MODAL REPRESENTATIONS FOR THE HIGH-FREQUENCY RESPONSE OF ELASTIC PLATES

Thesis by

Philip Wayne Randles

In Partial Fulfillment of the Requirements

For the Degree of

Doctor of Philosophy

California Institute of Technology

Pasadena, California

1969

(Submitted May 13, 1969)

ACKNOWLEDGMENTS

The author wishes to thank his thesis advisor, Professor J. Miklowitz, for his guidance and many helpful discussions throughout this work. The author would also like to thank Professor T. K. Caughey for his interest and help in this work.

The financial support of a National Science Foundation Graduate Fellowship, a National Science Foundation Traineeship and a teaching assistantship from the California Institute of Technology are greatly appreciated.

ABSTRACT

Representations for the high-frequency response of a suddenly loaded infinite plate are obtained from the modal form of the exact solution. The method of approach is presented by treating a linearly elastic, homogeneous, isotropic plate subjected to a normal impulsive line load on one face.

An investigation of the branches of the governing Rayleigh-Lamb frequency equation is given. These branches are closely related to the modes of propagation, the sum of which is the modal solution. The relationship between the high-frequency portions of the underlying frequency spectra and the high-frequency response is brought out.

Series representations for the branches are used to facilitate a summation over the branch (or mode) numbers. This results in convenient high-frequency representations, which exhibit all of the expected singular wave fronts in the plate.

The method appears to be applicable to a broader class of problems than other methods which have been used for the high-frequency response of a plate.

TABLE OF CONTENTS

LIST OF FIGURES

NOMENCLATURE

A	refers to asymmetrical part when used as a subscript
A_{pq}	see equations (4.2-4) and (4.2-5)
A'_{pq}	see equation (4.2-6)
Arg(~)	argument of a complex quantity
$a=\frac{c_d}{c_s}$	ratio of wave velocities, see equation (2.1-2)
B	see equation (4.2-10)
C	integration path in the χ-plane, see equation (2.3-15a) and Fig. 2
C_1	path in χ-plane on which $\|R\|=1$, see Appendix A
C_D, C_E	integration paths in χ-plane, see equation (4.1-2) and Fig. 21
C_{0A}, C_{0S}	integration paths in χ-plane, see equation (2.3-15a) and Fig. 3
c	refers to critical point or branch point when used as subscript
c_d, c_s	wave velocities, see equation (2.1-1)
c_g	group velocity, see equation (2.3-1)
c_p	phase velocity, see equation (2.3-1)
c_R	Rayleigh surface wave velocity
$D(\chi)$	see equation (2.3-12b)
d	refers to dilatational when used as subscript or superscript

e	refers to equivoluminal when used as subscript or superscript
$F(g_n,\chi)$	see equation (3.3-7b)
F_A, F_S	see equations (2.2-8) and (2.3-12)
F_ϕ	see equation (4.1-1a)
F_ψ	see equation (4.1-1b)
$g_d^{(k)}$	see equations (3.3-26) and (3.3-27)
$g_n^{(j)} \equiv g_e^{(j)}$	see equations (3.3-9) and (3.3-12)
$g_n(\chi)$	see equation (3.3-5)
H	half plate thickness
H(~)	Heaviside step function
I	see equation (2.1-7)
$I(\xi,\tau,\zeta)$	see equation (4.2-26a)
Im(~)	imaginary part of complex quantity
$i=\sqrt{-1}$	
$L=\frac{\xi}{\tau}$	normalized propagation coordinate
O	order symbol, see following equation (2.3-3)
p	used as Laplace transform variable only in Chapter 2
Q_{pq}^e, Q_{pq}^d	see equation (4.2-20)
$R(\chi) \equiv R(\chi,\nu)$	see equation (2.3-12a) and Appendix A

$\mathrm{Re}(\sim)$	real part of complex quantity
S	refers to symmetrical part when used as a subscript
$S_{k\ell}$	see equation (4.2-2a)
t	time
$U_{S\xi}$, $U_{A\xi}$, $U_{S\zeta}$, $U_{A\zeta}$	see equation (2.3-16)
$\underline{u}=(u_\xi,0,u_\zeta)$	displacement vector
u_x, u_z	see equation (2.1-5)
u_ξ, u_ζ	components of displacement vector, see equation (2.1-5)
$\tilde{u}_{S\xi}$, $\tilde{u}_{A\xi}$, $\tilde{u}_{S\zeta}$, $\tilde{u}_{A\zeta}$	see equation (2.2-9)
x	propagation coordinate
y	see equation (3.2-6)
z^e_{pq}, z^d_{pq}	normalized thickness coordinates, see equation (4.2-20)
z	thickness coordinate
$\alpha=\left(\frac{1}{a^2}\omega^2-\kappa^2\right)^{\frac{1}{2}}$	dilatational thickness wave number
$\beta=(\omega^2-\kappa^2)^{\frac{1}{2}}$	equivoluminal thickness wave number
$\Gamma(\chi)$	see equation (3.1-7a)

$\gamma(\theta)=\mathrm{ArgR}(e^{i\theta})$	see equation (A-6) in Appendix A
$\gamma_1(\chi)=\mathrm{ArgR}(\chi)$ for $\chi \in C_1$	see Appendix A
$\Delta^{\pm}_{jk}(\chi)$	see equation (3.1-9)
$\delta(\sim)$, $\delta_+(\sim)$	delta functions, see equation (2.1-7)
ε	used as a small quantity
$\varepsilon_n(\chi)$	see equation (3.3-7a)
$\zeta=\frac{z}{H}$	dimensionless thickness coordinate
$\eta=\beta+\alpha$	new variable replacing the dimensionless frequency
$\eta^{(0)}_{dm}(\chi)$	see equation (3.3-24)
$\eta^{(k)}_{d}(\chi)$	see equations (3.3-23) and (3.3-25)
$\eta^{(0)}_{en}(\chi)$	see equation (3.3-3)
$\eta^{(j)}_{e}(\chi)$	see equations (3.3-14) and (3.3-15)
$\eta_I=\mathrm{Im}\eta$	
$\eta_R=\mathrm{Re}\eta$	
η_n, η_m, η_p, η_q	branches of the frequency equation
$\theta=\mathrm{Arg}(\chi)$ for $\lvert\chi\rvert=1$	
θ_0	see equation (2.3-8) and Appendix A
θ_{-1}	see equation (A-1a) in Appendix A

κ	dimensionless wave number
λ, μ	Lamé constants
ν	Poisson's ratio
$\xi=\frac{x}{H}$	dimensionless propagation coordinate
ρ'	material density
$\sigma_{\zeta\zeta}$, $\sigma_{\xi\zeta}$	stress components, see equation (2.1-6)
$\tau=\frac{c_s t}{H}$	dimensionless time
Φ_ℓ	dilatational phase function, see equation (4.2-1)
$\Phi_{e\ell pq}$, $\Phi_{d\ell pq}$	see equation (4.2-7)
ϕ	dilatational potential, see equation (2.2-1)
$\chi=\frac{\beta-\alpha}{\beta+\alpha}$	new variable replacing the dimensionless wave number
χ_0	see equation (2.3-8) and Appendix A
χ_R	see equation (2.3-9) and Appendix A
χ_{-1}, χ_{01}, χ_{02}	see Appendix A
Ψ_ℓ	equivoluminal phase function, see equation (4.2-1)
$\Psi_{e\ell pq}$, $\Psi_{d\ell pq}$	see equation (4.2-7)
ψ	equivoluminal potential, see equation (2.2-1)
ω	dimensionless frequency
$\omega_n(\kappa)$	branches of the frequency equation

CHAPTER 1

INTRODUCTION

This work is concerned with representations for the high-frequency response of a suddenly loaded infinite plate governed by the equations of motion from linear elasticity theory. The problem has been given attention in the literature only recently. The method of attack has almost exclusively exploited Cagniard's method, geometric ray theory, and wave front approximations, as the most recent of these works, that by Rosenfeld and Miklowitz [1][1], exhibits. On the other hand, the present work is an investigation which logically asks whether high-frequency representations can be extracted from the modal form of the solution to the problem, which is based on the underlying frequency spectra. Indeed, it is shown here that such representations can be written, and the method appears to be applicable to a broader class of problems than those that Cagniard's method can handle.

The method, and representations, are brought forth here by treating the problem of an infinite plate, subjected to an impulsive line load applied normal to one of

---

[1]Numbers in brackets designate references in the bibliography.

the faces, which are otherwise free. The plate is assumed to be homogeneous and isotropic.

The modal form of the exact solution is a sum over an infinite number of integrals, each of which represents a mode of propagation. The modes are directly related to the branches, or roots, of the Rayleigh-Lamb frequency equation giving a functional relationship between the frequency and wave number of straight-crested waves propagating in the plate. The frequency spectrum of an infinite plate is then the plot of frequency versus wave number. The branches of the Rayleigh-Lamb frequency equation are now quite well understood, chiefly through the recent efforts of Mindlin and his coworkers (see [2]).

Most of the previous work on evaluating the modal solution has been limited to relatively low-frequency, long-wavelength calculations so as to limit consideration to a few of the lowest modes or just to the lowest mode of propagation. For example, Miklowitz [3] considered a plate, the faces of which were subjected to symmetrical normal point loads having a step dependence on time. Calculations were then based on the low-frequency portion of the lowest mode of propagation.

Such approaches are very useful when only the low-frequency response of the plate is of interest, however,

they cannot possibly predict the multitude of wave fronts, which are expected to be present in a plate subjected to an impulsive loading. The reason for this is that discontinuities identified as wave fronts must necessarily be composed of a superposition of high-frequency, short-wavelength waves.

To obtain the high frequency response of the plate, Rosenfeld and Miklowitz [1] used Cagniard's method which deals initially with a double-integral representation rather than with the modal solution. This representation results from use of integral transforms. The double-integral representation is expanded in a series, each term of which is finally warped into a single Laplace transform on time, then inverted by inspection to obtain wave front expansions. The wave front expansions are very accurate near the fronts, but they diverge quite rapidly away from them. Earlier uses of Cagniard's method of inversion for plate problems were given by Mencher [4], Broberg [5] and Davids [6]. Further studies on the high- and low-frequency response of plates are pointed out by Miklowitz [7].

Implicit in the problem of finding the high-frequency response of a plate is the need of a method of solution which is valid both at the wave fronts and for some distance behind the fronts. Also, there are two other very

important aspects of this problem. First, a clear indication of the relationship between the high-frequency portions of the frequency spectrum and the high-frequency response of the plate including possible singular wave fronts is needed. This will open the way for the investigation of the high-frequency response of other wave propagation problems whose solution can be formulated as a sum over modes of propagation. Such problems include other loading configurations on plates as well as wave propagation in anisotropic plates, circular rods, and layered media. Second, a method of solution for the high-frequency response which does not depend on Cagniard's method of inversion is needed since some of the problems just mentioned are apparently not solvable by his method.

In Chapter 2 the modal solution for the response of the plate is derived. The frequency and wave number are then replaced by new variables which allow a much more direct investigation of the high-frequency response of the plate.

An extension of Mindlin's [2] investigation of the branches of the Rayleigh-Lamb frequency equation is contained in Chapter 3. The most important new result found here, which relates to the high-frequency response, is the existence of analytic continuations of the branches which

are closely associated with the dilatational waves in the plate. These continuations are called the dilatational branches and they are found in a region where both the frequency and wave number are pure imaginary. The importance of these branches cannot be overemphasized in the context of this work. Series representations of the dilatational branches and of the usual branches of the Rayleigh-Lamb frequency equations, which are called the equivoluminal branches here, are given in Chapter 3. These series representations are extremely accurate for high frequency, making them the device which can be used to obtain representations of the high-frequency response of the plate. These series representations for the branches are quite unique since the individual terms in the series are found, in Chapter 4, to be closely related to the individual wave fronts in the plate. Also contained in Chapter 3 are descriptions of analytic continuations of the branches of the Rayleigh-Lamb frequency equations. These continuations are essential for manipulating the integrals involved in the modal solution.

In Chapter 4, the modal solution is shown to be equivalent to sums of integrals over the dilatational branches and over the equivoluminal branches. This equivalence is the key point in the solution method used in this

work. This is true since the series representations of Chapter 3 can then be used to derive representations of the response of the plate which are valid for high frequency and which exhibit all of the expected wave fronts. The series representations of Chapter 3 are used as if they were exact representations of the branches, and this makes the method approximate. However, the series representations for the branches are very good approximations and the validity of the final representations for the response of the plate does not diminish rapidly away from the wave fronts, as is the case for wave front expansions.

CHAPTER 2

STATEMENT OF THE PROBLEM AND THE MODAL SOLUTION

2.1. STATEMENT OF THE PROBLEM

An infinite plate subjected to an impulsive line load is considered in this work. The loading configuration, which makes this a plane strain problem, is shown in Fig. 1 with the space coordinates x and z indicated. The load is applied in the form of a stress normal to the upper face z=H (the uniform plate thickness being 2H) and it is concentrated on the line x=0. Otherwise the faces of the plate are traction-free. The plate material is linearly elastic, homogeneous and isotropic with no body forces acting.

The object is to obtain a representation which is capable of exhibiting the high-frequency response of the plate in terms of the displacement components.

It is convenient to define the material constants and wave velocities at this point.

$$c_d = \sqrt{\frac{\lambda+2\mu}{\rho'}} \quad , \quad c_s = \sqrt{\frac{\mu}{\rho'}} \qquad (2.1\text{-}1)$$

are the dilatational and equivoluminal body wave velocities respectively where λ and μ are the Lamé constants and ρ' is

the material density. The ratio of the velocities is

$$a = \frac{c_d}{c_s} = \sqrt{\frac{\lambda+2\mu}{\mu}} = \sqrt{\frac{2(1-\nu)}{1-2\nu}} \qquad (2.1\text{-}2)$$

where ν is Poisson's ratio.

The notation in the following work is simplified by writing this problem in terms of the dimensionless space and time coordinates

$$\xi = \frac{x}{H} \quad , \quad \zeta = \frac{z}{H} \quad , \quad \tau = \frac{c_s t}{H} \quad . \qquad (2.1\text{-}3)$$

This problem is governed by the equation of motion

$$(\lambda+\mu)\nabla\nabla\cdot\underline{u} + \mu\nabla^2\underline{u} = \rho' c_s^2 \frac{\partial^2 \underline{u}}{\partial \tau^2} \qquad (2.1\text{-}4)$$

for $-\infty<\xi<\infty, -1<\zeta<1, \tau>0$ where $\underline{u}=(u_\xi, 0, u_\zeta)$ is the displacement vector and ∇ is the del-operator with respect to the rectangular Cartesian coordinates ξ and ζ. (2.1-4) is homogeneous with respect to $\underline{u}$ and hence the dimensions are arbitrary. However, it is advantageous to take

$$u_\xi = Hu_x \quad , \quad u_\zeta = Hu_z \qquad (2.1\text{-}5)$$

where u_x and u_z are the original displacement components in the x,z coordinate system. Thus, the displacement components, u_ξ and u_ζ, have length squared dimensions.

The pertinent stress-strain relations are

$$\left.\begin{aligned} \sigma_{\zeta\zeta} &= (\lambda+2\mu)\frac{\partial u_\zeta}{\partial \zeta} + \lambda\frac{\partial u_\xi}{\partial \xi} \quad , \\ \sigma_{\xi\zeta} &= \mu\left(\frac{\partial u_\xi}{\partial \zeta} + \frac{\partial u_\zeta}{\partial \xi}\right) \quad . \end{aligned}\right\} \tag{2.1-6}$$

The boundary conditions on the faces $\zeta=\pm 1$ now take the form

$$\left.\begin{aligned} \sigma_{\zeta\zeta}(\xi,+1,\tau) &= -I\delta(\xi)\delta_+(\tau) \quad , \\ \sigma_{\zeta\zeta}(\xi,-1,\tau) &= 0 \quad , \\ \sigma_{\xi\zeta}(\xi,\pm 1,\tau) &= 0 \end{aligned}\right\} \tag{2.1-7}$$

where I is a positive constant, $\delta(\xi)$ is the Dirac delta function and $\delta_+(\tau)$ is the one-sided delta function. For example,

$$\delta(\xi) = \lim_{N\to+\infty}\left(\frac{N}{\pi}\right)^{\frac{1}{2}} e^{-N\xi^2} \quad ,$$

$$\delta_+(\tau) = \begin{cases} 0, & \tau<0 \\ \lim\limits_{N\to+\infty} N^2\tau e^{-N\tau}, & \tau\geq 0 \end{cases}$$

(N real and positive) are possible definitions of these generalized functions. Hence, from (2.1-7) and these

definitions, a quantity measuring the impulse is

$\int_{\xi=-\infty}^{\infty}\int_{\tau=0}^{\infty}\sigma_{\zeta\zeta}(\xi,+1,\tau)\,d\tau\,d\xi = -I$ so that I is the impulse per unit length along the line of loading.

The initial condition of quiescence at $\tau=0$ and the radiation condition (quantities vanish as $|\xi|\to\infty$) are imposed on all independent variables and their derivatives.

An important consideration is that (2.1-4) and (2.1-6) are physically accurate only if the strains are infinitesimal, which cannot be expected to be the case for the severe boundary conditions (2.1-7). This problem is justified on the grounds that any solution can be used in conjunction with convolution integrals to solve other more realistic problems in which only infinitesimal strains are expected.

2.2. THE MODAL SOLUTION

This problem is easily solved, formally at least, by first representing the displacement vector in terms of displacement potentials and then solving the resulting differential equations by means of integral transforms. This results in a double-integral representation or an infinite sum of single integrals (the modal solution) for the displacement components.

The representation

$$\underline{u} = \nabla\phi + \nabla\times(0,\psi,0) \quad , \tag{2.2-1}$$

where ϕ is the scalar displacement potential associated with dilatational motion and $(0,\psi,0)$ is the vector displacement potential associated with equivoluminal motion (ψ is a scalar), reduces the equation of motion (2.1-4) to

$$\left.\begin{aligned} \frac{\partial^2\phi}{\partial\xi^2} + \frac{\partial^2\phi}{\partial\zeta^2} &= \frac{1}{a^2}\frac{\partial^2\phi}{\partial\tau^2} \quad , \\ \frac{\partial^2\psi}{\partial\xi^2} + \frac{\partial^2\psi}{\partial\zeta^2} &= \frac{\partial^2\psi}{\partial\tau^2} \quad . \end{aligned}\right\} \tag{2.2-2}$$

(2.2-2) applies on the same domain as was indicated following (2.1-4). The boundary conditions on ϕ and ψ are given by (2.1-7) through (2.1-6) and (2.2-1). The required quiescence and radiation conditions are

$$\phi(\xi,\zeta,0) = \psi(\xi,\zeta,0) = \frac{\partial\phi}{\partial\tau}(\xi,\zeta,0) = \frac{\partial\psi}{\partial\tau}(\xi,\zeta,0) = 0 \tag{2.2-3}$$

and

$$\lim_{|\xi|\to\infty}[\phi(\xi,\zeta,\tau),\psi(\xi,\zeta,\tau),\ldots] = 0 \quad , \tag{2.2-4}$$

where (2.2-4) contains derivatives of ϕ and ψ up to and including the second order.

A Fourier transform with respect to the propagation coordinate ξ and a Laplace transform with respect to τ are applied to ϕ and ψ to reduce (2.2-2) to a pair of ordinary differential equations with ζ being the independent variable. Solution of these transformed equations subject to the boundary, initial and radiation conditions and also to the inversion integrals given by the pairs

$$\left.\begin{aligned} F(p) &= \int_0^\infty f(\tau)e^{-p\tau}d\tau \quad , \qquad f(\tau) = \frac{1}{2\pi i}\int_{Br_1} F(p)e^{p\tau}dp \\ \text{and} \\ F(\kappa) &= \int_{-\infty}^\infty f(\xi)e^{i\kappa\xi}d\xi \quad , \qquad f(\xi) = \frac{1}{2\pi}\int_{-\infty}^\infty F(\kappa)e^{-i\kappa\xi}d\kappa \end{aligned}\right\} \quad (2.2\text{-}5)$$

gives double-integral representations of the displacement components u_ξ and u_ζ . Br_1 is the Bromwich contour in the right half of the p-plane.

The following derivation of the modal solution was done for the symmetrical case by Miklowitz [3] and the double-integral representation appears in the work of Rosenfeld and Miklowitz [1]. Some of the derivation and the results are repeated here so that they can be used later in this work.

Without indicating the intervening algebraic calculations, the double-integral representations for the displacement components take the form

$$\left.\begin{aligned} u_\xi(\xi,\zeta,\tau) &= \frac{-I}{2\pi\mu}\int_{\kappa=0}^{\infty}\kappa\sin\kappa\xi\left[\frac{1}{2\pi i}\int_{Br_1}\left(\frac{\tilde{u}_{S\xi}}{F_S}+\frac{\tilde{u}_{A\xi}}{F_A}\right)e^{p\tau}dp\right]d\kappa \quad , \\ u_\zeta(\xi,\zeta,\tau) &= \frac{-I}{2\pi\mu}\int_{\kappa=0}^{\infty}\cos\kappa\xi\left[\frac{1}{2\pi i}\int_{Br_1}\alpha\left(\frac{\tilde{u}_{S\zeta}}{F_S}-\frac{\tilde{u}_{A\zeta}}{F_A}\right)e^{p\tau}dp\right]d\kappa \quad . \end{aligned}\right\} \tag{2.2-6}$$

$\omega=-ip$ is a dimensionless frequency, which is obviously real when p is pure imaginary, and κ is a dimensionless wave number for propogation in the ξ direction. The functions

$$\left.\begin{aligned} \alpha &= \left(\frac{1}{a^2}\omega^2-\kappa^2\right)^{\frac{1}{2}} \quad , \\ \beta &= \left(\omega^2-\kappa^2\right)^{\frac{1}{2}} \end{aligned}\right\} \tag{2.2-7}$$

are the dilatational and equivoluminal thickness wave numbers respectively and the functions

$$\left.\begin{aligned} F_S(\omega,\kappa) &= \left(\omega^2-2\kappa^2\right)^2\cos\alpha\sin\beta + 4\kappa^2\alpha\beta\sin\alpha\cos\beta \quad , \\ F_A(\omega,\kappa) &= \left(\omega^2-2\kappa^2\right)^2\sin\alpha\cos\beta + 4\kappa^2\alpha\beta\cos\alpha\sin\beta \end{aligned}\right\} \tag{2.2-8}$$

will be called the symmetrical and asymmetrical Rayleigh-Lamb functions respectively. The functions

$$\left.\begin{aligned}
\tilde{u}_{S\xi}(\omega,\kappa,\zeta) &= \left(\omega^2-2\kappa^2\right)\cos\alpha\zeta\sin\beta - 2\alpha\beta\sin\alpha\cos\beta\zeta \quad , \\
\tilde{u}_{A\xi}(\omega,\kappa,\zeta) &= \left(\omega^2-2\kappa^2\right)\sin\alpha\zeta\cos\beta - 2\alpha\beta\cos\alpha\sin\beta\zeta \quad , \\
\tilde{u}_{S\zeta}(\omega,\kappa,\zeta) &= \left(\omega^2-2\kappa^2\right)\sin\alpha\zeta\sin\beta + 2\kappa^2\sin\alpha\sin\beta\zeta \quad , \\
\tilde{u}_{A\zeta}(\omega,\kappa,\zeta) &= \left(\omega^2-2\kappa^2\right)\cos\alpha\zeta\cos\beta + 2\kappa^2\cos\alpha\cos\beta\zeta
\end{aligned}\right\} \quad (2.2\text{-}9)$$

are proportional to components of the transformed displacement. They are written so that the first term in each results from the dilatational potential ϕ through (2.2-1) and the second term in each results from the equivoluminal potential ψ. The decomposition into symmetrical and asymmetrical parts, denoted by the S and A subscripts respectively in (2.2-8) and (2.2-9), results from a convenient separation into two problems both with loadings on the upper and lower faces of the plate. In one problem the load is symmetrical with respect to $\zeta=0$ ($\sigma_{\zeta\zeta}(\xi,\pm1,\tau) = -\frac{1}{2}I\delta(\xi)\delta_+(\tau)$ from the loading (2.1-7)) and in the other the load is asymmetrical with respect to $\zeta=0$ ($\sigma_{\zeta\zeta}(\xi,\pm1,\tau) = \mp\frac{1}{2}I\delta(\xi)\delta_+(\tau)$). Superposition of the two problems gives the problem posed in this work. Actually the purpose of this

decomposition is to separate the Rayleigh-Lamb functions (2.2-8) as they appear in (2.2-6).

The integrands in (2.2-6) are even with respect to both α and β; hence the radicals in (2.2-7) do not give rise to branch points.

It is well known that each of the functions $F_S(\omega,\kappa)$ and $F_A(\omega,\kappa)$ in (2.2-8) have doubly infinite sets of simple zeros and no others for $0<\kappa<\infty$. Even though the symmetrical and asymmetrical sets of zeros are distinct, the zeros of both cases will be denoted by $\omega=\pm\omega_n(\kappa)$ with $n=0,1,2,...$ and it will be clear from the context whether they are symmetrical or asymmetrical zeros. For $0<\kappa<\infty$ the zeros are ordered as $0<\omega_0<\omega_1<\omega_2...$. The zeros were shown to be simple by Scott and Miklowitz [8] for the symmetrical case and it will become evident for both cases in this work. The zeros $\beta=0$ for $F_S(\omega,\kappa)$ and $\alpha=0$ for $F_A(\omega,\kappa)$ are superficial since they are seen to be removable in (2.2-6).

Thus, the integrands in (2.2-6) have doubly infinite sets of simple poles located on the imaginary p-axis for $0<\kappa<\infty$ and residue theory is used to carry out the integration over p. A detailed analysis of the representation (2.2-6) or the simple observation that (2.2-2) are hyperbolic differential equations leads to the conclusion that $\underline{u}\equiv\underline{0}$ for $\tau<\frac{1}{a}\sqrt{\xi^2+(1-\zeta)^2}$. For $\tau\geq\frac{1}{a}\sqrt{\xi^2+(1-\zeta)^2}$ the residue calculation results in

$$
\left.
\begin{aligned}
u_\xi(\xi,\zeta,\tau) &= \frac{I}{\pi\mu}\sum_{n=0}^{\infty}\int_0^{\infty}\kappa\sin\kappa\xi\sin\omega\tau\left.\frac{\tilde{u}_{S\xi}}{\frac{\partial F_S}{\partial\omega}}\right|_{\substack{F_S=0\\ \omega=\omega_n(\kappa)}}d\kappa \\
&+ \frac{I}{\pi\mu}\sum_{n=0}^{\infty}\int_0^{\infty}\kappa\sin\kappa\xi\sin\omega\tau\left.\frac{\tilde{u}_{A\xi}}{\frac{\partial F_A}{\partial\omega}}\right|_{\substack{F_A=0\\ \omega=\omega_n(\kappa)}}d\kappa \quad , \\
u_\zeta(\xi,\zeta,\tau) &= \frac{I}{\pi\mu}\sum_{n=0}^{\infty}\int_0^{\infty}\alpha\cos\kappa\xi\sin\omega\tau\left.\frac{\tilde{u}_{S\zeta}}{\frac{\partial F_S}{\partial\omega}}\right|_{\substack{F_S=0\\ \omega=\omega_n(\kappa)}}d\kappa \\
&- \frac{I}{\pi\mu}\sum_{n=0}^{\infty}\int_0^{\infty}\alpha\cos\kappa\xi\sin\omega\tau\left.\frac{\tilde{u}_{A\zeta}}{\frac{\partial F_A}{\partial\omega}}\right|_{\substack{F_A=0\\ \omega=\omega_n(\kappa)}}d\kappa \quad .
\end{aligned}
\right\} \qquad (2.2\text{-}10)
$$

The modal representation of the solution is precisely (2.2-10) with each of the terms n=0,1,2,... called a mode of propagation. The integrands represent residues and are evaluated at the simple poles resulting from $F_S=0$ or $F_A=0$ or equivalently at $\omega=\omega_n(\kappa)$ where $\omega_n(\kappa)$ are the zeros of the appropriate function F_S or F_A. Thus, the residue calculation has given rise to the Rayleigh-Lamb frequency equations. $F_S=0$ or from (2.2-8)

$$\frac{\tan\beta}{\tan\alpha} + \frac{4\kappa^2\alpha\beta}{\left(\omega^2-2\kappa^2\right)^2} = 0 \qquad (2.2\text{-}11)$$

is the symmetrical Rayleigh-Lamb frequency equation for a plate which admits branches $\omega_n(\kappa)$, n=0,1,2,... . F_A=0 or from (2.2-8)

$$\frac{\tan\beta}{\tan\alpha} + \frac{\left(\omega^2-2\kappa^2\right)^2}{4\kappa^2\alpha\beta} = 0 \qquad (2.2\text{-}12)$$

is the asymmetrical Rayleigh-Lamb frequency equation for a plate which admits branches $\omega_n(\kappa)$, n=0,1,2,... .

An important point is that the integration over κ and the summation over n have been interchanged in the representations (2.2-10) without mathematical justification. The singular loading (2.1-7) is expected to produce singular wave fronts; hence either the integration or the summation in (2.2-10) must diverge at these points. If theorems requiring uniform convergence with respect to the parameters are to be used to justify this interchange, either the loading must be made more smooth or the generalized functions in (2.1-7) must be replaced by their defining sequences with the limit to the generalized function taken after these summations and integrations are carried out. The latter is the most direct way to justify (2.2-10) as the response to the loading (2.1-7) and this can be

done in a manner similar to that which Lighthill [9] used to treat generalized functions.

2.3. CHANGE OF VARIABLES IN THE MODAL SOLUTION

Much of the high-frequency response of a plate, which must be contained in the representation (2.2-10), has apparently been inaccessible through direct integration and summation even when approximations such as asymptotic expansions are employed. The independent variable κ in (2.2-10) will be replaced by a new variable in an effort to make the modal solution and especially the frequency spectrum (made up of the branches $\omega_n(\kappa)$ as functions of κ) more easily handled with tools such as analytic function theory.

Various properties of the branches $\omega_n(\kappa)$ of the symmetrical and asymmetrical Rayleigh-Lamb frequency equations (2.2-11) and (2.2-12) respectively, which were given by Mindlin [2] or are implicit in his work, are useful to recount at this point. It is assumed throughout that κ is real and nonnegative. The properties are applicable to both the symmetrical and asymmetrical branches unless specified otherwise.

(1) The branches are ordered $0<\omega_0<\omega_1<\omega_2<\ldots$ for $0<\kappa<\infty$ with $\omega_n(0)>0$ for $n=1,2,3,\ldots$ and $\omega_0(0)=0$ ($\omega_0(\kappa)$ will be called the Rayleigh branch in this work; however, it is

usually called the lowest branch of the Rayleigh-Lamb frequency equation). Also, $\omega_{n-1}(0)<\omega_n(0)=\omega_{n+1}(0)<\omega_{n+2}(0)$ for certain integers $n\geq 1$ when Poisson's ratio ν is such that a in (2.1-2) is a rational number. Otherwise, $\omega_n(0)$, $n=1,2,3,\ldots$, are ordered just as for $0<\kappa<\infty$.

(2) The ratio $\frac{\omega_n(\kappa)}{\kappa}$ is a strictly decreasing function of $\kappa>0$ as κ increases from $0\to+\infty$ with $\lim_{\kappa\to\infty}\frac{\omega_n(\kappa)}{\kappa}=1$ for $n=1,2,3,\ldots$. Also, for the Rayleigh branches $n=0$, $\frac{\omega_0(\kappa)}{\kappa}$ is a strictly decreasing function of $\kappa>0$ for the symmetrical case and a strictly increasing function of $\kappa>0$ for the asymmetrical case as κ increases from $0\to+\infty$ with $\lim_{\kappa\to\infty}\frac{\omega_0(\kappa)}{\kappa}=\frac{c_R}{c_s}<1$ for both cases (c_R being the Rayleigh surface wave velocity for a half-space). The preceding remarks depend on the well-known fact that $c_p>c_g$ in the intervals mentioned (except for the asymmetrical Rayleigh branch $n=0$ on which $c_p<c_g$ for $\kappa>0$) where

$$\left.\begin{aligned} c_p &= \frac{\omega_n(\kappa)}{\kappa}c_s \quad , \\ c_g &= \frac{d\omega_n(\kappa)}{d\kappa}c_s \end{aligned}\right\} \quad (2.3\text{-}1)$$

are the phase and group velocities respectively for waves propagating in the ξ direction. These inequalities on c_p

and c_g will be seen to be related to the fact that the branches in the new variables have no singular points on the path of integration except possibly at the endpoints. It is also useful to state the results

$$\omega_0(\kappa) = \sqrt{\frac{2}{1-\nu}}\kappa + O(|\kappa|^3) \qquad (2.3\text{-}2)$$

for the symmetrical Rayleigh branch and

$$\omega_0(\kappa) = \sqrt{\frac{2}{3(1-\nu)}}\kappa^2 + O(|\kappa|^4) \qquad (2.3\text{-}3)$$

for the asymmetrical Rayleigh branch as $\kappa \to 0$ in each case. The order symbol O, as in (2.3-2) and (2.3-3), will be understood to mean the following in this work: if $f(\kappa) = g(\kappa) + O\left(|\kappa-\kappa_0|^\gamma\right)$ as $\kappa \to \kappa_0$ then $\dfrac{f(\kappa)-g(\kappa)}{|\kappa-\kappa_0|^\gamma}$ is bounded as $\kappa \to \kappa_0$.

(3) For any change of variables, $\omega_n(\kappa)$ and κ range through the values

$$0 \leq \omega_0(\kappa) < \infty \text{ for } 0 \leq \kappa < \infty \text{ and}$$

$$0 < \omega_n(\kappa) < \infty \text{ for } 0 \leq \kappa < \infty \ (n=1,2,3,\ldots).$$

The new variables are defined as

$$\left.\begin{aligned} \chi &= \frac{\beta-\alpha}{\beta+\alpha} \ , \\ \eta &= \beta+\alpha \end{aligned}\right\} \qquad (2.3\text{-}4)$$

where χ will replace κ as the independent variable in the integrals (2.2-10) and η will play the role of $\omega_n(\kappa)$ in that it is a function of χ through the Rayleigh-Lamb frequency equations. α and β are the thickness wave numbers defined by (2.2-7).

Holden [10] used α and β as variables to replace ω and κ in the Rayleigh-Lamb frequency equations, thus making the frequency spectrum simpler in some respects. The choice of the variables χ and η to replace ω and κ is not unlike using α and β and can be considered as a mapping of the frequency spectrum into yet another set of variables. However, the χ,η variables differ from the ω,κ and α,β variables in several respects one of which is that all infinities (cases where $\kappa\to\infty$ or $\omega\to\infty$) map into the finite χ-plane.

The thickness wave numbers have the inverses

$$\left.\begin{aligned} \alpha &= \tfrac{1}{2}\eta(1-\chi) \quad , \\ \beta &= \tfrac{1}{2}\eta(1+\chi) \end{aligned}\right\} \qquad (2.3\text{-}5)$$

in terms of χ and η. The particular branches of the radicals defining α and β in (2.2-7) were unimportant in the preceding integrals, however, now a definite branch must be assigned to each so that χ and η will be uniquely defined. This is arbitrary and the result of other choices

will be clear later. The branches of α and β are completely defined by requiring that

$$\left.\begin{aligned} &\alpha \geq 0 \text{ for } 0 \leq \kappa \leq \tfrac{1}{a}\omega_n(\kappa) \quad , \\ &\alpha = -i|\alpha| \text{ for } \tfrac{1}{a}\omega_n(\kappa) < \kappa \quad , \\ &\beta \geq 0 \text{ for } 0 \leq \kappa \leq \omega_n(\kappa) \quad , \\ &\beta = -i|\beta| \text{ for } \omega_n(\kappa) < \kappa \quad . \end{aligned}\right\} \tag{2.3-6}$$

The inverses of (2.3-4) giving ω and κ as functions of χ and η are

$$\left.\begin{aligned} \omega &= \frac{a}{\sqrt{a^2-1}}\eta\chi^{\frac{1}{2}} \quad , \\ \kappa &= \tfrac{1}{2}\eta\left[\left(\chi-\frac{a-1}{a+1}\right)\left(\frac{a+1}{a-1}-\chi\right)\right]^{\frac{1}{2}} \end{aligned}\right\} \tag{2.3-7}$$

where the branches of the radicals are chosen so that ω and κ are always real and nonnegative in the integrals (2.2-10) (unless the integration path is deformed).

The following remarks about χ result from (2.3-4) and the definitions (2.2-7) and (2.3-6) of α and β.

(1) χ is a real positive function of $\dfrac{\omega_n(\kappa)}{\kappa}$, $n=1,2,3,\ldots$, on $\infty \geq \dfrac{\omega_n(\kappa)}{\kappa} \geq a$ which is strictly increasing

from $\chi=\frac{a-1}{a+1}\to+1$ as $\frac{\omega_n(\kappa)}{\kappa}$ decreases from $+\infty\to a$. In this case and in the cases to follow, the strictly increasing or decreasing property of the functions does not necessarily include the endpoints of the intervals. The point

$$\frac{\omega_n(\kappa)}{\kappa} = +\infty\,(\kappa=0) \text{ maps into } \chi = \frac{a-1}{a+1}$$

and the point

$$\frac{\omega_n(\kappa)}{\kappa} = a\left(\kappa=\frac{1}{a}\omega_n(\kappa)\right) \text{ maps into } \chi = +1.$$

(2) $\chi=e^{i\theta}$ with $\theta=2\tan^{-1}\left(\frac{|\alpha|}{\beta}\right)$, $0\le\theta\le\pi$, where θ is a real positive function of $\frac{\omega_n(\kappa)}{\kappa}$, $n=1,2,3,\ldots$, on $a\ge\frac{\omega_n(\kappa)}{\kappa}\ge1$, which is strictly increasing from $\theta=0\to\pi$ as $\frac{\omega_n(\kappa)}{\kappa}$ decreases from $a\to1$. The point $\frac{\omega_n(\kappa)}{\kappa}=a$ maps into $\theta=0$ or $\chi=+1$ as given above and the point

$$\frac{\omega_n(\kappa)}{\kappa} = 1\,(\kappa=+\infty) \text{ maps into } \chi = -1.$$

(3) For the symmetrical Rayleigh branch $n=0$, $\chi=e^{i\theta}$ with $\theta=2\tan^{-1}\left(\frac{|\alpha|}{\beta}\right)$, $\theta_0\le\theta\le\pi$, where θ is a real positive function of $\frac{\omega_0(\kappa)}{\kappa}$ on $\sqrt{\frac{2}{1-\nu}}\ge\frac{\omega_0(\kappa)}{\kappa}\ge1$ (see (2.3-2)),

which is strictly increasing from $\theta=\theta_0 \to \pi$ as $\frac{\omega_0(\kappa)}{\kappa}$ decreases from $\sqrt{\frac{2}{1-\nu}} \to 1$. θ_0 is defined by

$$\chi_0 = e^{i\theta_0} = 1 - 2\nu^2 + 2i\nu\sqrt{1-\nu^2} \qquad (2.3\text{-}8)$$

so that $0 \leq \theta_0 < \frac{\pi}{2}$ for $0 \leq \nu \leq \frac{1}{2}$. The point

$$\frac{\omega_0(\kappa)}{\kappa} = \sqrt{\frac{2}{1-\nu}} \ (\kappa=0) \text{ maps into } \chi = \chi_0$$

and the point

$$\frac{\omega_0(\kappa)}{\kappa} = 1 \text{ maps into } \chi = -1.$$

(4) For the symmetrical Rayleigh branch n=0, χ is a real negative function of $\frac{\omega_0(\kappa)}{\kappa}$ on $1 \geq \frac{\omega_0(\kappa)}{\kappa} \geq \frac{c_R}{c_s}$, which is strictly increasing from $\chi=-1 \to \chi_R$ as $\frac{\omega_0(\kappa)}{\kappa}$ decreases from $1 \to \frac{c_R}{c_s}$, where

$$\chi_R = -\frac{\left(1-\frac{c_R^2}{c_d^2}\right)^{\frac{1}{2}} - \left(1-\frac{c_R^2}{c_s^2}\right)^{\frac{1}{2}}}{\left(1-\frac{c_R^2}{c_d^2}\right)^{\frac{1}{2}} + \left(1-\frac{c_R^2}{c_s^2}\right)^{\frac{1}{2}}} \qquad (2.3\text{-}9)$$

with all of the radicals positive and $0>\chi_R>-1$ for $0\leq\nu\leq\frac{1}{2}$.

The point $\frac{\omega_0(\kappa)}{\kappa}=1$ maps into $\chi=-1$ as given above and the point

$$\frac{\omega_0(\kappa)}{\kappa}=\frac{c_R}{c_s}\ (\kappa=+\infty)\ \text{maps into}\ \chi=\chi_R.$$

(5) For the asymmetrical Rayleigh branch n=0, χ is a real negative function of $\frac{\omega_0(\kappa)}{\kappa}$ on $0<\frac{\omega_0(\kappa)}{\kappa}\leq\frac{c_R}{c_s}$, which is strictly decreasing from $\chi=0\rightarrow\chi_R$ as $\frac{\omega_0(\kappa)}{\kappa}$ increases from $0\rightarrow\frac{c_R}{c_s}$. The point

$$\frac{\omega_0(\kappa)}{\kappa}=0\ (\kappa=0)\ \text{maps into}\ \chi=0$$

and the point

$$\frac{\omega_0(\kappa)}{\kappa}=\frac{c_R}{c_s}\ (\kappa=+\infty)\ \text{maps into}\ \chi=\chi_R.$$

The preceding remarks and the remarks at the first of this section about the variation of $\frac{\omega_n(\kappa)}{\kappa}$ as κ increases on the various branches specify a continuous one-to-one mapping of the real positive κ-axis, which is the integration path in the integrals (2.2-10), into the χ-plane for

each branch $\omega_n(\kappa)$.

In the following work

$$0 \leq \kappa \leq \frac{1}{a}\omega \tag{2.3-10}$$

will be called "the dilatational sector" of the ω,κ-plane and

$$\frac{1}{a}\omega \leq \kappa \leq \omega \tag{2.3-11}$$

will be called "the equivoluminal sector" of the ω,κ-plane. This terminology is not physically precise and is only used for identification purposes.

The mapping of the integration path on the real κ-axis $0\leq\kappa\leq\infty$ in the integrals (2.2-10) onto the integration path C in the χ-plane for the branches n=1,2,3,... is shown in Fig. 2. In that figure it is seen that the dilatational sector maps onto the segment $\frac{a-1}{a+1}\leq\chi\leq 1$ of the real χ-axis and that the equivoluminal sector maps onto the upper half unit circle $\chi=e^{i\theta}$, $0\leq\theta\leq\pi$. The direction on C in the χ-plane is $\frac{a-1}{a+1}\rightarrow 1\rightarrow -1$ corresponding to $0\rightarrow+\infty$ on the positive real κ-axis with $\frac{a-1}{a+1}\rightarrow 1$ on the positive real χ-axis and $1\rightarrow -1$ on the unit circle $\chi=e^{i\theta}$, $0\leq\theta\leq\pi$. The numbers 1, 2, 3 in Fig. 2 denote specific points on a given branch $\omega_n(\kappa)$, with 3 meant to indicate the limiting point $\kappa\rightarrow\infty$, and they also indicate the mapping of these points into the χ-plane. The integration path C is valid for all branches n=1,2,3,... .

The corresponding integration paths for the Rayleigh branches n=0 are shown in Fig. 3. For the symmetrical

Rayleigh branch the real κ-axis with the direction $0 \to +\infty$ maps onto the integration path C_{0S} in the χ-plane with the direction $\chi_0 \to -1 \to \chi_R$. χ_0 is given by (2.3-8) and χ_R by (2.3-9). The portion $\chi_0 \to -1$ of C_{0S} is on the upper half unit circle and the portion $-1 \to \chi_R$ is on the negative real axis. The numbers 1, 2, 3 in Fig. 3 denote points on the symmetrical Rayleigh branch and their mapping into the χ-plane with 3 indicating the limiting point $\kappa \to \infty$. For the asymmetrical Rayleigh branch the real κ-axis with the direction $0 \to +\infty$ maps onto the integration path C_{0A} in the χ-plane with the direction $0 \to \chi_R$ on the negative real χ-axis. The numbers I, II in Fig. 3 denote points on the asymmetrical Rayleigh branch and their mapping into the χ-plane. The ω and κ scales in Fig. 3 are expanded with respect to those in Fig. 2 so that the details of the Rayleigh branches can be seen more clearly.

If branches other than those defined by (2.3-6) are chosen for α and β, the integration path C in Fig. 2 and also the paths C_{0S} and C_{0A} in Fig. 3 are changed as follows: the paths of integration are reflected about the real χ-axis if the sign of α (or β) is changed only when it is pure imaginary; the paths of integration are reflected about the unit circle $|\chi|=1$ by the mapping $\chi \to \frac{1}{\chi}$ if the sign of α (or β) is changed throughout. In the latter case all points interior to $|\chi|=1$ map to the exterior like

$\frac{a-1}{a+1} \rightarrow \frac{a+1}{a-1}$, $\chi_R \rightarrow \frac{1}{\chi_R}$, etc., and the points on the unit circle are just reflected about the real χ-axis. Any of these three other choices represents the mapping of the positive real κ-axis into the χ-plane equally well.

It is significant that the mapping determined by (2.3-4) and (2.3-6) for this work has mapped all of the infinity points in the original ω,κ-plane, that is, the points where $\kappa \rightarrow \infty$ or $\omega_n(\kappa) \rightarrow \infty$ for any branch n=0,1,2,..., into the finite χ-plane with $|\chi| \leq 1$. Also, from the foregoing, it appears that all of the complex κ-plane, taken as a projection from the ω,κ-space with ω and κ related by one of the Rayleigh-Lamb frequency equations, has been mapped onto the unit disk $|\chi| \leq 1$. Likewise, the mapping can be onto $|\chi| \geq 1$ by choosing other branches of α or β.

Expressions required to change the integrals (2.2-10) from the κ independent variable to the χ independent variable are listed below in terms of χ and η. The Rayleigh-Lamb functions (2.2-8) become

$$\left.\begin{aligned} F_S &= \tfrac{1}{4}\eta^4 \chi D(\chi)[\sin\eta + R(\chi)\sin\chi\eta] \quad , \\ F_A &= \tfrac{1}{4}\eta^4 \chi D(\chi)[\sin\eta - R(\chi)\sin\chi\eta] \end{aligned}\right\} \qquad (2.3\text{-}12)$$

where

$$R(\chi) \equiv R(\chi,\nu) = \frac{1}{\chi}\,\frac{(1+\chi)^3 - 8(1-\nu)(1+\nu\chi)\chi}{(1+\chi)^3 - 8(1-\nu)(\nu+\chi)\chi}$$

$$= \frac{\left(\omega^2-2\kappa^2\right)^2 - 4\kappa^2\alpha\beta}{\left(\omega^2-2\kappa^2\right)^2 + 4\kappa^2\alpha\beta} \qquad (2.3\text{-}12a)$$

and

$$D(\chi) = (1+\chi)^3 - 8(1-\nu)(\nu+\chi)\chi$$

$$= \frac{2}{\eta^4\chi}\left[\left(\omega^2-2\kappa^2\right)^2 + 4\kappa^2\alpha\beta\right] \quad . \qquad (2.3\text{-}12b)$$

Hence, the symmetrical Rayleigh-Lamb frequency equation (2.2-11) becomes

$$\sin\eta = -R(\chi)\sin\chi\eta \qquad (2.3\text{-}13)$$

and the asymmetrical Rayleigh-Lamb frequency equation (2.2-12) becomes

$$\sin\eta = R(\chi)\sin\chi\eta \quad . \qquad (2.3\text{-}14)$$

These equations give the branches $\eta=\eta_n(\chi)$, $n=0,1,2,\ldots,$ which are identified with $\omega_n(\kappa)$ through (2.3-4). Henceforth (2.3-13) and (2.3-14) will just be called the symmetrical and asymetrical frequency equations respectively.

In the preceding forms of the frequency equations, use has been made of the fact that

$$\frac{1}{2}\eta^4\chi D(\chi) = \left(\omega^2-2\kappa^2\right)^2 + 4\kappa^2\alpha\beta$$

is precisely the equation whose zero gives the Rayleigh surface wave velocity. It is easy to show that, for α and β defined by (2.2-7) and (2.3-6), this equation has only the zero $\frac{\omega}{\kappa}=\frac{c_R}{c_s}$, that is, the asymptote of the Rayleigh branches, on $0<\kappa\leq\infty$. Hence, all of the branches of the Rayleigh-Lamb frequency equations (2.2-11) and (2.2-12) are contained in (2.3-13) and (2.3-14) respectively as branches defined in the χ-plane. It should be noted that $\chi=\chi_R$ from (2.3-9) is a zero of $D(\chi)$ and that, $D(\chi)$ being a cubic, the other two zeros are usually discarded as being identified with physically meaningless Rayleigh velocities.

There are other expressions such as $\frac{d\kappa}{d\chi}\left(\frac{\partial F}{\partial\omega}\bigg|_{F=0}\right)^{-1}$, which are required as functions of χ and η for the integrals; however, they will not be listed here. This particular expression requires the chain rule of differentiation to calculate $\frac{\partial F}{\partial\omega}$ from (2.3-12) and (2.3-7) and requires the derivative $\frac{d\eta}{d\chi}$ from (2.3-13) or (2.3-14) to calculate $\frac{d\kappa}{d\chi}$ from (2.3-7).

In terms of χ and η, the modal solution (2.2-10) becomes

$$\left.\begin{aligned} u_\xi(\xi,\zeta,\tau) &= \frac{aI}{4\pi\mu\sqrt{a^2-1}} \sum_{n=0}^{\infty} \left(u_{S\xi n}+u_{A\xi n}\right) , \\ u_\zeta(\xi,\zeta,\tau) &= \frac{aI}{4\pi\mu\sqrt{a^2-1}} \sum_{n=0}^{\infty} \left(u_{S\zeta n}-u_{A\zeta n}\right) \end{aligned}\right\} \qquad (2.3\text{-}15)$$

where

$$\left.\begin{aligned} u_{S\xi n} &= \int_C \frac{(1-\chi^2)\sin(\kappa\xi)\sin(\omega\tau)U_{S\xi}}{\chi^{\frac{3}{2}}D(\chi)(\cos\eta+\chi R\cos\chi\eta)}d\chi , \\ u_{A\xi n} &= \int_C \frac{(1-\chi^2)\sin(\kappa\xi)\sin(\omega\tau)U_{A\xi}}{\chi^{\frac{3}{2}}D(\chi)(\cos\eta-\chi R\cos\chi\eta)}d\chi , \\ u_{S\zeta n} &= \int_C \frac{(1-\chi)^2(1+\chi)\cos(\kappa\xi)\sin(\omega\tau)U_{S\zeta}}{\chi^{\frac{3}{2}}D(\chi)\left[\left(\chi-\frac{a-1}{a+1}\right)\left(\frac{a+1}{a-1}-\chi\right)\right]^{\frac{1}{2}}(\cos\eta+\chi R\cos\chi\eta)}d\chi , \\ u_{A\zeta n} &= \int_C \frac{(1-\chi)^2(1+\chi)\cos(\kappa\xi)\sin(\omega\tau)U_{A\zeta}}{\chi^{\frac{3}{2}}D(\chi)\left[\left(\chi-\frac{a-1}{a+1}\right)\left(\frac{a+1}{a-1}-\chi\right)\right]^{\frac{1}{2}}(\cos\eta-\chi R\cos\chi\eta)}d\chi . \end{aligned}\right\} \qquad (2.3\text{-}15a)$$

In (2.3-15a) ω and κ are given by (2.3-7) with $\eta=\eta_n(\chi)$, $n=0,1,2,\ldots$, understood to be branches of the symmetrical frequency equation (2.3-13) for integrals with an S subscript and branches of the asymmetrical frequency equation

(2.3-14) for integrals with an A subscript. C is the integration path shown in Fig. 2 for n=1,2,3,... and it is replaced by C_{0S} and C_{0A} shown in Fig. 3 for the symmetrical and asymmetrical Rayleigh branches n=0 respectively. The radicals in (2.3-15a) are defined just as in (2.3-7) so that ω and κ are real and nonnegative.

The two factors $\cos\eta \pm \chi R \cos\chi\eta$ in (2.3-15a) will be found to play a very important role in determining the properties of the branches $\eta=\eta_n(\chi)$. They result from the term $\frac{d\eta}{d\chi}$ which is required for calculating $\frac{d\kappa}{d\chi}$ in the change of variables. These factors replace the rather complicated functions of ω and κ, $\frac{\partial F_S}{\partial \omega}$ and $\frac{\partial F_A}{\partial \omega}$, in the representation (2.2-10).

The functions

$$U_{S\xi} = [\chi^2-2(1-2\nu)\chi+1]\cos\frac{\eta(1-\chi)\zeta}{2}\sin\frac{\eta(1+\chi)}{2}$$

$$- (1-\chi^2)\sin\frac{\eta(1-\chi)}{2}\cos\frac{\eta(1+\chi)\zeta}{2} \quad ,$$

$$U_{A\xi} = [\chi^2-2(1-2\nu)\chi+1]\sin\frac{\eta(1-\chi)\zeta}{2}\cos\frac{\eta(1+\chi)}{2}$$

$$- (1-\chi^2)\cos\frac{\eta(1-\chi)}{2}\sin\frac{\eta(1+\chi)\zeta}{2} \quad ,$$

$$U_{S\zeta} = [\chi^2-2(1-2\nu)\chi+1]\sin\frac{\eta(1-\chi)\zeta}{2}\sin\frac{\eta(1+\chi)}{2}$$

$$+ \left(\chi-\frac{a-1}{a+1}\right)\left(\frac{a+1}{a-1}-\chi\right)\sin\frac{\eta(1-\chi)}{2}\sin\frac{\eta(1+\chi)\zeta}{2} \quad ,$$

$$U_{A\zeta} = [\chi^2-2(1-2\nu)\chi+1]\cos\frac{\eta(1-\chi)\zeta}{2}\cos\frac{\eta(1+\chi)}{2}$$

$$+ \left(\chi-\frac{a-1}{a+1}\right)\left(\frac{a+1}{a-1}-\chi\right)\cos\frac{\eta(1-\chi)}{2}\cos\frac{\eta(1+\chi)\zeta}{2} \qquad (2.3\text{-}16)$$

are proportional to the functions $\tilde{u}$ in (2.2-9) and are also written with the first term in each deriving from the dilatational potential ϕ through (2.2-1) and the second term from the equivoluminal potential ψ.

The integrals (2.3-15a) actually offer no computational advantages over those in (2.2-10). Neither form can be integrated explicitly and they exhibit no characteristics which make numerical computation seem useful. These remarks should be qualified for the Rayleigh modes of propagation n=0 where a wave singularity arises from the single branches and no summation is involved if only this contribution to the response is sought. Also, the equivoluminal asymptotes, $\frac{\omega_n(\kappa)}{\kappa}\to 1$ as $\kappa\to+\infty$ for n=1,2,3,..., may lend themselves to computation which would yield some wave fronts traveling with the equivoluminal body wave velocity. The frequency spectrum is well understood due to Mindlin [2] and others; however, the complexity of much

of the high-frequency portion of the spectrum is not at all conducive to integration. Hence, any advantage which can be derived from the form (2.3-15a) must be obtained by manipulation of the integrals such as deforming the contours of integration, expanding functions, etc. As will be shown later, it is by these methods that the integrals in (2.3-15a) can be evaluated for the high-frequency response for the present problem.

CHAPTER 3

THE BRANCHES $\eta=\eta_n(\chi)$

A great deal must be known about the branches $\eta=\eta_n(\chi)$ satisfying the symmetrical frequency equation (2.3-13) and the asymmetrical frequency equation (2.3-14) before the integrals (2.3-15a) can be evaluated even in an approximate sense. In this chapter, existence of the branches on the real χ-axis and on the unit circle $|\chi|=1$ is shown and properties of these brances which may be useful in evaluating the integrals (2.3-15a) are developed.

The branches which map into the real ω, real κ- or the real ω, imaginary κ-plane by (2.3-7) were completely explained by Mindlin [2] and that work is repeated here only to show how these branches map into the χ,η-space. The branches on which ω is real and κ is complex (κ being neither pure real nor pure imaginary) map into the χ,η-space with both χ and η complex and are not convenient to examine in these variables. Other than for these real ω, complex κ branches, this chapter is a limited extension of Mindlin's work in that branches are considered on which both ω and κ are complex.

The function $R(\chi)$ defined by (2.3-12a) is obviously important in determining the properties of the branches η. $R(\chi)$ is treated in Appendix A and the results contained

there will be referred to throughout this chapter. Also, Figs. 4, 5 and 6 refer to $R(\chi)$. Fig. 4 shows some special points where $R=0$ or $[R]^{-1}=0$, Fig. 5 shows a sketch of R and of $[R]^{-1}$ on $-1\leq\chi\leq 1$ and Fig. 6 shows a sketch of $\gamma(\theta)=\text{Arg}R(e^{i\theta})$ on $\chi=e^{i\theta}$, $0\leq\theta\leq\pi$.

Appendix B supplements Section 3.2 and Appendix C pertains to the analytic continuations of the branches, which are discussed in Section 3.4.

3.1. ANALYTICITY OF THE BRANCHES

Perhaps the most important property of the branches is that they are analytic functions of the complex variable χ except at certain singular points in the χ-plane. Thus, the powerful tools of analytic continuation and the Cauchy-Goursat theorem for integration in the complex χ-plane are available for use on the modal solution integrals (2.3-15a). If a branch can be identified and understood on a subregion such as a segment of the real χ-axis or of the unit circle $|\chi|=1$, then the branch can be continued into any part of the χ-plane where it is known to be analytic. Analyticity of the branches is shown and an investigation of the singular points is given in this section.

3.1.1. Proof of Analyticity and the Criteria for Singular Points of the Branches.

The frequency equations, (2.3-13) and (2.3-14), can be written in the form

$$F(\chi,\eta) = 0 \tag{3.1-1}$$

where F is analytic with respect to both χ and η except at a few isolated subregions of the χ,η-space. For example, $F(\chi,\eta)$ can be taken as one of the Rayleigh-Lamb functions defined in (2.3-12), which are analytic functions of χ and η except at $\eta=\infty$ and at $\chi=\infty$. Hence, the derivative of η with respect to χ exists and is given by

$$\frac{d\eta}{d\chi} = -\frac{\frac{\partial F}{\partial \chi}}{\frac{\partial F}{\partial \eta}} \tag{3.1-2}$$

and, by definition, η is an analytic function of χ in any domain where $F(\chi,\eta)$ is analytic and where $\frac{\partial F}{\partial \eta}\neq 0$. The derivative (3.1-2) is written explicitly as

$$\frac{d\eta}{d\chi} = -\frac{\eta R\cos\chi\eta + R'\sin\chi\eta}{\cos\eta + \chi R\cos\chi\eta} \tag{3.1-3}$$

for the branches satisfying the symmetrical frequency equation (2.3-13) and as

$$\frac{d\eta}{d\chi} = \frac{\eta R\cos\chi\eta + R'\sin\chi\eta}{\cos\eta - \chi R\cos\chi\eta} \tag{3.1-4}$$

for the branches satisfying the asymmetrical frequency equation (2.3-14) where $R'=\frac{dR}{d\chi}$ in each case.

Singular points where the branches are not analytic because the derivatives (3.1-3) or (3.1-4) fail to exist may occur at any point where

$$\left.\begin{array}{ll} (1) & R \to \infty \quad , \\ (2) & \eta \to \infty \quad , \\ (3) & \cos\eta \pm \chi R\cos\chi\eta = 0 \quad . \end{array}\right\} \qquad (3.1\text{-}5)$$

The first case only occurs at $\chi=0$ and $\chi=\chi_R$ in $|\chi|\leq 1$ as can be seen from Appendix A and the second case will be found to occur only at a few isolated points. In fact, it can be shown directly from the frequency equations and the properties of $R(\chi)$ given in Appendix A that the branches η are always bounded on $|\chi|\leq 1$ except possibly on the real χ-axis. This is done by assuming that $\eta\to\infty$ and showing that both sides of the frequency equations cannot be balanced regardless of the manner in which η becomes unbounded as long as χ is not real. The cases on the real χ-axis where $\eta\to\infty$ will be considered in a later section. The third case in (3.1-5) occurs at many isolated points in the χ-plane which will be shown to be branch points common to pairs of branches.

A useful property of the branches is that they are also analytic with respect to Poisson's ratio ν as can be

seen by extending the foregoing argument. $R(\chi)=R(\chi,\nu)$ in (2.3-12a) is analytic with respect to both χ and ν except at isolated poles. Hence, the frequency equations can be written as in (3.1-1) with F also analytic with respect to ν. This property makes it possible to observe the branches as ν varies and to reach conclusions about $\eta=\eta_n(\chi)$ for ν fixed.

The third case of (3.1-5) is now considered in more detail. If this case is satisfied for the symmetrical branches, then some pairs χ,η (these are not yet known to be isolated points in the χ,η-space) must simultaneously satisfy

$$\left.\begin{aligned} \sin\eta &= -R\sin\chi\eta \quad , \\ \cos\eta &= -\chi R\cos\chi\eta \quad , \end{aligned}\right\} \qquad (3.1\text{-}6)$$

the first of these relations being the symmetrical frequency equation (2.3-13). Simultaneous satisfaction of these two equations is equivalent to requiring η to satisfy

$$\left.\begin{aligned} \eta &= k\pi \pm (-1)^k \sin^{-1}(\Gamma) \quad , \\ \eta &= \frac{j\pi}{\chi} \pm \frac{(-1)^k}{\chi}\sin^{-1}\left(\frac{1}{R}\Gamma\right) \end{aligned}\right\} \qquad (3.1\text{-}7)$$

simultaneously where

$$\Gamma = \Gamma(\chi) = \left(\frac{1-\chi^2 R^2}{1-\chi^2}\right)^{\frac{1}{2}} \quad . \qquad (3.1\text{-}7a)$$

j and k are arbitrary integers except that j+k must be odd. The choice of the ± signs must be consistent for both equations. The pair (3.1-7) is derived by squaring both equations in (3.1-6) and adding to give the second equation in (3.1-7) and by squaring both, multiplying the first by χ^2, and adding to give the first of (3.1-7). Requiring that j+k be odd insures that (3.1-7) are equivalent to (3.1-6). This is seen by taking η from the first of (3.1-7) for the left side of each of (3.1-6) and $\chi\eta$ from the second of (3.1-7) for the right side of each of (3.1-6). Then it is seen that $(-1)^{j+k}=-1$ is required to make (3.1-6) and (3.1-7) equivalent.

Γ is a single-valued, analytic function of χ in a cut χ-plane (meaning that the branch points resulting from the radical in (3.1-7a) are located and connected by branch cuts in such a way that Γ is single-valued on all of the χ-plane excepting the branch points and branch cuts). Γ only has branch points at $\chi=0,\infty,\chi_0$ and χ_0^* (χ_0^* is the complex conjugate of χ_0) as can be deduced from Appendix A. A branch cut can be taken on the negative imaginary χ-axis connecting $\chi=0$ and $\chi=-i\infty$ and another branch cut can connect $\chi=\chi_0$ and $\chi=\chi_0^*$ so that it is not interior to the unit

circle $|\chi|=1$. For definiteness, Γ is taken to be real and positive when $\frac{1-\chi^2R^2}{1-\chi^2}$ is real and positive. Hence, the two possible branches resulting from the radical are denoted by $\pm\Gamma$ which accounts for the $\pm$ signs in (3.1-7).

The inverse sine functions in (3.1-7) are also defined as single-valued, analytic functions of χ in a cut χ-plane and they approach zero as χ approaches zero.

The functions η defined by (3.1-7) have all of the branch points and branch cuts of Γ plus branch points at $\chi=\frac{a-1}{a+1}, \frac{a+1}{a-1}$ where $R=1$ and $\Gamma=1$, which produces square root branch points in the inverse sine functions. Also, η given by the first equation of (3.1-7) has logarithmic branch points at $\chi=\chi_R, \frac{1}{\chi_{01}}, \frac{1}{\chi_{02}}$ where $R=\infty$ and $\Gamma=\infty$ and η given by the second equation of (3.1-7) has logarithmic branch points at $\chi=\chi_{01}, \chi_{02}, \frac{1}{\chi_R}, \infty$ where $R=0$ and $\frac{1}{R}\Gamma=\infty$. Appendix A defines these points.

The multitude of combinations of $\pm,j,k$ in (3.1-7) then represents the various branches η (not to be confused with the branches $\eta=\eta_n(\chi)$ satisfying the frequency equation). A point χ where any branch η given by the first expression in (3.1-7) is common with any branch η given by the second expression is a possible singular point of some branch $\eta=\eta_n(\chi)$ of the symmetrical frequency equation. The point $\chi=-1$ is an exception for the symmetrical branches

since (3.1-7) are satisfied simultaneously at this point for some combinations of ±,j,k, but it will be shown not to be a singularity of the branches. This occurs only at $\chi=-1$ where the pair (3.1-6) reduces to the identities $\sin\eta=\sin\eta$ and $\cos\eta=\cos\eta$. These equations appear to be satisfied by any value $\eta(-1)$ and certainly (3.1-7) are satisfied simultaneously at $\chi=-1$ with the proper choice of ±,j,k. This is a special case on the symmetrical branches which is treated in B.1 of Appendix B where it is shown that the symmetrical branches are analytic at $\chi=-1$.

For the asymmetrical branches, simultaneous satisfaction of

$$\left.\begin{aligned} \sin\eta &= R\sin\chi\eta \quad , \\ \cos\eta &= \chi R\cos\chi\eta \quad , \end{aligned}\right\} \qquad (3.1\text{-}8)$$

the first being the asymmetrical frequency equation (2.3-14) and the second being the third case of (3.1-5), is analogous to the pair (3.1-6) for the symmetrical branches. This is equivalent to requiring η to satisfy (3.1-7) simultaneously with j+k even. Thus, simultaneous satisfaction of (3.1-7) locates singularities of both the symmetrical and asymmetrical branches with j+k determining the particular case.

The point $\chi=1$ is an exception for the asymmetrical branches for the same reason that $\chi=-1$ was for the

symmetrical branches. For $\chi=1$, (3.1-8) reduces to $\sin\eta=\sin\eta$ and $\cos\eta=\cos\eta$ allowing any value $\eta(1)$ as a solution and (3.1-7) are satisfied for certain choices of $\pm,j,k$. However, in B.1 of Appendix B it is shown that the asymmetrical branches are analytic at $\chi=1$.

In discussing these singular points, it is more natural to consider the zeros of the difference between the functions η defined by (3.1-7). This being done, the singular points of the branches arising from the third case of (3.1-5) are identified as zeros of the function

$$\Delta^{\pm}_{jk}(\chi) = k\pi - \frac{j\pi}{\chi} \pm (-1)^k\left[\sin^{-1}(\Gamma) - \frac{1}{\chi}\sin^{-1}\left(\frac{1}{R}\Gamma\right)\right] \qquad (3.1\text{-}9)$$

with $j+k$ odd for the symmetrical branches and $j+k$ even for the asymmetrical branches. For each fixed combination of j,k and either the plus or minus signs in (3.1-9) (again these distinguish a given branch $\Delta^{\pm}_{jk}$), $\Delta^{\pm}_{jk}$ is a single-valued, analytic function of χ in a cut χ-plane. The function $\Delta^{\pm}_{jk}$ has all of the branch points and branch cuts of the two functions η defined in (3.1-7).

The singular points of the branches $\eta=\eta_n(\chi)$, which are identified as zeros of $\Delta^{\pm}_{jk}$, are certainly isolated because the zeros of an analytic function are isolated (see Alfors [11], p. 102). Furthermore, it is obvious that if each of these zeros is identified by a pair, say

χ_c,η_c where χ_c is a zero of $\Delta^{\pm}_{jk}$ for a fixed combination $\pm,j,k$ and η_c corresponds to χ_c through either of (3.1-7) then this pair determines a point in the four-dimensional χ,η-space which is distinct from any other point corresponding to another pair χ_c',η_c' identified with a different combination $\pm,j,k$.

3.1.2. The Nature of the Singular Points.

Knowing that the singular points are isolated, it is advantageous to investigate the nature of these points before proceeding to determine their number and location. For this purpose the symmetrical branches are considered, and it is assumed that a singular point is given by the pair χ_c,η_c, which is identified with a zero of $\Delta^{\pm}_{jk}$, as in the foregoing, for a fixed combination $\pm,j,k$ with $j+k$ odd.

For the moment it is assumed that

$$\eta_c R(\chi_c)\cos\chi_c\eta_c + R'(\chi_c)\sin\chi_c\eta_c \neq 0 \qquad (3.1\text{-}10)$$

so that the derivative $\frac{d\eta}{d\chi}$ in (3.1-3) truly does not exist. Based on an argument analogous to that given for the branches $\eta=\eta_n(\chi)$, an inverse function $\chi=\chi(\eta)$ with $\chi_c=\chi(\eta_c)$ exists, which is analytic in a neighborhood of and including the point η_c in the η-plane. The derivative of this function is given by the inverse of (3.1-3) with $\frac{d\chi(\eta_c)}{d\eta}=0$

by the definition of the pair χ_c, η_c and the second derivative is

$$\frac{d^2\chi(\eta_c)}{d\eta^2} = \left.\frac{(1-\chi^2)\sin\eta}{\eta R\cos\chi\eta + R'\sin\chi\eta}\right|_{\substack{\chi=\chi_c \\ \eta=\eta_c}} . \qquad (3.1\text{-}11)$$

Hence, $\frac{d^2\chi(\eta_c)}{d\eta^2} \neq 0$ unless $\chi_c=\pm 1$ or $\sin\eta_c=0$. The points $\chi=\pm 1$ have already been seen to be exceptions and from (3.1-7) $\sin\eta_c=0$ implies that $\Gamma=0$ which only occurs at $\chi=0,\infty,\chi_0,\chi_0^*$ so that all of these are special points, which can be examined separately. Other than at these exceptional points, the local Taylor's series development of $\chi(\eta)$ about η_c is

$$\chi(\eta) = \chi_c + \frac{1}{2}\frac{d^2\chi(\eta_c)}{d\eta^2}(\eta-\eta_c)^2 + O(|\eta-\eta_c|^3) , \qquad (3.1\text{-}12)$$

which can be inverted locally to give

$$\eta(\chi) = \eta_c + \left(\frac{2(\chi-\chi_c)}{\frac{d^2\chi(\eta_c)}{d\eta^2}}\right)^{\frac{1}{2}} + O(|\chi-\chi_c|) . \qquad (3.1\text{-}13)$$

This behavior of $\eta(\chi)$ near $\chi=\chi_c$ shows clearly the nature of the singularity at this point, and it is a square root branch point with the function $\eta(\chi)$ being

double-valued. Thus, χ_c is a branch point common to two branches, say $\eta_n(\chi)$ and $\eta_{n'}(\chi)$, which are defined locally by (3.1-13) if they are identified with the two branches of the radical defined to be single-valued in the χ-plane with a branch cut emanating from χ_c.

The case where (3.1-10) does not hold and $\frac{d\eta}{d\chi}$ in (3.1-3) takes the $\frac{0}{0}$ indeterminant form at $\chi=\chi_c$ is now considered. This gives another relation, in addition to the two in (3.1-6), since the numerator of $\frac{d\eta}{d\chi}$ also vanishes and these three conditions can be shown to cause $\Delta^{\pm}_{jk}$ and $\frac{d\Delta^{\pm}_{jk}}{d\chi}$ to vanish at $\chi=\chi_c$. Hence, if $\frac{d\eta}{d\chi}$ takes the $\frac{0}{0}$ form, χ_c is a zero of order higher than one of $\Delta^{\pm}_{jk}$. This can also be interpreted as a point of tangency between the functions η defined by (3.1-7). Such a case is like the end result of a merging of two or more zeros of $\Delta^{\pm}_{jk}$ to the single point χ_c. For all of the points satisfying this situation, other than some of the exceptional points already mentioned, this merging can be made to occur by varying Poisson's ratio ν. If this involves the merging of only two branch points, as will be shown later to be the case, and if they are common to the same pair of branches, say $\eta_n(\chi)$ and $\eta_{n'}(\chi)$, then the branch points merge to cancel each other and the branches become analytic at the point χ_c. A simple example illustrating this local

behavior of two merging branch points is given by the double-valued function $(\chi^2-\varepsilon^2)^{\frac{1}{2}}$ as $\varepsilon\to 0$. This can be shown to be precisely the behavior of the branches $\eta=\eta_n(\chi)$ as ν varies when the case under discussion occurs.

It will soon become apparent that this is a very restricted case. In fact, it is precisely the case which was investigated by Onoe, McNiven and Mindlin [12] for the similar circular rod frequency equation. In that work this critical point was called a saddle point in the ω,κ,ν-space.

The asymmetrical branches have branch points which are exactly analogous to those just discussed for the symmetrical branches.

3.1.3. The Number of Branch Points and Their Location.

With the exception of the points $\chi=0$ and $\chi=\chi_0$, it can be shown that there are no branch points resulting from the third case of (3.1-5) on the segments $\frac{a-1}{a+1}<\chi\leq 1$ and $-1\leq\chi\leq 0$ or on the unit circle $\chi=e^{i\theta}$ for $0<\theta<\pi$. This is done by using the inequalities (A-5) and the form (A-6) from Appendix A and just showing that the frequency equations and the equations in the third case of (3.1-5) cannot be satisfied simultaneously on these segments. The exceptions include the $\omega=\kappa=0$ points of the Rayleigh branches

where $\chi=\chi_0=e^{i\theta_0}$ and $\eta=0$, with χ_0 given by (2.3-8), for the symmetrical Rayleigh branch and $\chi=\eta=0$ for the asymmetrical Rayleigh branch.

On the segment $0<\chi<\frac{a-1}{a+1}$, there are zeros of the functions $\Delta^{\pm}_{jk}$ in (3.1-9) and, hence, there are branch points common to pairs of branches $\eta=\eta_n(\chi)$. This is shown in Fig. 7 by indicating the intersection points of the functions η given in (3.1-7). The functions η are sketched, rather than the functions $\Delta^{\pm}_{jk}$, so that the branch points occur in the $Re\chi, Re\eta$-plane and they are actually points common to pairs of branches $\eta=\eta_n(\chi)$ which will be considered in the next section (Re and Im are used to denote the real and imaginary parts respectively of the quantities in question). Each function $\Delta^{\pm}_{jk}$ can be deduced from Fig. 7 as the difference between two of the functions η, the two being given by (3.1-7) for a fixed choice of $\pm,j,k$.

Each branch point in Fig. 7 is designated by the triplet $(\pm,j,k)$ indicating that it is a zero of $\Delta^{\pm}_{jk}$ given by (3.1-9). A given function $\Delta^{\pm}_{jk}$ has either one zero or no zeros at all on $0<\chi<\frac{a-1}{a+1}$ except possibly near $\chi=\frac{a-1}{a+1}$ where some functions $\Delta^{\pm}_{jk}$ with $\pm(-1)^k=+1$ and $j,k\geq 1$ may have two zeros. Two such zeros of $\Delta^{-}_{3,11}$ corresponding to branch points of asymmetrical branches are shown in Fig. 7 between $\eta=11\pi$ and $\eta=12\pi$ and near $\chi=\frac{a-1}{a+1}$. If a function $\Delta^{\pm}_{jk}$ does have two distinct zeros, then a slight increase in

Poisson's ratio ν causes these to merge into a double zero and then vanish completely from the real χ-axis. This is the case of branch points merging to cancel each other that was spoken of earlier. Alternatively, decreasing ν causes branch points to migrate onto the real χ-axis for $0<\chi<\frac{a-1}{a+1}$ and they apparently come from the complex χ-plane.

The point $\chi=\frac{a-1}{a+1}$ is a singular point of the function $\Delta^{\pm}_{jk}$. Specifically, it is a branch point through the inverse sine functions since $R=1$ and $\Gamma=1$ at this point; however, it is possible for this point to also be a branch point of the branches $\eta=\eta_n(\chi)$ for some integers n. This will be the case if (3.1-6) or (3.1-8) are simultaneously satisfied at $\chi=\frac{a-1}{a+1}$ or if

$$\Delta^{\pm}_{jk}\left(\frac{a-1}{a+1}\right) = k\pi - j\pi\frac{a+1}{a-1} \mp \frac{(-1)^k\pi}{a-1} = 0 \quad ,$$

where $\frac{\pi}{2}$ has been taken for the value of the inverse sine functions at this point. This equation can be solved for a to give the rational number

$$a = \frac{k+j\pm(-1)^k}{k-j} \quad ,$$

which indicates that these branch points are precisely the mapping into the χ-plane of the points on $\kappa=0$ where $\omega_n(0)=\omega_{n+1}(0)$ is possible as was discussed in Chapter 2.

These points are not singular in the ω,κ-space and they have become branch points in the χ,η-space as a result of the particular mapping (2.3-4) introduced in this work.

The question of branch points interior to the upper half unit disk ($|\chi|<1$ and $\mathrm{Im}\chi>0$) is now investigated. This is accomplished by use of the argument principle (see Alfors [11], p. 123). The argument principle is applicable since each branch, $\Delta_{jk}^{\pm}$, is analytic and single-valued interior to the upper half unit disk except for a logarithmic branch point at $\chi=\chi_{01}$ due to the fact that $R(\chi_{01})=0$ (χ_{01} is interior only if $\nu_c<\nu\leq\frac{1}{2}$ with ν_c defined following (A-3) in Appendix A). This logarithmic branch point can be excluded by a branch cut from χ_{01} to the boundary $\frac{a-1}{a+1}<\chi<1$, which avoids any of the zeros of $\Delta_{jk}^{\pm}$. The point χ_{01} is not a branch point of the branches $\eta=\eta_n(\chi)$ since neither (3.1-6) nor (3.1-8) can be satisfied simultaneously at this point.

Actually, knowledge of $\Delta_{jk}^{\pm}$ interior to the upper half unit disk, other than the property of analyticity, is not required for application of the argument principle; however $\Delta_{jk}^{\pm}$ must be known on the boundary of this region. As mentioned before, the functions $\Delta_{jk}^{\pm}$ are implicit in Fig. 7 for $0<\chi<\frac{a-1}{a+1}$. The form of $\Delta_{jk}^{\pm}$ is not complicated on the remainder of the real χ-axis. On the unit circle, $\Delta_{jk}^{\pm}$ takes a simple form due to (A-6) in Appendix A. With the form of $\Delta_{jk}^{\pm}$ known, the real and imaginary parts of $\Delta_{jk}^{\pm}$ and,

hence, the change in the argument of $\Delta^{\pm}_{jk}$ can be deduced for one traversal of the boundary in the positive direction. Once this is done for a fixed combination $\pm,j,k$, it is a simple matter to deduce the results for other combinations due to the simple dependence of $\Delta^{\pm}_{jk}$ on $\pm,j,k$ in (3.1-9).

The number of zeros of the functions $\Delta^{\pm}_{jk}(\chi)$ in (3.1-9) or, equivalently, the number of branch points of the branches $\eta=\eta_n(\chi)$, as calculated by the argument principle, is given below.

Case I: $\pm(-1)^k=+1$.

(a) The function $\Delta^{\pm}_{jk}(\chi)=k\pi-\frac{j\pi}{\chi}+\sin^{-1}(\Gamma)-\frac{1}{\chi}\sin^{-1}\left(\frac{1}{R}\Gamma\right)$ has one simple zero interior to the upper half unit disk for each pair j,k with $j=1,2,3,\ldots$ and $k=1,2,3,\ldots$ provided that

$$(j-2)\pi < k\pi < \min_{0<\chi<\frac{a-1}{a+1}}\left[\frac{j\pi}{\chi} - \sin^{-1}(\Gamma) + \frac{1}{\chi}\sin^{-1}\left(\frac{1}{R}\Gamma\right)\right]$$

(these will be called "the set of positive branch points" henceforth). The upper bound on k involves a minimum over $0<\chi<\frac{a-1}{a+1}$ of a quantity in brackets which is actually just $k\pi-\Delta^{\pm}_{jk}$. This bound is explained by saying that when it is violated the function $\Delta^{\pm}_{jk}$ has one or two zeros on $0<\chi<\frac{a-1}{a+1}$ as shown in Fig. 7. Hence, this bound on k defines the transition between branch points on the real χ-axis and

branch points in the complex χ-plane off the real axis. The bound $j-2<k$ has no obvious explanation, but it can be shown to distinguish between branch points exterior to and those interior to the unit circle $|\chi|=1$.

At these branch points the bounds

$$k\pi < \mathrm{Re}\eta < (k+1)\pi$$

on $\mathrm{Re}\eta$ result from (3.1-7) and knowledge of the range of $\sin^{-1}(\Gamma)$ on the upper half unit disk.

(b) $\Delta^{\pm}_{jk}$ has one simple zero interior to the upper half unit disk for each pair j,k with k=1,2,3,... and j=-1,-2,-3,... provided that

$$k > -(j+1)$$

(these will be called "the set of negative branch points" henceforth). Again, the bound on k has no obvious explanation, but it can be shown to distinguish between branch points exterior to and those interior to the unit circle.

The value of $\mathrm{Re}\eta$ at these branch points satisfies

$$k\pi < \mathrm{Re}\eta < (k+1)\pi$$

with the bounds explained just as in (a).

This includes all of the zeros of Case I for $k=0,1,2,\ldots$ and $j=0,\pm1,\pm2,\ldots$.

Case II: $\pm(-1)^k=-1$.

The function $\Delta^{\pm}_{jk}(\chi)=k\pi-\frac{j\pi}{\chi}-\sin^{-1}(\Gamma)+\frac{1}{\chi}\sin^{-1}\left(\frac{1}{R}\Gamma\right)$ has no zeros interior to the upper half unit disk for any pair j,k with k=0,1,2,... and j=0,±1,±2,... . A natural analytic continuation of this function into the lower half unit disk does have zeros which are complex conjugates of the zeros found in Case I.

Negative values of the integer k have not been considered since they only lead to branch points for branches with $\mathrm{Re}\eta<0$ which are simple reflections of the branches whose branch points were just considered.

In summary, all of the branch points or singularities due to the three cases in (3.1-5) have been identified for those branches with $\mathrm{Re}\eta\geq 0$ at the point with some exceptions on the real χ-axis. These exceptions will be examined when the branches $\eta=\eta_n(\chi)$ are understood in more detail.

It is interesting to examine the mapping of these branch points back into the ω,κ-space by (2.3-7). With the exception of the branch points which may occur at $\chi=\frac{a-1}{a+1}$ and map into $\kappa=0$ with $\omega\neq 0$, all branch points with the local behavior (3.1-13) give the local behavior

$$\omega = \frac{\omega_c}{\kappa_c}\kappa + O\left(|\kappa-\kappa_c|^2\right)$$

in the ω,κ-space with ω_c,κ_c (both may be complex) being

the mapping of the branch point χ_c,η_c. This is equivalent to requiring that

$$\frac{\omega_c}{\kappa_c} = \left.\frac{d\omega}{d\kappa}\right|_{\kappa=\kappa_c} ,$$

which means that the phase and group velocities defined in (2.3-1) are equal at $\kappa=\kappa_c$ in the special case where both ω_c and κ_c are real. Thus, absence of branch points of the branches $\eta=\eta_n(\chi)$ on the integration paths C in Fig. 2 and C_{0S} and C_{0A} in Fig. 3, as has been shown in all but a few exceptional cases, guarantees that the phase and group velocities are not equal on the real positive κ-axis for any of the branches $\omega=\omega_n(\kappa)$, $n=0,1,2,\ldots$.

3.2. THE BRANCHES ON THE REAL χ-AXIS AND ON THE UNIT CIRCLE $|\chi|=1$

One result of the change to the variables χ,η in Chapter 2 is that the frequency equations (2.3-13) and (2.3-14) are satisfied by simple forms of the branches $\eta=\eta_n(\chi)$ on the real χ-axis and on the unit circle $|\chi|=1$. This section contains verification of the existence and form of $\eta=\eta_n(\chi)$ on which both ω and κ are real from (2.3-7), plus other branches on these subregions. These other branches will be shown in a later section to be

analytic continuations of $\eta=\eta_n(\chi)$; however the notation $\eta_n(\chi)$ is reserved for the branches on which ω and κ are real with η_m,η_q, etc., denoting other branches.

The discussion is restricted to values of η with $Re\eta\geq 0$ since it is obvious that if η satisfies either of the frequency equations then $-\eta$ does also.

3.2.1. The Real Branches on the Real χ-Axis.

In this subsection the branches η which are real on the real χ-axis are considered and most of the results are shown in Fig. 8. Only the segment $-1\leq\chi\leq 1$ of the real χ-axis is considered since B.2 in Appendix B gives the mapping of the branches under $\chi\rightarrow\frac{1}{\chi}$.

A convenient form of the symmetrical frequency equation (2.3-13) on $\frac{a-1}{a+1}<\chi<1$ is

$$\eta = n\pi + (-1)^{n+1}\sin^{-1}[R(\chi)\sin\chi\eta] \quad , \qquad (3.2\text{-}1)$$

$n=1,2,3,\ldots$. If η is assumed to be real, the inverse sine function is defined by requiring that

$$-\frac{\pi}{2} < \sin^{-1}[R(\chi)\sin\chi\eta] < \frac{\pi}{2}$$

as can be done on this interval since $-1<R(\chi)<1$ by (A-5) in Appendix A. The form (3.2-1) does not yield explicit solutions η; however it immediately shows the existence

of the branches $\eta=\eta_n(\chi)$ and also it provides a method of finding solution points if they are required. This is seen by considering the simultaneous solution of the two parametric equations

$$\left.\begin{aligned} \eta &= n\pi + (-1)^{n+1}\sin^{-1}[R(\chi)\sin P\pi] \quad , \\ \eta &= \frac{P\pi}{\chi} \end{aligned}\right\} \qquad (3.2\text{-}2)$$

where P is a positive, constant parameter. This pair is equivalent to (3.2-1) as can be seen by setting $\chi\eta=P\pi$. As P is varied continuously, the solution points of (3.2-2) form a branch $\eta=\eta_n(\chi)$, which is a real, analytic function of χ in this interval for each n=1,2,3,... .

The bounds

$$n\pi - \sin^{-1}|R(\chi)| \le \eta_n(\chi) \le n\pi + \sin^{-1}|R(\chi)| \qquad (3.2\text{-}3)$$

result from (3.2-1) and (3.2-2) by setting $\sin\chi\eta=\pm 1$ to make $|(-1)^{n+1}\sin^{-1}[R(\chi)\sin\chi\eta]|$ a maximum. Thus, one of the equalities in (3.2-3) is taken by a branch $\eta_n(\chi)$ at a point χ only if $\eta_n(\chi)$ also satisfies $\eta_n(\chi)=\frac{(2m+1)\pi}{2\chi}$, m=0,1,2,..., so that $\sin\chi\eta_n=(-1)^m$ (or equivalently, if $P=\frac{2m+1}{2}$ in (3.2-2)) with the upper equality taken in the case where $(-1)^{m+n}R(\chi)\le 0$ and the lower equality in the case where $(-1)^{m+n}R(\chi)\ge 0$. These requirements on the sign

of $(-1)^{m+n}R(\chi)$ merely indicate whether the plus or minus sign precedes $\sin^{-1}|R(\chi)|$ in (3.2-3).

All of the results to this point apply equally well to the asymmetrical frequency equation (2.3-14) and to its branches $\eta=\eta_n(\chi)$, $n=1,2,3,\ldots$, if $R(\chi)$ is replaced by $-R(\chi)$ throughout.

Analogous to (3.2-1), on the interval $-1<\chi<\frac{a-1}{a+1}$, a convenient form of the symmetrical frequency equation is

$$\eta = \frac{m\pi}{\chi} + \frac{(-1)^{m+1}}{\chi}\sin^{-1}\left[\frac{1}{R(\chi)}\sin\eta\right] \quad , \qquad (3.2\text{-}4)$$

$m=0,\pm1,\pm2,\ldots$, where, if η is assumed to be real,

$$-\frac{\pi}{2} < \sin^{-1}\left[\frac{1}{R(\chi)}\sin\eta\right] < \frac{\pi}{2}$$

defines the inverse sine function since $-1<\frac{1}{R(\chi)}<1$ from (A-5) in Appendix A. It should be stressed that (3.2-1) and (3.2-4) are equivalent and, in turn, are both equivalent to the symmetrical frequency equation (2.3-13). The new forms are introduced only because they are open to each interpretation in the respective intervals mentioned.

The form (3.2-4) lends itself to a parametric solution just as did (3.2-2). However, the interpretation of continuing branches of the frequency equations is not so obvious because of the branch points on $0<\chi<\frac{a-1}{a+1}$, which were found in Section 3.1 and sketched in Fig. 7. These branch

points show up as vertical tangents of the functions η in Fig. 8. This only means that, if a continuous function is to be traced through solution points from the parametric solution, multiple-valued functions must be accepted. This is certainly not a difficulty and the presence of branch points does not hinder the parametric method of finding solution points which form continuous functions be they multiple- or single-valued. Further analysis will be done later to identify analytic continuations of single branches, but that is not important here.

The bounds

$$\left|\frac{m\pi}{\chi}\right| - \left|\frac{1}{\chi}\sin^{-1}\left(\frac{1}{R(\chi)}\right)\right| \leq \eta(\chi) \leq \left|\frac{m\pi}{\chi}\right| + \left|\frac{1}{\chi}\sin^{-1}\left(\frac{1}{R(\chi)}\right)\right| \tag{3.2-5}$$

result from (3.2-4) and are valid on the whole range $-1<\chi<\frac{a-1}{a+1}$. These bounds are derived just as (3.2-3) was derived from (3.2-1). One of the equalities in (3.2-5) is taken at a point χ only if η also satisfies $\eta=\frac{(2n+1)\pi}{2}$, $n=0,1,2,\ldots$, with the upper equality being taken if $\frac{(-1)^{m+n}}{\chi R(\chi)} \leq 0$ and the lower equality being taken if $\frac{(-1)^{m+n}}{\chi R(\chi)} \geq 0$. For the case $m=0$, $0\leq\eta(\chi)\leq\left|\frac{1}{\chi}\sin^{-1}\left(\frac{1}{R(\chi)}\right)\right|$ can be used as an improved bound to replace (3.2-5).

Again, all of the results for $-1<\chi<\frac{a-1}{a+1}$ apply to the asymmetrical branches if $R(\chi)$ is replaced by $-R(\chi)$.

The hyperbolas $\eta=\frac{p\pi}{1-\chi}$, $p=1,2,3,\ldots$, and $\eta=\frac{q\pi}{1+\chi}$, $q=1,2,3,\ldots$, are curves of constant α and β by (2.3-5) and they form a grid in the χ,η-plane, which can be used as an aid for sketching the real branches. This grid is precisely the mapping of Mindlin's [2] "grid of bounds," which also consists of hyperbolas, but in the ω,κ-plane.

The real η branches are sketched on the real χ-axis in Fig. 8 by using the bounds (3.2-3) and (3.2-5) and the special solution pairs from B.1 in Appendix B. The symmetrical branches are shown in heavy solid lines and the asymmetrical branches are shown in dashed lines in Fig. 8. Also, the hyperbolic grid consisting of $\eta=\frac{p\pi}{1-\chi}$ and $\eta=\frac{q\pi}{1+\chi}$ is shown in Fig. 8.

The branches, shown in Fig. 8 on $\frac{a-1}{a+1}\leq\chi\leq 1$, are denoted by η_n, $n=1,2,3,\ldots$, for both the symmetrical and asymmetrical branches and they are one-to-one mappings of the real branches $\omega_n(\kappa)$, $n=1,2,3,\ldots$, from the dilatational sector (2.3-10) of the $\mathrm{Re}\omega,\mathrm{Re}\kappa$-plane into the χ,η-plane by (2.3-4). The branches on $0<\chi\leq\frac{a-1}{a+1}$ are one-to-one mappings of the branches in the $\mathrm{Re}\omega,\mathrm{Im}\kappa$-plane, which were discussed by Mindlin [2]. The branches on $-1\leq\chi<0$ give both ω and κ pure imaginary by (2.3-7) and apparently these branches of the Rayleigh-Lamb frequency equation have not been considered before.

All of these branches will play a role in the analytic

continuation of the branches $\eta=\eta_n(\chi)$. Those with ω and κ pure imaginary seem to have no special physical significance except that they add to the overall understanding of the branches of the frequency equations.

As mentioned before, the branch points on $0<\chi\leq\frac{a-1}{a+1}$ appear in Fig. 8 as vertical tangents on the branches and they can be identified with the branch points shown in Fig. 7 by comparing the two figures. The scale of the real χ-axis in Fig. 7 is expanded five times that of Fig. 8, however, the vertical scale for real η is the same in both figures.

3.2.2. The Branches on the Unit Circle $|\chi|=1$.

In Chapter 2 it was found that the portions of the branches $\omega_n(\kappa)$, $n=1,2,3,\ldots$, and the portion of the symmetrical Rayleigh branch $\omega_0(\kappa)$ which occur in the equivoluminal sector (2.3-11) map onto the upper half unit circle $\chi=e^{i\theta}$, $0\leq\theta\leq\pi$. The definition (2.3-6) of α and β determines the particular mapping given by (2.3-4). It is sufficient to consider the upper half of the circle since simple relations in B.2 of Appendix B give the continuations onto the lower half of the circle.

In this subsection these branches $\eta=\eta_n(\chi)$ are investigated as functions of θ through $\chi=e^{i\theta}$. Also, a second set of branches are found on the upper half unit circle which

map into the ω,κ-space with both ω and κ pure imaginary. The former set of branches, which map into the usual real branches $\omega_n(\kappa)$, is shown in Fig. 9 as continuations of the real branches $\eta=\eta_n(\chi)$ on the real χ-axis (shown in Fig. 8 and discussed in Subsection 3.2.1) through the point $\chi=1$ or $\theta=0$. The latter set of branches, which map into branches with ω and κ imaginary, is shown in Fig. 10 as continuations of the real branches on the real χ-axis through the point $\chi=-1$ or $\theta=\pi$.

In B.1 of Appendix B, it is shown that all of the branches of the frequency equations which are bounded at $\chi=1$ and $\chi=-1$ are analytic at these points.

The function η satisfying either of the frequency equations, (2.3-13) or (2.3-14), is just an unknown complex function of θ on $\chi=e^{i\theta}$; hence, it is just as well to take

$$\eta(e^{i\theta}) = ye^{-i\frac{\theta}{2}} \qquad (3.2\text{-}6)$$

where y is another unknown complex function of θ. η is taken in the form (3.2-6) to simplify the frequency equations on $\chi=e^{i\theta}$.

(3.2-6) and the form (A-6) of $R(e^{i\theta})$ from Appendix A are used to write the symmetrical frequency equation (2.3-13) in the form

$$\sin\eta + R(\chi)\sin\chi\eta\Big|_{\chi=e^{i\theta}} = e^{i\frac{\gamma}{2}}\left[e^{-i\frac{\gamma}{2}}\sin\left(ye^{-i\frac{\theta}{2}}\right)\right.$$

$$\left. + e^{i\frac{\gamma}{2}}\sin\left(ye^{i\frac{\theta}{2}}\right)\right] = 2e^{i\frac{\gamma}{2}}\left[\cos\tfrac{\gamma}{2}\sin\left(y\cos\tfrac{\theta}{2}\right)\cosh\left(y\sin\tfrac{\theta}{2}\right)\right.$$

$$\left. - \sin\tfrac{\gamma}{2}\cos\left(y\cos\tfrac{\theta}{2}\right)\sinh\left(y\sin\tfrac{\theta}{2}\right)\right] = 0$$

on $\chi=e^{i\theta}$. Thus, the symmetrical frequency equation can be written as

$$\tan\left(y\cos\tfrac{\theta}{2}\right) = \tan\tfrac{\gamma}{2}\tanh\left(y\sin\tfrac{\theta}{2}\right) \qquad (3.2\text{-}7)$$

on the unit circle $\chi=e^{i\theta}$.

If (3.2-7) is written as

$$\tan\left(y\cos\tfrac{\theta}{2}\right)\coth\left(y\sin\tfrac{\theta}{2}\right) = \tan\tfrac{\gamma}{2} \quad ,$$

the right side of this equation is real since γ in (A-6a) in Appendix A is real and it is a simple matter to show that the left side is real only if y is either pure real or pure imaginary. Thus, using (3.2-6), η must take one of the forms

$$\left.\begin{aligned} &(1) \quad \eta(e^{i\theta}) = |\eta|e^{-i\frac{\theta}{2}} \quad , \\ &(2) \quad \eta(e^{i\theta}) = i|\eta|e^{-i\frac{\theta}{2}} \quad . \end{aligned}\right\} \qquad (3.2\text{-}8)$$

These forms are chosen so that $\mathrm{Re}\eta \geq 0$. As mentioned previously, $-\eta$ is also a solution if η given by either of (3.2-8) satisfies the symmetrical frequency equation.

The form (1) of η in (3.2-8) maps into ω and κ real and nonnegative by (2.3-7) by taking $\chi^{\frac{1}{2}} = e^{i\frac{\theta}{2}}$, etc., and branches of this description map into the branches $\omega_n(\kappa)$ in the equivoluminal sector (2.3-11) which were discussed in Chapter 2. Likewise, the form (2) of η in (3.2-8) maps into ω and κ both pure imaginary by (2.3-7). For reasons which will become apparent shortly, branches $\eta(e^{i\theta})$ of the form (1) in (3.2-8) are called "the equivoluminal branches" and those of the form (2) are called "the dilatational branches."

The symmetrical frequency equation, (2.3-13) or (3.2-7), takes the form

$$\tan\left(|\eta|\cos\tfrac{\theta}{2}\right) = \tan\tfrac{\gamma}{2}\tanh\left(|\eta|\sin\tfrac{\theta}{2}\right) \qquad (3.2\text{-}9)$$

for the symmetrical equivoluminal branches $\eta_n(e^{i\theta}) = |\eta_n| e^{-i\frac{\theta}{2}}$, $n=0,1,2,\ldots$, and the form

$$\cot\left(|\eta|\sin\tfrac{\theta}{2}\right) = \tan\tfrac{\gamma}{2}\coth\left(|\eta|\cos\tfrac{\theta}{2}\right) \qquad (3.2\text{-}10)$$

for the symmetrical dilatational branches $\eta_m(e^{i\theta})=i|\eta_m|e^{-i\frac{\theta}{2}}$, $m=0,1,2,\ldots$.

Just as the real branches in the preceding subsection satisfied the form (3.2-1) or (3.2-4) of the symmetrical frequency equation, the symmetrical equivoluminal branches $\eta_n(e^{i\theta})=|\eta_n|e^{-i\frac{\theta}{2}}$, $n=0,1,2,\ldots$, satisfy the form

$$|\eta_n| = \frac{n\pi}{\cos\frac{\theta}{2}} + \frac{1}{\cos\frac{\theta}{2}}\tan^{-1}\left[\tan\tfrac{\gamma}{2}\tanh\left(|\eta_n|\sin\tfrac{\theta}{2}\right)\right] \qquad (3.2\text{-}11)$$

of (3.2-9) and the symmetrical dilatational branches $\eta_m(e^{i\theta})=i|\eta_m|e^{-i\frac{\theta}{2}}$, $m=0,1,2,\ldots$, satisfy the form

$$|\eta_m| = \frac{\left(m+\frac{1}{2}\right)\pi}{\sin\frac{\theta}{2}} - \frac{1}{\sin\frac{\theta}{2}}\tan^{-1}\left[\tan\tfrac{\gamma}{2}\coth\left(|\eta_m|\cos\tfrac{\theta}{2}\right)\right] \qquad (3.2\text{-}12)$$

of (3.2-10). From knowledge of the function $\gamma=\gamma(\theta)$ defined by (A-6a) in Appendix A and sketched in Fig. 6, the ranges

$$0 \le \tan\tfrac{\gamma}{2}\tanh\left(|\eta_n|\sin\tfrac{\theta}{2}\right) \le +\infty \quad ,$$

$$0 \le \tan\tfrac{\gamma}{2}\coth\left(|\eta_m|\cos\tfrac{\theta}{2}\right) \le +\infty$$

apply on $0\le\theta\le\pi$; thus (3.2-11) and (3.2-12) are completely defined by requiring that

$$0 \leq \tan^{-1}\left[\tan\tfrac{\gamma}{2}\tanh\left(|\eta_n|\sin\tfrac{\theta}{2}\right)\right] \leq \frac{\pi}{2} \quad ,$$

$$0 \leq \tan^{-1}\left[\tan\tfrac{\gamma}{2}\coth\left(|\eta_m|\cos\tfrac{\theta}{2}\right)\right] \leq \frac{\pi}{2} \quad .$$

The forms (3.2-11) and (3.2-12) lend themselves to easy solution for $|\eta|$ by considering simultaneous solutions of equivalent parametric equations as was done in (3.2-2) for (3.2-1).

It should be indicated that the branches n=0 in (3.2-11) and m=0 in (3.2-12) can be shown, by solving for $|\eta|$ using parametric equations or otherwise, to terminate in a branch point at the point $\chi_0=e^{i\theta_0}$ given by (2.3-8). The behavior of these branches near the branch point χ_0 is given by (B.1-1) in Appendix B, and this can also be derived from either (3.2-11) or (3.2-12). The branch n=0 defined by (3.2-11) is the symmetrical Rayleigh branch and it only exists on the portion $\theta_0 \leq \theta \leq \pi$ of the upper half unit circle. Likewise, the branch m=0, defined by (3.2-12), is a continuation of the symmetrical Rayleigh branch about $\chi_0=e^{i\theta_0}$ and it exists only on the portion $0<\theta\leq\theta_0$ of the upper half unit circle. The termination of these branches in a branch point at $\theta=\theta_0$ is seen in Figs. 9 and 10.

From (3.2-11) the moduli of the symmetrical equivoluminal branches $\eta_n(e^{i\theta})=|\eta_n|e^{-i\frac{\theta}{2}}$, n=0,1,2,..., have the

bounds

$$\frac{n\pi}{\cos\frac{\theta}{2}} \leq |\eta_n| \leq \frac{\left(n+\frac{1}{2}\right)\pi}{\cos\frac{\theta}{2}} \tag{3.2-13}$$

with the upper equality occurring only at $\theta=\theta_{-1}$ where $\gamma(\theta_{-1})=\pi$ and the lower equality occurring only at $\theta=0$ (the branch n=0 does not extend to $\theta=0$). The bounds (3.2-13) result from the allowable range of the inverse tangent function in (3.2-11)

Likewise, from (3.2-12) the moduli of the dilatational branches $\eta_m(e^{i\theta})=i|\eta_m|e^{-i\frac{\theta}{2}}$, m=0,1,2,..., have the bounds

$$\frac{m\pi}{\sin\frac{\theta}{2}} \leq |\eta_m| \leq \frac{\left(m+\frac{1}{2}\right)\pi}{\sin\frac{\theta}{2}} \tag{3.2-14}$$

with the lower equality occurring only at θ_{-1} for m=1,2,3,... and the upper equality never occurring. These branches satisfy (B.1-10) in Appendix B at $\theta=\pi$ and they approach the upper equality in (3.2-14) for m large as can be seen from the asymptotic expansion for $\eta_m(-1)$ following (B.1-10).

The solution points at $\chi=1$ or $\theta=0$, $\chi=\chi_{-1}$ or $\theta=\theta_{-1}$, and $\chi=-1$ or $\theta=\pi$ are listed in B.1 in Appendix B where the

subscripts n and m refer to equivoluminal and dilatational branches respectively. These solution points can also be deduced from (3.2-11) and (3.2-12) and they make up some of the points where the bounds (3.2-13) and (3.2-14) are taken. These points are evident in Figs. 9 and 10.

It is apparent from the bounds (3.2-13) that the symmetrical equivoluminal branches n=1,2,3,... become unbounded as $\theta \to \pi$ or $\chi \to -1$ on the unit circle (the symmetrical Rayleigh branch n=0 is an exception since it is bounded at $\chi=-1$, yet it is natural to call it an equivoluminal branch in the present context). Also, from (3.2-14) the symmetrical dilatational branches are unbounded as $\theta \to 0$ or $\chi \to 1$ on the unit circle. As was mentioned in Chapter 2, the phase velocity c_p in (2.3-1) takes the value c_s, the equivoluminal body wave velocity, at $\chi=-1$ and the value c_d, the dilatational body wave velocity, at $\chi=1$. Hence, the names equivoluminal and dilatational branches have been used since these branches give the equivoluminal and dilatational phase velocities at their singular points $\chi=-1$ and $\chi=1$ respectively.

The equivoluminal branches are well known and are just the mapping of the usual real ω, real κ branches from the equivoluminal sector (2.3-11) into the χ,η-space.

The dilatational branches apparently have not been investigated because they map into the ω,κ-space with both

ω and κ pure imaginary. However, these branches are highly significant since they have an asymptote (point where $|\eta|\to\infty$) where the phase velocity takes the value of the dilatational body wave velocity in the limit. Also, they are smooth monotonic functions of θ as contrasted with the terraced portion of the frequency spectrum in the dilatational sector (2.3-10) or on $\frac{a-1}{a+1}\leq\chi\leq 1$ in Fig. 8, which is the only place that the dilatational body wave velocity is approached in the $\mathrm{Re}\omega,\mathrm{Re}\kappa$-plane. Thus, if analytic continuations can be found onto these branches, an improved representation for the dilatational waves in the plate may be possible by manipulating the integrals (2.3-15a).

The branches satisfying the asymmetrical frequency equation (2.3-14) on the upper half unit circle $\chi=e^{i\theta}$, $0\leq\theta\leq\pi$, are now considered. Just as in the symmetrical case, the asymmetrical branches must take one of the forms (3.2-8) with those of the first form called the equivoluminal branches and those of the second form called the dilatational branches. In the same manner as (3.2-9) and (3.2-10) were derived, the asymmetrical frequency equation (2.3-14) takes the form

$$\cot\left(|\eta|\cos\frac{\theta}{2}\right) = -\tan\frac{\gamma}{2}\coth\left(|\eta|\sin\frac{\theta}{2}\right) \qquad (3.2\text{-}15)$$

for the asymmetrical equivoluminal branches $\eta_n(e^{i\theta})=|\eta_n|e^{-i\frac{\theta}{2}}$, $n=1,2,3,\ldots$, and the form

$$\tan\left(|\eta|\sin\tfrac{\theta}{2}\right) = -\tan\tfrac{\gamma}{2}\tanh\left(|\eta|\cos\tfrac{\theta}{2}\right) \qquad (3.2\text{-}16)$$

for the asymmetrical dilatational branches $\eta_m(e^{i\theta})=i|\eta_m|e^{-i\frac{\theta}{2}}$, $m=1,2,3,\ldots$. Analogous to (3.2-11) and (3.2-12), (3.2-15) and (3.2-16) can be written as

$$|\eta_n| = \frac{\left(n-\frac{1}{2}\right)\pi}{\cos\frac{\theta}{2}} + \frac{1}{\cos\frac{\theta}{2}}\tan^{-1}\left[\tan\tfrac{\gamma}{2}\coth\left(|\eta_n|\sin\tfrac{\theta}{2}\right)\right], \qquad (3.2\text{-}17)$$

$n=1,2,3,\ldots$, and

$$|\eta_m| = \frac{m\pi}{\sin\frac{\theta}{2}} - \frac{1}{\sin\frac{\theta}{2}}\tan^{-1}\left[\tan\tfrac{\gamma}{2}\tanh\left(|\eta_m|\cos\tfrac{\theta}{2}\right)\right], \qquad (3.2\text{-}18)$$

$m=1,2,3,\ldots$, respectively.

The inverse tangent functions in (3.2-17) and (3.2-18) have the same ranges as those given following (3.2-12), which results in the bounds

$$\frac{\left(n-\frac{1}{2}\right)\pi}{\cos\frac{\theta}{2}} \leq |\eta_n| \leq \frac{n\pi}{\cos\frac{\theta}{2}} \quad , \qquad (3.2\text{-}19)$$

$n=1,2,3,\ldots$, for the moduli of the asymmetrical equivoluminal branches $\eta_n(e^{i\theta})=|\eta_n|e^{-i\frac{\theta}{2}}$ and the bounds

$$\frac{(m-\frac{1}{2})\pi}{\sin\frac{\theta}{2}} \leq |\eta_m| \leq \frac{m\pi}{\sin\frac{\theta}{2}} \quad , \tag{3.2-20}$$

$m=1,2,3,\ldots$, for the moduli of the asymmetrical dilatational branches $\eta_m(e^{i\theta})=i|\eta_m|e^{-i\frac{\theta}{2}}$.

The upper equality in (3.2-19) is taken only at the point θ_{-1} where $\gamma(\theta_{-1})=\pi$ and the lower equality is not taken. At $\theta=0$ or $\chi=1$, (3.2-17) takes a limiting form which is equivalent to (B.1-4) in Appendix B; hence $|\eta_n|$ in (3.2-19) approaches the lower equality at $\theta=0$ for n very large. This can be seen from the asymptotic expansion for $\eta_n(1)$ following (B.1-4).

The lower equality in (3.2-20) is taken only at the point θ_{-1} and the upper equality is taken only at the point $\theta=\pi$ or $\chi=-1$.

These asymmetrical equivoluminal and asymmetrical dilatational branches are also unbounded at $\chi=-1$ and $\chi=1$ respectively and the description of the symmetrical branches also applies here.

The point $\chi_{-1}=e^{i\theta_{-1}}$ defined by (A-1a) in Appendix A maps into the Lamé point $\omega=\sqrt{2}\kappa$ and the special solutions

(B.1-12) and (B.1-14) in Appendix B taken by the equivoluminal branches at this point are identified with the Lamé modes of harmonic wave propagation. These consist of equivoluminal waves meeting and reflecting from a boundary at an angle of 45° with no mode conversion to dilatational waves. This is expected since $R(\chi_{-1})=-1$ and R is the reflection coefficient as stated in Appendix A.

Both the symmetrical (in heavy solid lines) and the asymmetrical (in dashed lines) equivoluminal branches are sketched in Fig. 9 with the continuations through the point $\theta=0$ or $\chi=1$ onto the real branches of Fig. 8 shown at the left side. Likewise, the symmetrical (in heavy solid lines) and the asymmetrical (in dashed lines) dilatational branches are sketched in Fig. 10 with the continuations through the point $\theta=\pi$ or $\chi=-1$ onto the real branches of Fig. 8 shown at the right side. The hyperbolas $|\eta|=\frac{q\pi}{2\cos\frac{\theta}{2}}$ or $\eta=\frac{q\pi}{1+\chi}$, $q=1,2,3,\ldots$, are also shown in Fig. 9 and the hyperbolas $|\eta|=\frac{p\pi}{2\sin\frac{\theta}{2}}$ or $\eta=\frac{p\pi}{1-\chi}$, $p=1,2,3,\ldots$, are shown in Fig. 10. These branches can be calculated approximately by a few simple iterations on equations (3.2-11), (3.2-12), (3.2-17) and (3.2-18). This is done by taking $|\eta_n|=\frac{n\pi}{\cos\frac{\theta}{2}}$ as a first try in the expression of the right side of (3.2-11) to give an improved value of $|\eta_n|$, etc.

3.2.3. The Complex Branches on the Real χ-Axis.

These complex branches serve to complete the picture of the branches of the Rayleigh-Lamb frequency equations on the real χ-axis and on the unit circle $|\chi|=1$. In principle at least, analytic continuations of the branches can then be made to the interior of the unit circle and the mappings to the exterior are given by (B.2-2) and (B.2-4) in Appendix B.

Actually, a detailed description of these branches serves no other purpose than to complete the understanding of the branches so that such continuations can be made with more confidence. The method to be employed in this work for evaluating the high-frequency response of the plate does not depend on the complex branches. Hence, the complex branches are treated in B.3 of Appendix B and only a description of the branches is given here by referring to B.3 and to Figs. 11 and 12.

The complex loops in the ω,κ-space with ω real and κ complex as given by Mindlin [2] are somewhat like the branches which are described here, however, they are not the same since both ω and κ will be complex by (2.3-7) for branches with η complex (not pure imaginary) and χ real. Such complex branches must surely be analytic continuations of the real ω, complex κ branches.

$\eta_I=\text{Im}\eta$, the imaginary part of η, is determined by (B.3-3) and $\eta_R=\text{Re}\eta$, the real part of η, is determined by (B.3-4) by the method described in B.3 of Appendix B.

Fig. 11 shows the upper and lower bounds of $\eta_I=\text{Im}\eta$ given by (B.3-7) where the lower bound is the asymmetrical Rayleigh branch on $\chi_R<\chi\leq 0$ and it is a portion of the symmetrical Rayleigh branch on $-1\leq\chi<\chi_R$. The remaining portion of the symmetrical Rayleigh branch is on $\chi=e^{i\theta}$ and it is shown in Fig. 9.

A sketch of some of the complex branches is shown in Fig. 12 as a perspective in the $\text{Re}\chi,\text{Re}\eta,\text{Im}\eta$-space along with the projections onto the $\text{Re}\chi,\text{Re}\eta$- and $\text{Re}\chi,\text{Im}\eta$-planes. Only branches with $\text{Im}\eta\geq 0$ are shown, but the complex conjugates, η^*, are also branches satisfying the frequency equations. Portions of the real branches on $\chi>0$ from Fig. 8 are shown at the right of Fig. 12 to illustrate that the branch points on $0\leq\chi\leq\frac{a-1}{a+1}$ are common points of the real and complex branches. Loops between branch points occur above the level $\text{Re}\eta=5\pi$ in this figure and they become very numerous for $\text{Re}\eta$ large. All of the projections onto the $\text{Re}\chi,\text{Re}\eta$-plane up to the level included in Fig. 12 are sketched, but only a few of the projections onto the $\text{Re}\chi,\text{Im}\eta$-plane are shown since these fall on top of each other and just become confusing. Only the lowest asymmetrical complex branch (the branch with the smallest value

of $\mathrm{Re}\eta=\eta_R$) is sketched as $\chi\to-1$ where $\eta_R\to\infty$ and $\mathrm{Im}\eta=\eta_I$ oscillates more and more rapidly as shown in the projection onto the $\mathrm{Re}\chi,\mathrm{Im}\eta$-plane. All other complex branches behave in the same manner and their general form can be deduced from their projections onto the $\mathrm{Re}\chi,\mathrm{Re}\eta$-plane in Fig. 12 and by the limited variation of $\mathrm{Im}\eta=\eta_I$ allowed by its bounds. The real part of η jumps by an amount $\pm\frac{\pi}{1+\chi_R}$ as the complex branches are continued about the logarithmic branch point at $\chi=\chi_R$. This can be seen in Fig. 12 or from the asymptotic approximation (B.3-9) in Appendix B.

In general, the imaginary part of η consists of loops between the branch points on $0<\chi\leq\frac{a-1}{a+1}$ where $\mathrm{Im}\eta=0$, and the loops are tangent to the upper bound given by the second equation in (B.3-7) with the equality. The branch points on this interval are shown as points in the $\mathrm{Re}\chi,\mathrm{Re}\eta$-plane in Fig. 7. A final loop from a branch point near $\chi=0$ fails to return to the $\mathrm{Re}\chi,\mathrm{Re}\eta$-plane with $\mathrm{Im}\eta=0$ and, instead, it crosses $\chi=0$ with a value of η satisfying (B.1-7) of Appendix B if it is a symmetrical complex branch or (B.1-8) if it is an asymmetrical complex branch. On $-1\leq\chi<0$, η_I oscillates between the upper and lower bounds given by (B.3-7) and shown in Fig. 11 and becomes unbounded as $\chi\to\chi_R$. The approximation to the complex branches near $\chi=\chi_R$ is given by (B.3-9). Since η_I takes

the lower bound when $\sin^2\eta_R=\sin^2(1+\chi)\eta_R=0$ and the upper bound when $\sin^2\eta_R=1$ and $\sin^2(1+\chi)\eta_R=0$, it oscillates more and more rapidly as $\chi=-1$ is approached with the frequency of oscillation going to infinity at $\chi=-1$. As is mentioned following (B.3-8) of B.3 in Appendix B, the separation of the bounds remains finite as $\chi=-1$ is approached. The oscillation of η_I is a result of an essential singularity at $\chi=-1$ on all of the complex branches except the symmetrical Rayleigh branch, which is analytic at $\chi=-1$.

The unexpected feature of all complex branches having a singularity at $\chi=\chi_R$ seems to have little physical significance. The Rayleigh branches are unique in this respect simply because they are pure imaginary and, of course, ω and κ given by (2.3-7) are real. All other complex branches have a finite real part, η_R, as $\chi\to\chi_R$ with the imaginary part, η_I, unbounded. Then by (2.3-7), ω and κ have real parts which become unbounded just as do the Rayleigh branches, but they also have finite imaginary parts which are usually identified with a disturbance that decays in time and space and does not give rise to wave fronts. More important is the fact that analytic continuations of the Rayleigh branches are now known about the infinity point $(\omega,\kappa\to\infty)$ and the continuation goes onto other neighboring complex branches all of which are interconnected by a common logarithmic branch point at $\chi=\chi_R$.

This gives further information needed to make analytic continuations in the complex χ-plane.

With regard to analytic continuations, there is a striking similarity between the singularity of the complex branches at $\chi=-1$ and the singularity of the equivoluminal branches on $|\chi|=1$ at the same point $\chi=-1$ or $\theta=\pi$. This is seen by solving (B.3-4) in Appendix B for η_R so that it has the leading term $\frac{q\pi}{1+\chi}$, $q=1,2,3,\ldots$, and comparing this with (3.2-11) and (3.2-17). Then the dominate term of η in each case is $\frac{n\pi}{1+\chi}$ or $\frac{q\pi}{1+\chi}$ and this makes it seem likely that the complex branches continue about $\chi=-1$ onto the equivoluminal branches. A comparison of Figs. 9 and 12 also indicates this possibility.

The fact that there are no complex branches on the real χ-axis near $\chi=1$ which can be considered as analytic continuations of the dilatational branches on $|\chi|=1$ and shown in Fig. 10 poses a difficult problem which can be answered only by investigating the analytic continuations about the branch points near $\chi=1$.

3.3. SERIES REPRESENTATIONS OF THE BRANCHES η ABOUT THE POINTS $\chi=1$ AND $\chi=-1$

All of the preceding work in Section 3.2 concerning the existence and form of the branches on certain sub-regions in the χ-plane is not sufficient to allow even a

good approximate evaluation of the integrals (2.3-15). The infinite sums of integrals and the complicated relationship between η and χ present the same difficulties that were present in the integrals (2.2-10) with ω and κ as the variables.

In this section representations of the branches η as explicit functions of χ are derived in the form of a series of functions of χ. These series are derived by expanding the frequency equations about the points $\chi=1$ and $\chi=-1$, which are singular points of the dilatational and equivoluminal branches respectively of Subsection 3.2.2. The fact that $\eta\to\infty$ on these branches as $\chi\to 1,-1$ or as $\theta\to 0,\pi$ on $\chi=e^{i\theta}$ means that $\omega\to\infty$ and $\kappa\to\infty$ from (2.3-7).

These singular points are expected to be very significant with regard to their contribution to the high-frequency wave fronts in the plate. The reason for this is that $\frac{\omega}{\kappa}$ and $\frac{d\omega}{d\kappa}$ both approach 1 as $\chi\to -1$ or as $\theta\to\pi$ on the equivoluminal branches, other than on the symmetrical Rayleigh branch, and they both approach $a=\frac{c_d}{c_s}$ as $\chi\to 1$ or as $\theta\to 0$ on the dilatational branches. $\frac{\omega}{\kappa}c_s$ and $\frac{d\omega}{d\kappa}c_s$ are the phase and group velocities respectively as defined by (2.3-1) when both ω and κ are real, which is the case on the equivoluminal branches. It is recalled from Subsection 3.2.2 that both ω and κ are pure imaginary on the

dilatational branches and it remains to be seen if these branches contribute to the response of the plate.

For much the same reason as was given in Subsection 3.2.2 for using the names equivoluminal and dilatational branches, the points $\chi=-1$ and $\chi=1$ are assumed to be identified with equivoluminal and dilatational wave fronts respective.

Apparently, the only convenient series representations, such as ω as a function of κ, have been about points where both ω and κ are finite. These usually consist of Taylor's series. Obviously such representations are of very little use for high-frequency calculations where ω may become unbounded. It is true that a few terms are apparent in an asymptotic approximation as $\kappa\to\infty$ on the Rayleigh branches or on any of the other branches. For example, $\omega_0(\kappa)\sim\frac{c_R}{c_s}\kappa$ on the Rayleigh branches as $\kappa\to\infty$ and $\beta \equiv \left(\omega_n^2(\kappa)-\kappa^2\right)^{\frac{1}{2}}\sim\frac{1}{2}m\pi$ as $\kappa\to\infty$ on all other branches with $m=2n$ and $n=1,2,3,\ldots$ on the symmetrical branches and with $m=2n-1$ and $n=1,2,3,\ldots$ on the asymmetrical branches. Attempts to find more than a few succeeding terms or to find an expression for a general term in these expansions appear to be doomed to failure. The reason for this is the complicated functional relationship between ω and κ in the frequency equations (2.2-11) and (2.2-12). It seems

to be practical to seek asymptotic expansions only if the variables ω and κ are grouped into convenient functional forms such as χ and η.

The symmetrical branches η_n, which are identical to the equivoluminal branches of the form (1) of (3.2-8) when $\chi=e^{i\theta}$, will be considered first. χ will not necessarily be restricted to the unit circle $\chi=e^{i\theta}$, however, the branches considered are analytic continuations of the equivoluminal branches.

As has been the usual practice, the form (2.3-13) of the symmetrical frequency equation is altered to obtain the more convenient form

$$\tan\frac{(1+\chi)\eta}{2} = \frac{R-1}{R+1}\tan\frac{(1-\chi)\eta}{2} \quad . \tag{3.3-1}$$

This can be recognized as the original form (2.2-11) of the symmetrical frequency equation by using (2.3-5) and (2.3-12a) to return to the ω,κ variables.

Series representations are now sought for the symmetrical branches η which satisfy (3.3-1) and are singular as $\chi\to-1$ in some sector about that point. The sector must include the path $\chi=e^{i\theta}$, $0\leq\theta<\pi$, as $\theta\to\pi$ since the equivoluminal branches are on this circle. Also this sector may include the real χ-axis as $\chi\to-1$ from the right where the complex branches on the real χ-axis of Subsection 3.2.3 were found

to be singular. It was speculated there that these branches might be analytic continuations of the equivoluminal branches. The singular nature of the equivoluminal branches is shown in Fig. 9 and that of the complex branches in Fig. 12 as $\chi \to -1$ in each case.

It is convenient to examine the case $\chi = e^{i\theta}$ first, realizing that by means of analytic continuations most of the results will extend to neighboring portions of the χ-plane. η takes the form (1) of (3.2-8) and the frequency equation (3.3-1) becomes (3.2-9) on $\chi = e^{i\theta}$ where $R(e^{i\theta}) = e^{i\gamma(\theta)}$ by (A-6) in Appendix A. Further, (3.2-9) can be written as (3.2-11) which has the obvious approximation

$$\left|\eta_n(e^{i\theta})\right| \sim \left|\eta_{en}^{(0)}(e^{i\theta})\right| \qquad (3.3\text{-}2)$$

as $\theta \to \pi$ where

$$\left|\eta_{en}^{(0)}(e^{i\theta})\right| = \frac{n\pi}{\cos\frac{\theta}{2}} + \frac{\gamma(\theta)}{2\cos\frac{\theta}{2}} \quad . \qquad (3.3\text{-}2a)$$

The subscript e refers to equivoluminal branches. (3.3-2) is valid for n=1,2,3,... since $|\eta_n| \to \infty$ and $\tanh\left(|\eta_n|\sin\frac{\theta}{2}\right) \to 1$ as $\theta \to \pi$.

This result is extended to the general χ-plane by replacing $e^{i\theta}$ with χ and $\gamma(\theta)$ with $-i\mathrm{Log}R(\chi)$ and recalling

the form (1) of (3.2-8) for $\eta_n(e^{i\theta})$ and $\eta_{en}^{(0)}(e^{i\theta})$. Then

$$\eta_{en}^{(0)}(\chi) = \frac{2n\pi}{1+\chi} - i\frac{\mathrm{LogR}(\chi)}{1+\chi} \tag{3.3-3}$$

is taken for the first term in the series expansion for $\eta_n(\chi)$ as $\chi\to-1$. The term is well-defined by taking $\mathrm{LogR}(\chi)=i\gamma(\theta)$ when $\chi=e^{i\theta}$, $0\le\theta\le\pi$. The approximation $\eta_n(\chi)\sim\frac{2n\pi}{1+\chi}$ gives $\beta=\frac{1}{2}(1+\chi)\eta_n\sim n\pi$, which was mentioned as an asymptotic approximation to the symmetrical branches relating $\omega_n(\kappa)$ to κ as $\kappa\to\infty$. The second term in (3.3-3) is finite as $\chi\to-1$ with

$$\lim_{\chi\to-1}\frac{\mathrm{LogR}(\chi)}{1+\chi} = \frac{2}{1-\nu} \tag{3.3-4}$$

by (A-4) in Appendix A. The single term $\left|\eta_{en}^{(0)}(e^{i\theta})\right|$ in (3.3-2a) gives an excellent approximation to the equivoluminal branches on $\chi=e^{i\theta}$ being exact at $\theta=0,\theta_{-1}$ and as $\theta\to\pi$. θ_{-1} is defined by (A-1a) in Appendix A. The approximation is so accurate that, on the scale shown in Fig. 9, no apparent difference exists between $\left|\eta_n(e^{i\theta})\right|$ and $\left|\eta_{en}^{(0)}(e^{i\theta})\right|$ for the symmetrical branches. By comparing Figs. 6 and 9, it is seen that the fact that $\gamma(\theta_{-1})=\pi$ gives the exact solution at $\theta=\theta_{-1}$ since

$$\left|\eta_n\left(e^{i\theta_{-1}}\right)\right| = \left|\eta_{en}^{(0)}\left(e^{i\theta_{-1}}\right)\right| = \frac{\left(n+\frac{1}{2}\right)\pi}{\cos\frac{\theta_{-1}}{2}}$$

in agreement with (B.1-12) in Appendix B. Another result of this good approximation is that succeeding terms in the series representation must be very small on $\chi=e^{i\theta}$.

The one-term approximation $\eta_n(\chi)\sim\eta_{en}^{(0)}(\chi)$ given by (3.3-3) also has many of the characteristics of the complex branches on the real χ-axis of Subsection 3.2.3. This is true both as $\chi\to-1$ and near the point $\chi=\chi_R$ as can be seen by comparing (3.3-3) with (B.3-9) in Appendix B.

The question of a region or sector of convergence of the series representation is discussed at the end of this section and it is only assumed here that such a region will include the circular path $\chi=e^{i\theta}$, $0\leq\theta\leq\pi$, as $\theta\to\pi$.

For the purpose of deriving a series representation, it is convenient to define another variable, $g_n(\chi)$, replacing $\eta_n(\chi)$ by setting

$$\eta_n(\chi) = \eta_{en}^{(0)}(\chi) + \frac{2g_n(\chi)}{1+\chi} \qquad (3.3\text{-}5)$$

where $\eta_{en}^{(0)}(\chi)$ is given by (3.3-3). There is no reason to exclude the Rayleigh branch n=0, and (3.3-5) will be taken for the definition of $g_n(\chi)$ for n=0,1,2,... with $g_n(\chi)$ expected to vanish as $\chi\to-1$.

The form (3.3-1) of the symmetrical frequency equation then becomes

$$e^{-i(1-\chi)\eta_{en}^{(0)}(\chi)} = \frac{-2R\sin g_n}{(R^2+1)\sin g_n - i(R^2-1)\cos g_n} e^{2i\frac{1-\chi}{1+\chi}g_n} \qquad (3.3\text{-}6)$$

by using (3.3-5). The left side of (3.3-6) approaches zero exponentially fast as $\chi\to-1$ in $0<\mathrm{Arg}(1+\chi)<\pi$ and, since $R^2-1=O(|1+\chi|)$ as $\chi\to-1$ from (A-1), $\frac{g_n}{1+\chi}$ must also approach zero exponentially fast as $\chi\to-1$ in this sector. The Rayleigh branch n=0 is an exception with $e^{-i(1-\chi)\eta_{e0}^{(0)}(\chi)} \to e^{-\frac{4}{1-\nu}}$ as $\chi\to-1$ regardless of $\mathrm{Arg}(1+\chi)$, but this exception is of very little concern in this work.

The definitions

$$\varepsilon_n(\chi) = e^{-i(1-\chi)\eta_{en}^{(0)}(\chi)}, \qquad (3.3\text{-}7a)$$

$$F(g_n,\chi) = \frac{-2R\sin g_n}{(R^2+1)\sin g_n - i(R^2-1)\cos g_n} e^{2i\frac{1-\chi}{1+\chi}g_n}, \qquad (3.3\text{-}7b)$$

with $\eta_{en}^{(0)}(\chi)$ given by (3.3-3), reduce (3.3-6) to

$$\varepsilon_n = F(g_n,\chi) \quad . \qquad (3.3\text{-}8)$$

For the present ε_n, g_n and χ are thought of as three completely independent complex variables except that they are

related by the functional relationship (3.3-8). That is, the fact that ε_n is a function of χ by (3.3-7a) is not critical in this derivation. $F(g_n,\chi)$, defined by (3.3-7b), is an analytic function of both g_n and χ with three obvious exceptions: $g_n=\infty$, $\chi=-1$, and $\tanh g_n=i\frac{R^2-1}{R^2+1}$ with $\sinh g_n\neq 0$ in the last two cases.

The inverse of (3.3-8) must then exist in any domain of the χ,ε_n-space in which $\frac{\partial F}{\partial g_n}\neq 0$ and F is an analytic function of g_n and χ. Furthermore, the representation of the analytic function g_n can be taken as a Taylor's series in ε_n about $\varepsilon_n=0$ with the coefficients being functions of χ. Thus, a representation of the form

$$g_n = \sum_{j=1}^{\infty} g_n^{(j)}(\chi)\,\varepsilon_n^j \qquad (3.3\text{-}9)$$

which satisfies (3.3-8) will be sought. The question of the existence of an explicit inverse function has been answered by the analytic properties of the functional relationship (3.3-8) and it is left to find the coefficients $g_n^{(j)}(\chi)$ in (3.3-9).

It simplifies the algebra of finding these coefficients to consider the special case $\chi=e^{i\theta}$, $0\leq\theta\leq\pi$, and then return to the χ-plane in general. The form of $\varepsilon_n(e^{i\theta})$ is not important since it is still considered to be an

independent complex variable, however, it is listed here along with $F(g_n,e^{i\theta})$ and from (3.3-7a) and (3.3-7b) they take the forms

$$\varepsilon_n(e^{i\theta}) = e^{-(2n\pi+\gamma)\tan\frac{\theta}{2}} , \qquad (3.3\text{-}10a)$$

$$F(g_n,e^{i\theta}) = -\frac{\sin g_n}{\sin(\gamma+g_n)} e^{2g_n\tan\frac{\theta}{2}} . \qquad (3.3\text{-}10b)$$

$R(e^{i\theta})=e^{i\gamma(\theta)}$ from (A-6) has been used again. The symmetrical frequency equation (3.3-8) then becomes

$$\varepsilon_n = -\frac{\sin g_n}{\sin(\gamma+g_n)} e^{2g_n\tan\frac{\theta}{2}} ,$$

which can also be written as

$$\frac{1}{\varepsilon_n} g_n e^{2g_n\tan\frac{\theta}{2}} = -g_n \cot g_n \sin\gamma - g_n\cos\gamma . \qquad (3.3\text{-}11)$$

(3.3-11) is expanded in powers of g_n and (3.3-9) is substituted for g_n to give relationships for the coefficients $g_n^{(j)}$ by equating the coefficients of ε_n^j. The first few of these coefficients are easy to find, but it becomes increasingly more difficult as more coefficients are sought. A general recurrence relation can be

determined which gives $g_n^{(j+1)}$ in terms of $g_n^{(j)}, g_n^{(j-1)}, \ldots, g_n^{(1)}$ for j=1,2,3,..., however, the form of the general term as a function only of θ has not been found. Further work on the integrals (2.3-15a) will show that only a finite number of the terms in this series are required to represent a finite number of wave fronts in the plate; hence it is not so important to find all of the coefficients $g_n^{(j)}$. An interesting feature of these coefficients is that they are independent of the branch number n. Thus, the coefficients are denoted by $g_e^{(j)} \equiv g_n^{(j)}$ with the subscript e added to distinguish these as equivoluminal coefficients as opposed to the dilatational case, which will be considered. A few of these coefficients, derived by the procedure just described, are

$$g_e^{(1)} = -\sin\gamma \quad ,$$

$$g_e^{(2)} = \tfrac{1}{2}\sin 2\gamma - 2\sin^2\gamma\tan\tfrac{\theta}{2} \quad ,$$

$$g_e^{(3)} = -\tfrac{1}{3}\sin 3\gamma + 3\sin\gamma\sin 2\gamma\tan\tfrac{\theta}{2} - 6\sin^3\gamma\tan^2\tfrac{\theta}{2} \quad ,$$

$$g_e^{(4)} = \tfrac{1}{4}\sin 4\gamma - 4\sin\gamma\left(\sin 3\gamma + \tfrac{1}{3}\sin^3\gamma\right)\tan\tfrac{\theta}{2}$$

$$+ 16\sin^2\gamma\sin 2\gamma\tan^2\tfrac{\theta}{2} - \tfrac{64}{3}\sin^4\gamma\tan^3\tfrac{\theta}{2} \quad . \qquad (3.3\text{-}12)$$

A pattern does emerge in the form of $g_e^{(j)}$ and it is clear that $g_e^{(j)} = O(\pi-\theta)$ as $\theta\to\pi$ for fixed j since $\gamma(\theta) = -i\text{LogR}(e^{i\theta}) = \frac{2}{1-\nu}(\pi-\theta)+O(\pi-\theta)^2$ from (A-4). Also, the first and last terms in $g_e^{(j)}$ can be written in general as $\frac{(-1)^j}{j}\sin j\gamma$ and $-\frac{(2j)^{j-1}}{j!}\sin^j\gamma\tan^{j-1}\frac{\theta}{2}$ respectively, however, the other terms become more numerous and complicated as j increases. It is true that the last term in $g_e^{(j)}$ dominates for j very large and it becomes unbounded as $j\to\infty$ for a general point θ; however this is of very little consequence in the power series (3.3-9) since the magnitude of ε_n greatly influences convergence.

The symmetrical branches on $\chi=e^{i\theta}$, $0\le\theta\le\pi$, were described in Subsection 3.2.2 by the modulus $\left|\eta_n(e^{i\theta})\right|$ where $\eta_n(e^{i\theta}) = \left|\eta_n(e^{i\theta})\right| e^{-i\frac{\theta}{2}}$ from (1) of (3.2-8) for the equivoluminal branches. Thus, from (3.3-2a), (3.3-5), (3.3-9) and (3.3-10a), the series representation for the symmetrical equivoluminal branches is

$$\left|\eta_n(e^{i\theta})\right| = \frac{1}{\cos\frac{\theta}{2}}\left[n\pi + \frac{1}{2}\gamma(\theta) + \sum_{j=1}^{\infty} g_e^{(j)} e^{-j(2n\pi+\gamma(\theta))\tan\frac{\theta}{2}}\right], \tag{3.3-13}$$

$n=0,1,2,\ldots$, where the first four coefficients $g_e^{(j)}$ are given in (3.3-12).

Before the series representations are derived for the

asymmetrical equivoluminal, symmetrical dilatational and asymmetrical dilatational branches; it is useful to write the series representation for the symmetrical equivoluminal branches $\eta_n(\chi)$ for a point χ not necessarily on the unit circle $\chi=e^{i\theta}$. From (3.3-5) and (3.3-9), this series is written as

$$\eta_n(\chi) = \eta_{en}^{(0)}(\chi) + \sum_{j=1}^{\infty} \eta_e^{(j)}(\chi) e^{-ij(1-\chi)\eta_{en}^{(0)}(\chi)} , \qquad (3.3\text{-}14)$$

$n=0,1,2,\ldots$, where $\eta_{en}^{(0)}(\chi)$ is given by (3.3-3) and $\eta_e^{(j)}(\chi) = \frac{2}{1+\chi} g_e^{(j)}(\chi)$. The form (3.3-7a) of $\varepsilon_n(\chi)$ has been used. The first four coefficients result directly from (3.3-12) by replacing $e^{i\theta}$ with χ and $e^{i\gamma}$ with $R(\chi)$ to give $g_e^{(j)}(\chi)$ and then $\eta_e^{(j)}(\chi) = \frac{2}{1+\chi} g_e^{(j)}(\chi)$. These coefficients are

$$\eta_e^{(1)}(\chi) = \frac{i}{R} \frac{R^2-1}{1+\chi} ,$$

$$\eta_e^{(2)}(\chi) = -\frac{i}{R^2} \frac{R^2-1}{1+\chi} \left[\frac{1}{2}(R^2+1) - (1-\chi) \frac{R^2-1}{1+\chi} \right] ,$$

$$\eta_e^{(3)}(\chi) = \frac{i}{R^3} \frac{R^2-1}{1+\chi} \left[\frac{1}{3}(R^4+R^2+1) - \frac{3}{2}(1-\chi)(R^2+1) \frac{R^2-1}{1+\chi} \right.$$

$$\left. + \frac{3}{2}(1-\chi)^2 \left(\frac{R^2-1}{1+\chi} \right)^2 \right] ,$$

$$\eta_e^{(4)}(\chi) = -\frac{i}{R^4}\frac{R^2-1}{1+\chi}\left[\frac{1}{4}(R^4+1)(R^2+1) - 2(1-\chi)(R^4+R^2+1)\frac{R^2-1}{1+\chi}\right.$$

$$+ \frac{1}{6}(1-\chi)(R^2-1)^2\frac{R^2-1}{1+\chi} + 4(1-\chi)^2(R^2+1)\left(\frac{R^2-1}{1+\chi}\right)^2$$

$$\left. - \frac{8}{3}(1-\chi)^3\left(\frac{R^2-1}{1+\chi}\right)^3\right] . \qquad (3.3\text{-}15)$$

The term $\frac{R^2-1}{1+\chi}$ is bounded, except at points where R is unbounded, and $\lim_{\chi\to-1}\frac{R^2-1}{1+\chi}=\frac{4}{1-\nu}$ from (A-3) and (A-4) in Appendix A.

The series representation for the asymmetrical equivoluminal branches $\eta_n(\chi)$, n=1,2,3,..., is obtained by simply replacing $R(\chi)$ with $-R(\chi)$ in all of the foregoing expressions. This is valid because the sign of $R(\chi)$ is the only difference between the frequency equations (2.2-13) and (2.2-14). In this case the Rayleigh branch n=0 is not expected to occur in the domain of interest which includes $\chi=e^{i\theta}$, $0\le\theta\le\pi$. In order to have $\mathrm{Re}\eta_n(\chi)\ge 0$ on all branches n=1,2,3,..., it is necessary to take $\mathrm{Log}(-R)=\mathrm{Log}R-i\pi$ which is equivalent to replacing n with $n-\frac{1}{2}$ in the definition (3.3-3) of $\eta_{en}^{(0)}(\chi)$. Therefore, $\gamma(\theta)$ is replaced with $\gamma(\theta)-\pi$ on $\chi=e^{i\theta}$. In summary, the series representation for the asymmetrical equivoluminal branches $\eta_n(\chi)$, n=1,2,3,..., is

$$\eta_n(\chi) = \eta^{(0)}_{en-\frac{1}{2}}(\chi) + \sum_{j=1}^{\infty}(-1)^j \eta_e^{(j)}(\chi) e^{-ij(1-\chi)\eta^{(0)}_{en-\frac{1}{2}}(\chi)} \qquad (3.3\text{-}16)$$

where $\eta^{(0)}_{en-\frac{1}{2}}(\chi)=\frac{(2n-1)}{1+\chi} - i\,\frac{\mathrm{LogR}(\chi)}{1+\chi}$ results directly from the definition (3.3-3) for $\eta^{(0)}_{en}(\chi)$, and the first four coefficients $\eta_e^{(j)}(\chi)$ are given by (3.3-15). On $\chi=e^{i\theta}$, $0\leq\theta<\pi$,

$$\left|\eta_n(e^{i\theta})\right| = \frac{1}{\cos\frac{\theta}{2}}\left[\left(n-\tfrac{1}{2}\right)\pi + \tfrac{1}{2}\gamma(\theta) + \sum_{j=1}^{\infty}(-1)^j g_e^{(j)} e^{-j\left((2n-1)\pi+\gamma(\theta)\right)\tan\frac{\theta}{2}}\right] \qquad (3.3\text{-}17)$$

with $\eta_n(e^{i\theta})=\left|\eta_n(e^{i\theta})\right| e^{-i\frac{\theta}{2}}$ from (1) of (3.2-8), and the first four coefficients $g_e^{(j)}$ are given by (3.3-12).

The symmetrical dilatational branches are now considered. The series representation of these branches can be derived in much the same way as was done for the equivoluminal branches. However, due to the unusual symmetry of the frequency equations, these representations for both the symmetrical and asymmetrical cases can be derived directly from the equivoluminal representations by simple changes of variables.

This comes about as follows for the symmetrical case: The representation (3.3-14) is an explicit function of χ and R which satisfies the symmetrical frequency equation (2.3-13). This, of course, assumes that all of the coefficients $\eta_e^{(j)}$ can be found and that the series converges to η_n in some domain. Hence, that function can be written as

$$\eta = f(\chi,R) \tag{3.3-18}$$

and it is incidental that R is a function of χ. It will be assumed for the time being that χ and R are independent complex variables and then η given by (3.3-18) satisfies the equation

$$\sin\eta = -R\sin\chi\eta \tag{3.3-19}$$

on some domain D in the χ,R-space. (3.3-19) includes the symmetrical frequency equation as the special case where $R=R(\chi)$ given by (2.3-12a). Now, if the mappings $\chi\to-\frac{1}{\chi}$ and $R\to-\frac{1}{R}$ are carried out,

$$\sin[f(\chi,R)] = -R\sin[\chi f(\chi,R)]$$

becomes

$$\sin\left[f\left(-\frac{1}{\chi},-\frac{1}{R}\right)\right] = \frac{1}{R}\sin\left[-\frac{1}{\chi}f\left(-\frac{1}{\chi},-\frac{1}{R}\right)\right] \quad ,$$

which can be written as

$$\sin\left[-\frac{1}{\chi}f\left(-\frac{1}{\chi},-\frac{1}{R}\right)\right] = -R\sin\left\{\chi\left[-\frac{1}{\chi}f\left(-\frac{1}{\chi},-\frac{1}{R}\right)\right]\right\} .$$

Thus, the function

$$\eta = -\frac{1}{\chi}f\left(-\frac{1}{\chi},-\frac{1}{R}\right) \qquad (3.3\text{-}20)$$

satisfies the same equation (3.3-19) as does $f(\chi,R)$. In this case, η given by (3.3-20) satisfies (3.3-19) on the domain D^{-1} which is the mapping of D under $\chi\rightarrow-\frac{1}{\chi}$ and $R\rightarrow-\frac{1}{R}$ in the χ,R-space. Setting $R=R(\chi)$, this means that η given by (3.3-20) is an equally good solution of the symmetrical frequency equation.

For the special case when $\chi=e^{i\theta}$, $0\leq\theta\leq\pi$, (3.3-18) for the symmetrical equivoluminal branches becomes

$$\eta(e^{i\theta}) = f(e^{i\theta},e^{i\gamma}) = e^{-i\frac{\theta}{2}}\left|f(e^{i\theta},e^{i\gamma})\right| \qquad (3.3\text{-}21)$$

where form (1) of (3.2-8) has been used. The changes indicated by (3.3-20) are applied to (3.3-21) for $f(e^{i\theta},e^{i\gamma})$, with $\chi\rightarrow-\frac{1}{\chi}$ and $R\rightarrow-\frac{1}{R}$ being equivalent to $\theta\rightarrow\pi-\theta$ and $\gamma\rightarrow\pi-\gamma$ respectively, to give new solutions

$$\eta(e^{i\theta}) = -e^{-i\theta}e^{-i\frac{\pi-\theta}{2}}\left|f\left(e^{i(\pi-\theta)},e^{i(\pi-\gamma)}\right)\right| =$$

$$ie^{-i\frac{\theta}{2}}\left|f\left(e^{i(\pi-\theta)},e^{i(\pi-\gamma)}\right)\right| \qquad (3.3\text{-}22)$$

on $\chi=e^{i\theta}$. Hence, the new set of branches obtained in this manner must be the symmetrical dilatational branches since (3.3-22) is identical with form (2) of (3.2-8).

The changes indicated by (3.3-20) are carried out on (3.3-14) where the right side of that equation is taken to be $f(\chi,R)$. Replacing n with m and using the subscript d to distinguish these as dilatational branches, this operation gives the series representation

$$\eta_m(\chi) = \eta_{dm}^{(0)}(\chi) + \sum_{k=1}^{\infty}\eta_d^{(k)}(\chi)e^{ik(1+\chi)\eta_{dm}^{(0)}(\chi)} \qquad (3.3\text{-}23)$$

for the symmetrical dilatational branches $\eta_m(\chi)$, m=0,1,2, ..., where $\eta_{dm}^{(0)}(\chi)=-\frac{1}{\chi}\left[\eta_{en}^{(0)}(\chi)\right]\Big|_{\substack{\chi\to\frac{-1}{\chi}\\ R\to-\frac{1}{R}\\ n\to m}}$ with the indicated changes applying only to $\eta_{en}^{(0)}(\chi)$ given by (3.3-3). By taking $\mathrm{Log}\left(-\frac{1}{R}\right)=i\pi-\mathrm{Log}R$, this gives

$$\eta_{dm}^{(0)}(\chi) = \frac{(2m+1)\pi}{1-\chi} + i\frac{\mathrm{Log}R(\chi)}{1-\chi} \quad . \qquad (3.3\text{-}24)$$

The coefficients $\eta_d^{(k)}(\chi)$ are obtained by performing the same operations indicated by (3.3-20) on the coefficients $\eta_e^{(j)}(\chi)$ given by (3.3-15). Thus, the first four coefficients $\eta_d^{(k)}(\chi)$ to be used in (3.3-23) are

$$\eta_d^{(1)}(\chi) = -\frac{1}{\chi}\left[-iR\frac{(1-R^2)(-\chi)}{R^2(1-\chi)}\right] = -\frac{i}{R}\frac{1-R^2}{1-\chi} \quad ,$$

$$\eta_d^{(2)}(\chi) = -\frac{i}{R^2}\frac{1-R^2}{1-\chi}\left[\frac{1}{2}(1+R^2) + (1+\chi)\frac{1-R^2}{1-\chi}\right] \quad ,$$

$$\eta_d^{(3)}(\chi) = -\frac{i}{R^3}\frac{1-R^2}{1-\chi}\left[\frac{1}{3}(1+R^2+R^4) + \frac{3}{2}(1+\chi)(1+R^2)\frac{1-R^2}{1-\chi}\right.$$

$$\left. + \frac{3}{2}(1+\chi)^2\left(\frac{1-R^2}{1-\chi}\right)^2\right] \quad ,$$

$$\eta_d^{(4)}(\chi) = -\frac{i}{R^4}\frac{1-R^2}{1-\chi}\left[\frac{1}{4}(1+R^4)(1+R^2) + 2(1+\chi)(1+R^2+R^4)\frac{1-R^2}{1-\chi}\right.$$

$$- \frac{1}{6}(1+\chi)(1-R^2)^2\frac{1-R^2}{1-\chi} + 4(1+\chi)^2(1+R^2)\left(\frac{1-R^2}{1-\chi}\right)^2$$

$$\left. + \frac{8}{3}(1+\chi)^3\left(\frac{1-R^2}{1-\chi}\right)^3\right] . \qquad (3.3\text{-}25)$$

The series for $\left|\eta_m(e^{i\theta})\right|$, the modulus of the symmetrical dilatational branches on $\chi=e^{i\theta}$, can be obtained from

(3.3-13) by simply making the changes $\theta\to\pi-\theta$ and $\gamma\to\pi-\gamma$ in that expression. This is true since the term $-\frac{1}{\chi}=-e^{-i\theta}$ multiplying f in (3.3-20) has unity modulus. Thus, since $\theta\to\pi-\theta$ implies that $\cos\frac{\theta}{2}\to\sin\frac{\theta}{2}$ and $\tan\frac{\theta}{2}\to\cot\frac{\theta}{2}$, and $\gamma\to\pi-\gamma$ implies that $\sin j\gamma\to(-1)^{j+1}\sin j\gamma$, the series representation for the symmetrical dilatational branches, $\eta_m(e^{i\theta})=i\left|\eta_m\right|e^{-i\frac{\theta}{2}}$, $m=0,1,2,\ldots$, on $\chi=e^{i\theta}$ is

$$\left|\eta_m(e^{i\theta})\right| = \frac{1}{\sin\frac{\theta}{2}}\left[\left(m+\tfrac{1}{2}\right)\pi - \tfrac{1}{2}\gamma(\theta) + \sum_{k=1}^{\infty} g_d^{(k)} e^{-k\left((2m+1)-\gamma(\theta)\right)\cot\frac{\theta}{2}}\right] \qquad (3.3\text{-}26)$$

as obtained from (3.3-13). The first four coefficients $g_d^{(k)}$ in (3.3-26) result from (3.3-12) in the same manner and they are

$$g_d^{(1)} = -\sin\gamma \ ,$$

$$g_d^{(2)} = -\tfrac{1}{2}\sin 2\gamma - 2\sin^2\gamma\cot\tfrac{\theta}{2} \ ,$$

$$g_d^{(3)} = -\tfrac{1}{3}\sin 3\gamma - 3\sin\gamma\sin 2\gamma\cot\tfrac{\theta}{2} - 6\sin^3\gamma\cot^2\tfrac{\theta}{2} \ ,$$

$$g_d^{(4)} = -\frac{1}{4}\sin 4\gamma - 4\sin\gamma\left(\sin 3\gamma+\frac{1}{3}\sin^3\gamma\right)\cot\frac{\theta}{2}$$

$$- 16\sin^2\gamma\sin 2\gamma\cot^2\frac{\theta}{2} - \frac{64}{3}\sin^4\gamma\cot^3\frac{\theta}{2} \quad . \qquad (3.3\text{-}27)$$

The series representation for the asymmetrical dilatational branches, $\eta_m(\chi)$, m=1,2,3,..., is obtained by replacing $R(\chi)$ with $-R(\chi)$ in all of the expressions for the symmetrical dilatational branches. In this case $\mathrm{Log}(-R) = \mathrm{Log}R+i\pi$ is taken so that all branches with $\mathrm{Re}\eta_m(\chi)\geq 0$ for m=1,2,3,... are included. On $\chi=e^{i\theta}$, $\gamma(\theta)$ is replaced with $\gamma(\theta)+\pi$. Thus, the series representation for the asymmetrical dilatational branches is

$$\eta_m(\chi) = \eta^{(0)}_{dm-\frac{1}{2}}(\chi) + \sum_{k=1}^{\infty}(-1)^k\eta_d^{(k)}(\chi)\,e^{ik(1+\chi)\eta^{(0)}_{dm-\frac{1}{2}}(\chi)}, \qquad (3.3\text{-}28)$$

m=1,2,3,..., with $\eta^{(0)}_{dm}(\chi)$ given by (3.3-24) and the first four coefficients $\eta_d^{(k)}(\chi)$ given by (3.3-25). Likewise, on $\chi=e^{i\theta}$, $0\leq\theta\leq\pi$,

$$\left|\eta_m(e^{i\theta})\right| = \frac{1}{\sin\frac{\theta}{2}}\left[m\pi - \frac{1}{2}\gamma(\theta)\right.$$

$$\left. + \sum_{k=1}^{\infty}(-1)^k g_d^{(k)}\,e^{-k\left(2m\pi-\gamma(\theta)\right)\cot\frac{\theta}{2}}\right] \qquad (3.3\text{-}29)$$

where $\eta_m(e^{i\theta})=i\left|\eta_m(e^{i\theta})\right|e^{-i\frac{\theta}{2}}$ by form (2) of (3.2-8) and the first four coefficients $g_d^{(k)}$ are given by (3.3-27).

The forms of the representations (3.3-23) and (3.3-28) for the symmetrical and asymmetrical dilatational branches respectively show that there is no chance of convergence on the real χ-axis. In fact, these series are complex for χ real and only real branches are possible on $\frac{a-1}{a+1}\leq\chi\leq 1$. Also, the individual terms in the series seem to increase in magnitude as k increases. This is contrasted with the representations for the equivoluminal branches which seem to converge to the complex branches on some of the interval $-1\leq\chi\leq 0$. This difference can be shown to be closely related to the distribution of branch points near the points $\chi=1,-1$.

The derivation of these representations has revealed a very significant symmetry of the branches of the Rayleigh-Lamb frequency equations. This symmetry is evident in the close relationship between the equivoluminal and dilatational branches as demonstrated by (3.3-18) and (3.3-20), and it is not necessary to derive the series representations to find this relationship. Symmetries have long been known to exist between the symmetrical and asymmetrical branches, shown in this work by replacing $R(\chi)$ with $-R(\chi)$, but the lack of any equivoluminal-dilatational symmetry has been a troublesome aspect in modal solutions. The

only part of the frequency spectrum with both ω and κ real which seems to be related to dilatational waves is a portion in the dilatational sector (2.3-10) where the branches are terraced and very dissimilar to the branches in the shear sector (2.3-11). However, this symmetry between branches with an equivoluminal singularity and those with a dilatational singularity is not really surprising. Once the dilatational branches have been identified and sketched, it is almost obvious in Figs. 9 and 10 that the equivoluminal and dilatational branches are closely related. Also, on physical grounds, there is a great similarity between the geometry and form of the dilatational and equivoluminal wave fronts, which will be found to be closely identified with the dilatational and equivoluminal branches.

Convergence of the series representations that were derived in this section can be shown on certain regions in the χ-plane by a lengthy method, which is not included here. Instead, the method is described briefly and the results are listed.

Uniform convergence of the series representations can be shown on certain regions by taking advantage of the similarity between series such as (3.3-9) and a Taylor's series in powers of ε_n. Actually, (3.3-9) is not a Taylor's series since both ε_n and the coefficients $g_n^{(j)}(\chi)$ are functions of χ.

As might be expected, the region of convergence of the series is determined by the location of the branch points and other singular points of the branches η. The region of convergence is then determined by locating the singularity "nearest" to $\varepsilon_n=0$. However, since both ε_n and $g_n^{(j)}(\chi)$ in (3.3-9) are functions of χ, the term "nearest" must be interpreted very carefully. This fact makes the problem quite difficult and too lengthy to include here.

Convergence of the series representations is only considered on $\chi=e^{i\theta}$, $0\leq\theta\leq\pi$, and on the path C_1, which is described at the end of Appendix A. These paths are good choices for possible alternate integration paths for the modal solution (2.3-15), and they are convenient to investigate due to the simple forms of $R(\chi)$ given by (A-6) and (A-8) in Appendix A.

The results for convergence are listed below.

The series (3.3-14) for the symmetrical equivoluminal branch n=0 (the symmetrical Rayleigh branch) converges uniformly with respect to $\chi=e^{i\theta}$ on any closed segment interior to $\theta_0<\theta\leq\pi$. θ_0 is defined by (2.3-8).

The series (3.3-23) for the symmetrical dilatational branch m=0 converges uniformly with respect to $\chi=e^{i\theta}$ on any closed segment interior to $0\leq\theta<\theta_0$. In B.1 of Appendix B it is shown that the symmetrical Rayleigh branch n=0 and the symmetrical dilatational branch m=0 share a branch

point at $\chi_0=e^{i\theta_0}$. This branch point determines the limit $\theta=\theta_0$ of these regions of uniform convergence.

The series (3.3-14) for the symmetrical equivoluminal branches n=1,2,3,... and the series (3.3-16) for the asymmetrical equivoluminal branches m=1,2,3,... converge uniformly with respect to $\chi=e^{i\theta}$ on any closed segment interior to $0<\theta\leq\pi$.

The series (3.3-23) for the symmetrical dilatational branches m=1,2,3,... and the series (3.3-28) for the asymmetrical dilatational branches m=1,2,3,... converge uniformly with respect to $\chi=e^{i\theta}$ on any closed segment interior to $0\leq\theta<\pi$.

None of the series representations converge on all of the path C_1, which has the endpoints $\chi=\frac{a-1}{a+1}$ and χ_{-1} given by (A-1a) in Appendix A. However, as the branch number, n for the equivoluminal branches and m for the dilatational branches, increases the series representations converge uniformly with respect to $\chi\in C_1$ on a larger and larger closed segment of C_1 which includes the endpoint χ_{-1} and approaches the endpoint $\chi=\frac{a-1}{a+1}$. A conclusion, which can be verified by investigating the branch points near $\chi=\frac{a-1}{a+1}$, is that the extent of the region of uniform convergence is determined by the location of branch points on or near C_1 which are common to the branch η in question.

This result for uniform convergence on C_1 is precisely that which is required since this work involves the high-frequency response of a plate. As such, calculations are necessary which require an approximation that improves in accuracy as the branch number and, hence, the frequency increases.

3.4. ANALYTIC CONTINUATIONS OF THE BRANCHES

The purpose of this section is to incorporate the information already derived about the branches in this chapter. Specifically, analytic continuations will be used to continue the branches η on a closed curve consisting of the boundary of the upper half unit disk ($|\chi|<1$, $\mathrm{Im}\chi>0$) with the singularities on the boundary being excluded. Also, by excluding the branch points which are interior to the half disk, the branches become single-valued, analytic functions of χ on the closed curve. The branches as a function of χ are described in Section 3.2 for all of this boundary and the branch points are described in Section 3.1. Analytic continuations about each of the particular classes of branch points and continuations about the aforementioned closed curve are described in this section. Reference is made to Appendix C where supplementary material is given for the continuations and continuations for specific branches are described.

3.4.1. Analytic Continuations About the Branch Points.

In this subsection the nature of the analytic continuations of the branches of the frequency equations about their branch points is investigated by varying Poisson's ratio ν. This causes many of the branch points to migrate onto the real χ-axis where they are much easier to understand. In this context, the nature of the analytic continuations about the branch points merely means the knowledge of which branches are common to the particular branch points. It is recalled from Subsection 3.1.2 that each branch point is common to only two branches.

An argument was given in Subsection 3.1.1 showing that the branches η are analytic functions of Poisson's ratio ν as well as being analytic functions of χ. Hence, ν is varied and the fact that the position of all the branch points, except the branch point of the asymmetrical Rayleigh branch at $\chi=0$, are functions of η makes it possible to bring many of these points into view on the real χ-axis. The analyticity of the branches η with respect to ν insures that the nature of the branches remains generally the same as ν is varied. Specifically, given branch points continue to be shared by the same two branches.

From Subsection 3.1.3 and from Figs. 7 and 8, branch points are plainly visible and easily understood on the

segment $0 \leq \chi \leq \frac{a-1}{a+1}$ of the real χ-axis. Also, from (2.1-2) giving a as a function of ν, the point

$$\frac{a-1}{a+1} = \frac{\sqrt{2(1-\nu)} - \sqrt{1-2\nu}}{\sqrt{2(1-\nu)} + \sqrt{1-2\nu}} = 3 - 4\nu - 2\sqrt{2(1-\nu)(1-2\nu)} \qquad (3.4\text{-}1)$$

is an increasing function of ν for $0 \leq \nu \leq \frac{1}{2}$. Hence, increasing η to $\frac{1}{2}$ causes $\frac{a-1}{a+1}$ to increase to 1 and the interval containing branch points on the real χ-axis becomes $0 \leq \chi \leq 1$.

The branches are sketched on the interval $0 \leq \chi \leq 1$ for $\nu = \frac{1}{2}$ in Fig. 13. The general behavior of the branches remains essentially the same on $-1 \leq \chi \leq 0$ and on $\chi = e^{i\theta}$, $0 \leq \theta \leq \pi$, for all of the range $0 \leq \nu \leq \frac{1}{2}$ with no change in the number of branch points.

The transition of the branches which occurs as ν increases toward $\frac{1}{2}$ is caused by the merging of the branch points from "the set of positive branch points" of Subsection 3.1.3 with their complex conjugates. As ν continues to increase, the complex conjugate pairs then separate and remain on $0 < \chi \leq \frac{a-1}{a+1}$. This can be visualized in Fig. 8 for various pairs of branches. For example, the symmetrical branches η_4 and η_5 approach in a maximum on η_4 and a minimum on η_5 near $\chi = \frac{a-1}{a+1}$. A slight increase in ν over the value $\nu = 0.3$ in Fig. 8 will cause branch points common to η_4 and η_5 to merge on the real χ-axis near $\chi = \frac{a-1}{a+1}$; hence,

η_4 and η_5 also merge at this point and, as described in Subsection 3.1.2, the branch points cancel and leave the branches analytic at this point. A further increase in ν will cause these branch points to separate and remain on $0<\chi\leq\frac{a-1}{a+1}$ on the real χ-axis. η_4 and η_5 will then be left connected by one of the branch points, as are the symmetrical branches η_9 and η_{10} near $\chi=\frac{a-1}{a+1}$ in Fig. 8. By this method, branch points common to η_4 and η_5 are identified as (+,1,4) from "the set of positive branch points" and as (+,2,5) which is the complex conjugate of (+,1,4) for $\nu=0.3$. The triplets (±,j,k) identify these branch points as zeros of the function $\Delta^{\pm}_{jk}$ in (3.1-9).

The transition just described has occurred for all of the branch points which are seen on $0<\chi<1$ in Fig. 13 as ν increased to $\nu=\frac{1}{2}$. These branch points are identified as the vertical tangents where $\frac{d\eta}{d\chi}=\infty$ in Fig. 13 and they are circled and labeled with the triplets (±,j,k) to identify them as zeros of the functions $\Delta^{\pm}_{jk}$ in (3.1-9).

For $\nu=\frac{1}{2}$ all of the branch points from "the set of positive branch points" have migrated onto the segment $0<\chi<1$ of the real χ-axis with the exception of an infinite subset of branch points. Before discussing this subset, the nature of the branch points which do migrate onto the real χ-axis can be described by comparing Figs. 8 and 13.

All of the branch points $(\pm,j,k)$ with $\pm(-1)^k=+1$, which migrate onto the real χ-axis as ν increases to $\nu=\frac{1}{2}$, are common to the real branches η_k and η_{k+1}. Referring to Subsection 3.1.3, $\pm(-1)^k=+1$ identifies these as branch points from "the set of positive branch points" and they are common to symmetrical branches if j+k is odd while they are common to asymmetrical branches if j+k is even.

The previously mentioned subset of branch points which remains off the real χ-axis is just "the set of positive branch points" for $\nu=\frac{1}{2}$. The identification of these branch points by the triplets $(\pm,j,k)$ depends on the definition of the functions $\Delta^{\pm}_{jk}$ from (3.1-9). This definition is made precise by specifying the branch cut to the logarithmic branch point at χ_{01} which is common to all of the functions $\Delta^{\pm}_{jk}$. χ_{01} is located as shown in Fig. 4 for $\nu=\frac{1}{2}$. In Fig. 13 for $\nu=\frac{1}{2}$ the choice of this branch cut is indicated by a vertical line at $\chi=0.6$ which represents the intersection of the real χ-axis and the branch cut to χ_{01}. This is chosen quite arbitrarily so as to avoid the lower branch points on $0<\chi<1$. This being the case, "the set of positive branch points" for $\nu=\frac{1}{2}$ which remain off the real χ-axis are identified by the triplets (-,2,1), (+,3,2), (-,2,3), (+,3,4), (-,4,5), etc., for the symmetrical branches and by (-,1,1), (+,2,2), (-,3,3), (+,4,4), (-,3,5), etc., for the asymmetrical branches.

"The set of negative branch points" of Subsection 3.1.3 does not appear on the real χ-axis for $\nu=\frac{1}{2}$. These branch points are investigated in the following by letting ν exceed $\frac{1}{2}$.

There is no physical reason to consider values of Poisson's ratio ν exceeding $\frac{1}{2}$, however, the branches are analytic functions of ν for $\nu>\frac{1}{2}$ and they can be studied for any range of ν. For $\frac{1}{2}<\nu<1$ the branches remain essentially the same as they were for $\nu=\frac{1}{2}$ with no more branch points appearing on the real χ-axis or on $|\chi|=1$. The point $\frac{a-1}{a+1}$ given by (3.4-1) does move onto $\chi=e^{i\theta}$ with $0<\theta<\pi$ causing some change in the branches.

The limiting case $\nu=1$ causes many things to happen to the branches. All of the points $\frac{a-1}{a+1}$, χ_R, χ_{01}, χ_{-1} and χ_0 and their inverses and complex conjugates have merged to $\chi=-1$ leaving $R=\frac{1}{\chi}$ from (2.3-12a). The frequency equations then become $\sin\eta=\pm\frac{1}{\chi}\sin\chi\eta$. The first obvious result is that the branches η are now even functions of χ.

The branches are sketched in Fig. 13 for $\nu=1$ on $0\leq\chi\leq1$ beside the case $\nu=\frac{1}{2}$ for comparison. The sketch is also valid for $-1\leq\chi\leq0$ by just replacing χ by $-\chi$ because the branches are even functions of χ.

A result, which is of no importance here, is that the asymmetrical Rayleigh branch $\eta_0(\chi)$ and the asymmetrical branch $\eta_1(\chi)$, which shared the branch point at $\chi=0$, have

become identically zero for $\nu=1$.

The reason for looking at the branches for $\nu=1$ is apparent from Fig. 13. The branch points on $0\leq\chi\leq 1$ for $\frac{1}{2}\leq\nu<1$ have merged together in pairs to form third order branch points with $\frac{d\chi}{d\eta}=\frac{d^2\chi}{d\eta^2}=0\neq\frac{d^3\chi}{d\eta^3}$ at the points. For example, the two symmetrical branch points (+,1,2) and (-,1,2) in Fig. 13 for $\nu=\frac{1}{2}$ have merged at $\chi=\frac{1}{2}$ and $\eta=2\pi$ for $\nu=1$, the two asymmetrical branch points (-,1,3) and (+,1,3) have merged at $\chi=\frac{1}{3}$ and $\eta=3\pi$, etc. More importantly, the situation is the same on $-1\leq\chi\leq 0$ for $\nu=1$ since the branches are even functions of χ; therefore, "the set of negative branch points" have merged with their complex conjugates on that segment of the real χ-axis.

Now all of the branch points have been located since the branches have no branch points other than those on the real χ-axis for $\nu=1$. This can be seen by setting $R=\frac{1}{\chi}$ in (3.1-7a) to give $\Gamma=0$ and $\Delta^{\pm}_{jk}=k-\frac{j\pi}{\chi}$ from (3.1-9) so that zeros of $\Delta^{\pm}_{jk}$, which are also branch points of the branches, occur only at $\chi=\frac{j}{k}$ with $\eta=k\pi$ resulting from (3.1-7). This value of η causes $\sin\eta$ to vanish in (3.1-11) to explain how $\frac{d^2\chi}{d\eta^2}=0$ comes about at the branch points.

This discussion has not explained what has happened to "the set of positive branch points" for $\nu=\frac{1}{2}$, which remained off the real χ-axis as $\nu\to\frac{1}{2}$. These branch points have

migrated toward $\chi=-1$ as $\nu\to 1$ and at $\nu=1$ they merge with their complex conjugates at $\chi=-1$ to cancel each other and leave the branches η analytic except for the branch points already discussed.

The nature of the branch points belonging to "the set of negative branch points" is not apparent even though they have migrated onto the real χ-axis for $\nu=1$. These branch points are investigated in C.1 of Appendix C where the frequency equations are approximated under the assumption that Poisson's ratio ν is slightly less than $\nu=1$.

The result of great importance which is found in C.1 is that only the complex branches with $\mathrm{Im}\eta>0$ have branch points belonging to "the set of negative branch points" and these branch points are shared with real branches on $-1<\chi<0$. The complex branches with $\mathrm{Im}\eta<0$ have no branch points from "the set of negative branch points" and, in fact, these complex branches share branch points with the real branches on $-1<\chi<0$ which are the complex conjugates of branch points from this set.

It is interesting that the form of the branch points, which occur on the real χ-axis or in complex conjugate pairs adjacent to the real χ-axis, is related to the bounds on $R(\chi)$ and $\chi R(\chi)$ given by (A-5) in Appendix A. That is, on $\frac{a-1}{a+1}<\chi<1$ where $-1<R<1$ and $-1<\chi R<1$, the branch points are

in complex conjugate pairs which are common to neighboring real branches. On $0<\chi\leq\frac{a-1}{a+1}$ where $R\geq 1$ and $-1<\chi R\leq 1$, the branch points are in pairs on the real χ-axis and they are common to complex loops and real branches. On $-1<\chi<0$ where $-1<[R]^{-1}<1$ and $-1<[\chi R]^{-1}<1$, the branch points are in complex conjugate pairs with the upper branch points ($Im\chi>0$) common to the real branches and only the complex branches with $Im\eta>0$.

Continuations about the singular points $\chi=-1$ and $\chi=1$ of the equivoluminal and dilatational branches respectively are described in C.2 of Appendix C. There it is found that the equivoluminal branches on $\chi=e^{i\theta}$, $0\leq\theta\leq\pi$, continue about $\chi=-1$ onto the complex branches with $Im\eta<0$ on $-1<\chi<0$. The complex branches with $Im\eta>0$ continue about $\chi=-1$ onto the dilatational branches on $\chi=e^{i\theta}$, $0\leq\theta\leq\pi$. This difference is a result of the nature of the branch points from "the set of negative branch points," which was just discussed.

Not surprisingly, the dilatational branches continue about $\chi=1$ onto the real branches on $\frac{a-1}{a+1}<\chi<1$ since these are the only branches on this segment of the real χ-axis.

These continuations of the equivoluminal and dilatational branches provide information about the branch points near $\chi=-1$ and $\chi=1$.

Additional information about the branch points can be gained by approximating the function $\Delta^{\pm}_{jk}$ in (3.1-9) in a

Taylor's series about $\chi=-1$ and $\chi=1$. The zeros of the approximated function $\Delta^{\pm}_{jk}$ then gives the approximate location of branch points near these points. Sets of branch points corresponding to j fixed and k large and varying are found corresponding to the triplets $(\pm,j,k)$. Obviously, these sets become infinite as $k\to+\infty$ and it is found that they have limit points at $\chi=1$. For $\pm(-1)^k=+1$ and the appropriate requirements on j and k, these branch points belong to "the set of positive branch points," which were found to be common to neighboring real branches, η_k and η_{k+1}, for k fixed and j varying. These branch points are also common to the dilatational branch η_j for j fixed and k varying.

Likewise, "the set of negative branch points," represented by $(\pm,j,k)$ with $\pm(-1)^k=+1$ and $j=-1,-2,-3,\ldots$, was found to be common to real and complex branches as described. For j fixed and k varying, the approximate location of these branch points shows that the infinite sets as $k\to\infty$ have limit points at $\chi=-1$. The abundance of these branch points near the real χ-axis as $\chi\to-1$ is reflected by the rapid oscillation of the imaginary part of η on the complex branches.

The details of the local analytic continuation about a branch point where $\frac{d\chi}{d\eta}=0$ and $\frac{d^2\chi}{d\eta^2}\neq0$, which includes all but

a few branch points, is given by (3.1-13); thus, the nature of any branch point can now be understood so that analytic continuations can proceed.

3.4.2. Analytic Continuations on a Closed Path.

A discussion of analytic continuations of a general branch of either frequency equation is given in this subsection. In C.3 of Appendix C, "the set of positive branch points" for $\nu=\frac{1}{2}$, which were not satisfactorily explained in Subsection 3.4.1, are examined by using these analytic continuations on a closed path. The conclusions of the present subsection are based on the analytic continuations of three specific branches of the frequency equations corresponding to a closed path in the χ-plane, which are described in C.4 of Appendix C.

The continuations of the branches are conformal mappings since the branches η are analytic functions of χ and they are single-valued mappings if no singular points of η are interior to or on the closed path in the χ-plane.

The paths for the analytic continuations described here and in C.4 of Appendix C consist of the boundary of the upper half unit disk ($|\chi|<1$, $\mathrm{Im}\chi>0$) taken in a counterclockwise direction with all of the branch points of the branch in question excluded by making indentions about the

points and their branch cuts. The branch cuts can be taken perpendicular to the real χ-axis for convenience.

The continuation illustrated by Figs. 14 and 15 involves the symmetrical branch η_1 at $\chi=\frac{a-1}{a+1}$, the symmetrical dilatational branch η_0 on $\chi=e^{i\theta}$, $0<\theta<\theta_0$, and the symmetrical equivoluminal branch η_0 (the symmetrical Rayleigh branch) on $\chi=e^{i\theta}$, $\theta_0<\theta\leq\pi$. This analytic continuation is explained in C.4 of Appendix C. The point $\chi_0=e^{i\theta_0}$ is defined by (2.3-8) and it is a branch point common to these two branches on $\chi=e^{i\theta}$ as is seen from (B.1-1) in Appendix B.

Similarly, Figs. 16 and 17 illustrate a continuation which involves the asymmetrical branch η_1 at $\chi=\frac{a-1}{a+1}$ and the asymmetrical dilatational branch η_1 on $\chi=e^{i\theta}$, $0<\theta\leq\pi$; and Figs. 18 and 19 illustrate a continuation which involves the symmetrical branch η_5 at $\chi=\frac{a-1}{a+1}$ and the symmetrical equivoluminal branch η_2 on $\chi=e^{i\theta}$, $0\leq\theta<\pi$. These analytic continuations are also explained in C.4 of Appendix C.

Continuations involving branches with higher branch numbers follow from the last two examples in C.4 of Appendix C with the only difference being that more branch points are involved. However, the details of continuations about individual branch points is the same.

It is noted that the continuation described by Figs. 16 and 17 is called a dilatational continuation while the

continuation described by Figs. 18 and 19 is called an equivoluminal continuation. These names for the continuations are explained as follows: If a given real branch is continued in the χ-plane, as shown in Figs. 16 and 18, so that the path circles all of the branch points from "the set of positive branch points" which are common to this continuation of the branch, then it is called a dilatational continuation if the branch continues onto a dilatational branch on $\chi=e^{i\theta}$, $0\leq\theta\leq\pi$. Likewise, it is called an equivoluminal continuation if the branch continues onto an equivoluminal branch on $\chi=e^{i\theta}$, $0\leq\theta\leq\pi$. These names are used both for continuations on closed paths, as in Figs. 16 and 18, and also for unclosed paths.

The continuation described by Figs. 14 and 15 is not designated in this manner simply because it involves both a dilatational and an equivoluminal branch on $\chi=e^{i\theta}$, $0\leq\theta\leq\pi$. However, this is the only such case since only these branches share a branch point on $\chi=e^{i\theta}$, $0<\theta<\pi$.

A point of interest is that equivoluminal continuations involve branch points from "the set of positive branch points" which have j+k constant while dilatational continuations involve those with k-j constant. This assumes that the branch points are designated by the triplets $(\pm,j,k)$ so that they are also zeros of the functions $\Delta^{\pm}_{jk}$ in (3.1-9).

In Fig. 20 the branch points from "the set of positive branch points," which are common to neighboring real branches, are shown on $\frac{a-1}{a+1}\leq\chi<1$. The branch points in Fig. 20 are designated by points on vertical lines connecting the real branches which share the branch points. Some of the points are labeled by the triplets $(\pm,j,k)$ identifying them as zeros of the functions $\Delta^{\pm}_{jk}$ in (3.1-9).

Fig. 20 serves to illustrate the equivoluminal and dilatational continuations. If continuations about the branch points, as in Figs. 16 and 18, are visualized, an equivoluminal continuation involves starting at $\chi=\frac{a-1}{a+1}$ on a real branch $\eta_n(\chi)$, such as the symmetrical branches $\eta_3,\eta_5,\eta_6,\eta_8,\ldots$ or the asymmetrical branches $\eta_2,\eta_4,\eta_5,\eta_7,\eta_8,\ldots$, and stair-stepping down a branch at every branch point encountered by continuing toward $\chi=1$ on the real χ-axis. Similarly, a dilatational continuation involves starting at $\chi=\frac{a-1}{a+1}$ on a real branch $\eta_n(\chi)$, such as the symmetrical branches $\eta_1,\eta_2,\eta_4,\eta_7,\ldots$ or the asymmetrical branches $\eta_1,\eta_3,\eta_6,\ldots$, and stair-stepping up a branch at every branch point encountered by continuing toward $\chi=1$ on the real χ-axis.

A close relationship exists between the type of continuation just described and the value of the real branch at $\chi=\frac{a-1}{a+1}$. For all but a few of the lowest branches (this

depends on the value of ν), those branches which take the values at $\chi=\frac{a-1}{a+1}$ given by the first of (B.1-5) in Appendix B or by the first of (B.1-6) lead to equivoluminal continuations. Likewise, those branches which take the values at $\chi=\frac{a-1}{a+1}$ given by the second of (B.1-5) or by the second of (B.1-6) lead to dilatational continuations.

CHAPTER 4

THE APPROXIMATE REPRESENTATION OF THE HIGH-FREQUENCY RESPONSE

The modal solution (2.3-15) can now be replaced by an equivalent representation which makes the high-frequency response much more accessible. By utilizing the analytic continuations of Section 3.4, the modal solution is found to be equivalent to integrals over the integration paths C_E and C_D in Fig. 21, and these integrals involve the equivoluminal and dilatational branches from Subsection 3.2.2 respectively. The series representations in Section 3.3 for the equivoluminal and dilatational branches are then used in these integrals to obtain approximations to the high-frequency response of the plate. The geometry of the resulting wave fronts in the plate is shown in Fig. 22 and a discussion is given relating the various wave fronts to the frequency spectrum in the χ,η-space or in the ω,κ-space.

This method requires expansions of the integrands, which are much like those used by Rosenfeld and Miklowitz [1] to obtain wave front expansions. However, relatively convenient representations of the high-frequency response are found here, which appear to be valid without the

restriction of nearness to the wave front as is required for wave front expansons.

A specific representation is further approximated near a wave front to make a comparison with an amplitude in the wave front expansion given by Rosenfeld [13].

4.1. THE MODAL SOLUTION ON THE EQUIVOLUMINAL AND DILATATIONAL BRANCHES

In this section the modal solution (2.3-15), with the exception of the Rayleigh modes n=0, is shown to be equivalent to a sum of integrals over the equivoluminal branches plus a sum of integrals over the dilatational branches of Subsection 3.2.2. This is done so as to make use of the series representations in Section 3.3 to approximate the high-frequency response of the plate. The Rayleigh modes are not included because this method offers no advantage over the usual ω,κ representation for these modes.

The integrals (2.3-15a) separate into two parts consisting of that part which results from the dilatational potential ϕ through the first term in each of the functions U in (2.3-16) and that part which results from the equivoluminal potential ψ through the second term in each of the functions U.

With some foresight about the task of identifying the wave fronts, it is helpful, and perhaps necessary, to write those parts of the integrals (2.3-15a) which result from the dilatational potential ϕ as the imaginary part of integrals of the form

$$\int_C F_\phi(\chi,\eta_n(\chi),\zeta)\sin(\omega\tau)e^{i\kappa\xi}d\chi \quad . \tag{4.1-1a}$$

Similarly, those parts of (2.3-15a) which result from the equivoluminal potential ψ are written as the imaginary part of integrals of the form

$$\int_C F_\psi(\chi,\eta_n(\chi),\zeta)\begin{bmatrix}\sin(\kappa\xi)\\ \cos(\kappa\xi)\end{bmatrix}e^{i\omega\tau}d\chi \quad . \tag{4.1-1b}$$

In both (4.1-1a) and (4.1-1b), C is the integration path shown in Fig. 2 and κ and ω are given by (2.3-7) with $\eta=\eta_n(\chi)$, n=1,2,3,... . The bracket term in (4.1-1b) just means that either $\sin(\kappa\xi)$ or $\cos(\kappa\xi)$ may occur in the integrand as in (2.3-15a). These forms are to be used to examine the response of the right half of the plate, $\xi>0$.

As was mentioned, the representation (2.3-15) is not a form which readily yields information about the wave fronts or about the high-frequency response in general. Thus, it is expected to be advantageous to write the response as a sum of integrals over the equivoluminal and

dilatational branches since these branches seem closely related to the equivoluminal and dilatational wave fronts respectively.

By using the forms (4.1-1a) and (4.1-1b), either the symmetrical or asymmetrical parts of the representation (2.3-15) can be written as the imaginary part of

$$\sum_{n=1}^{\infty}\int_{C_E}\left[F_\phi \sin(\omega\tau)e^{i\kappa\xi} + F_\psi\begin{bmatrix}\sin(\kappa\xi)\\ \cos(\kappa\xi)\end{bmatrix}e^{i\omega\tau}\right]d\chi$$

$$+ \sum_{m=0,1}^{\infty}\int_{C_D}\left[F_\phi \sin(\omega\tau)e^{i\kappa\xi} + F_\psi\begin{bmatrix}\sin(\kappa\xi)\\ \cos(\kappa\xi)\end{bmatrix}e^{i\omega\tau}\right]d\chi \qquad (4.1\text{-}2)$$

where the integration paths C_E and C_D are shown in the first sketch of Fig. 21. The justification of the equivalence of (4.1-2) and the modal solution (2.3-15) will be given shortly. On C_E, $F_\phi \equiv F_\phi(\chi,\eta_n(\chi),\zeta)$ and $F_\psi \equiv F_\psi(\chi,\eta_n(\chi),\zeta)$ where $\eta_n(\chi)$, n=1,2,3,..., are the equivoluminal branches shown in Fig. 9 or analytic continuations of these branches. On C_D, $F_\phi \equiv F_\phi(\chi,\eta_m(\chi),\zeta)$ and $F_\psi \equiv F_\psi(\chi,\eta_m(\chi),\zeta)$ where $\eta_m(\chi)$ are the dilatational branches shown in Fig. 10 or analytic continuations of these branches. The lower limit on the sum in the second term of (4.1-2) is from m=0 for the symmetrical case and from m=1 for the asymmetrical case. Again, ω and κ are given

by (2.3-7) with $\eta=\eta_n(\chi)$ being the equivoluminal branches in the first integral of (4.1-2) and $\eta=\eta_m(\chi)$ being the dilatational branches in the second integral.

The first sketch of Fig. 21 shows C_E going from $\chi=\frac{a-1}{a+1}$ to $\chi_{-1}=e^{i\theta}-1$ given by (A-1a) on the path C_1 on which $|R|=1$ as discussed in Appendix A. From χ_{-1}, C_E proceeds counterclockwise on the unit circle $|\chi|=1$ to the point $\chi=-1$. C_E is meant to be such that all of the branch points common to the particular equivoluminal branch $\eta_n(\chi)$ which belong to "the set of positive branch points" of Subsection 3.1.3 are to the right of the portion of C_E from $\chi=\frac{a-1}{a+1}$ to $\chi=\chi_{-1}$. Likewise, all of the branch points common to the particular branch which belong to "the set of negative branch points" should be to the left of this portion of C_E. If this is not possible due to the location of some of the branch points, small indentions can be made in C_E so as to leave all of these branch points on the proper side of the integration path.

The first sketch of Fig. 21 also shows the integration path C_D going from $\chi=\frac{a-1}{a+1}$ to χ_{-1} exactly as did C_E and the same comments hold for those branch points common to the particular dilatational branch $\eta_m(\chi)$. C_D then continues clockwise on the unit circle $|\chi|=1$ toward the point $\chi=1$. A small indention in C_D about $\chi=1$ must be included because

the integrals in (4.1-2) fail to exist for certain values of ξ,ζ,τ as $\theta\to 0$ on $\chi=e^{i\theta}$, $0<\theta<\pi$. This difficulty can be seen from (2.3-7), (3.2-8) and Fig. 10 showing that on the dilatational branches $\omega=i|\omega|$ and $\kappa=i|\kappa|$ with both ω and κ unbounded as $\theta\to 0$ on $\chi=e^{i\theta}$, $0<\theta<\pi$, and $\lim_{\theta\to 0}\frac{\omega}{\kappa}=a$. a is the ratio of velocities given by (2.1-2). The indention in C_D passes above all of the branch points from "the set of positive branch points" which are common to the particular dilatational branch $\eta_m(\chi)$. Yet C_D approaches $\chi=1$ tangent to the real χ-axis. This is possible since the locus of this infinite set of branch points is also tangent to the real χ-axis.

Justification of the equivalence of the representations (4.1-2) and (2.3-15) still requires considerable explanation. This is not done rigorously since it involves rearranging infinite series which are not expected to converge everywhere due to the presence of singular wave fronts. However, the representation (4.1-2) can be shown to involve precisely the same integrals over the same branches as does (2.3-15) and that is done in the following.

For each equivoluminal branch, the path C_E is deformed onto the real χ-axis and the unit circle $\chi=e^{i\theta}$, $0\leq\theta\leq\pi$. This is done as in Fig. 18 so that the deformed path goes from $\chi=\frac{a-1}{a+1}$ along the real χ-axis in a positive

direction with vertical indentions for the branch points from "the set of positive branch points" which are common to this particular equivoluminal branch. Finally, $\chi=1$ is reached and the deformed path remains on $\chi=e^{i\theta}$, $0\leq\theta\leq\pi$, to the end point $\chi=-1$.

Likewise, the integration path C_D is deformed onto the segment $\frac{a-1}{a+1}\leq\chi\leq 1$ of the real χ-axis for each dilatational branch with similar vertical indentions for the branch points common to the particular branch. Examples of these deformations of C_D are shown in Figs. 14 and 16 from $\chi=\frac{a-1}{a+1}$ to $\chi=1$.

By the Cauchy-Goursat theorem, these deformations of the integration paths C_E and C_D do not change the values of the integrals.

(4.1-2) is then equivalent to sums of integrals over all equivoluminal and dilatational continuations of the branches $\eta_n(\chi)$, $n=1,2,3,\ldots$, with the equivoluminal continuations extending from $\chi=\frac{a-1}{a+1}$ to $\chi=1$ and then to $\chi=-1$ while the dilatational continuations extend from $\chi=\frac{a-1}{a+1}$ to $\chi=1$. The equivoluminal and dilatational continuations are defined in Subsection 3.4.2 and examples are shown in Figs. 19 and 17 respectively.

(4.1-2) then involves integrals over all of the equivoluminal branches on $\chi=e^{i\theta}$, $0\leq\theta\leq\pi$, which is identical on both C in (2.3-15) and the path C_E deformed as described

for (4.1-2). This portion of the integrals is then identical in (2.3-15) and (4.1-2).

The remaining portion of (4.1-2) involves integrals over the equivoluminal and dilatational continuations of all branches $\eta_n(\chi)$, n=1,2,3,..., on $\frac{a-1}{a+1}\leq\chi\leq 1$ plus the branch line integrals around the various branch points from "the set of positive branch points." Referring to Fig. 20 and to the description of equivoluminal and dilatational continuations from $\chi=\frac{a-1}{a+1}$ to $\chi=1$ which is given in Subsection 3.4.2, it is seen that (4.1-2), with the paths C_E and C_D deformed, covers every portion of every real branch on $\frac{a-1}{a+1}\leq\chi\leq 1$. This fact along with the fact that the equivoluminal branches are covered on $\chi=e^{i\theta}$, $0\leq\theta\leq\pi$, means that the same branches have been covered in (4.1-2) as have been in (2.3-15).

Only the integrals on the indentions about the branch points adjacent to $\frac{a-1}{a+1}\leq\chi\leq 1$ as shown in Figs. 14, 16 and 18 remain. Every branch point belonging to "the set of positive branch points" is easily seen from Fig. 20 to be involved twice in these integrals--once on an equivoluminal branch and once on a dilatational branch. It is then a simple matter to show that the two branch line integrals about a particular branch point cancel each other. The integrals on the small circular paths can also be shown to cancel. Also, by making a simple expansion about the

branch points and by using (3.1-13) it is seen that $\cos\eta \pm \chi R\cos\chi\eta = O\left(\left|\chi-\chi_c\right|^{\frac{1}{2}}\right)$ near a branch point $\chi=\chi_c$. Since $(\cos\eta\pm\chi R\cos\chi\eta)^{-1}$ are the only singular terms at the branch points in the integrands of (2.3-15a), the integrals on the small circular paths give zero contribution as the paths are shrunk to the branch point.

Thus, (4.1-2) results from (2.3-15) by a rearrangement of the series representation. The representation (4.1-2) is taken as the response of the plate to the loading (2.1-7). To justify this form as a solution of the governing equations of motion (2.1-4) requires the procedure discussed at the end of Section 2.2.

4.2. THE HIGH-FREQUENCY APPROXIMATION

4.2.1. The High-Frequency Expansion of the Modal Solution.

The representation (4.1-2) is to be approximated by using the series representations for the equivoluminal and dilatational branches from Section 3.3.

Before proceeding with this approximation, it is convenient to write portions of the integrands of (4.1-2) or (2.3-15a) as sums of exponential functions. A product of the terms $\sin(\omega\tau)e^{i\kappa\xi}$ and the first terms of U in (2.3-16) and of $\begin{bmatrix}\sin(\kappa\xi)\\ \cos(\kappa\xi)\end{bmatrix}e^{i\omega\tau}$ and the second terms of U are required.

In order to write these products, the phase functions Φ_ℓ and Ψ_ℓ, $\ell=1,2,\ldots,8$, are defined as

$$\left.\begin{aligned}
\Phi_\ell(\xi,\tau,\zeta,\chi) &= \tfrac{1}{2}\xi\left[\left(\chi-\frac{a-1}{a+1}\right)\left(\frac{a+1}{a-1}-\chi\right)\right]^{\frac{1}{2}} - (-1)^\ell\frac{a}{\sqrt{a^2-1}}\tau\chi^{\frac{1}{2}} \\
&\quad + \tfrac{1}{2}(1-\chi)\zeta \pm \tfrac{1}{2}(1+\chi) \quad , \\
\Psi_\ell(\xi,\tau,\zeta,\chi) &= \frac{a}{\sqrt{a^2-1}}\tau\chi^{\frac{1}{2}} - \tfrac{1}{2}(-1)^\ell\xi\left[\left(\chi-\frac{a-1}{a+1}\right)\left(\frac{a+1}{a-1}-\chi\right)\right]^{\frac{1}{2}} \\
&\quad \pm \tfrac{1}{2}(1-\chi) + \tfrac{1}{2}(1+\chi)\zeta
\end{aligned}\right\} \quad (4.2\text{-}1)$$

where the upper sign applies for $\ell=1,2,3,4$, the lower sign applies for $\ell=5,6,7,8$ and ζ is replaced with $-\zeta$ for $\ell=3,4,7,8$. Φ_ℓ is called the dilatational phase function and Ψ_ℓ is called the equivoluminal phase function since they are to be related to the dilatational potential ϕ and the equivoluminal potential ψ respectively through (2.2-1) and (2.3-16) defining the functions U. The spatial and time dependence of the response depends strongly on Φ_ℓ and Ψ_ℓ and the geometry of the wave fronts is determined entirely by these functions since they will contain all of the dependence of the integrals on the variables ξ, τ and ζ.

The phase functions (4.2-1) are now used to write the

required products in two parts where the first and second terms in the expressions (2.3-16) for the functions U are separated to give

$$e^{i\kappa\xi}\sin(\omega\tau)\begin{bmatrix}\cos\frac{\eta(1-\chi)\zeta}{2}\sin\frac{\eta(1+\chi)}{2}\\ \sin\frac{\eta(1-\chi)\zeta}{2}\cos\frac{\eta(1+\chi)}{2}\\ i\sin\frac{\eta(1-\chi)\zeta}{2}\sin\frac{\eta(1+\chi)}{2}\\ i\cos\frac{\eta(1-\chi)\zeta}{2}\cos\frac{\eta(1+\chi)}{2}\end{bmatrix} = \frac{1}{8}\sum_{\ell=1}^{8} e^{i\eta\Phi_\ell}\begin{bmatrix}S_{1\ell}\\ S_{2\ell}\\ S_{3\ell}\\ S_{4\ell}\end{bmatrix},$$

$$e^{i\omega\tau}\begin{bmatrix}\sin(\kappa\xi)\sin\frac{\eta(1-\chi)}{2}\cos\frac{\eta(1+\chi)\zeta}{2}\\ \sin(\kappa\xi)\cos\frac{\eta(1-\chi)}{2}\sin\frac{\eta(1+\chi)\zeta}{2}\\ \cos(\kappa\xi)\sin\frac{\eta(1-\chi)}{2}\sin\frac{\eta(1+\chi)\zeta}{2}\\ \cos(\kappa\xi)\cos\frac{\eta(1-\chi)}{2}\cos\frac{\eta(1+\chi)\zeta}{2}\end{bmatrix} = \frac{1}{8}\sum_{\ell=1}^{8} e^{i\eta\Psi_\ell}\begin{bmatrix}S_{1\ell}\\ S_{2\ell}\\ (-1)^{\ell+1}S_{3\ell}\\ (-1)^{\ell+1}S_{4\ell}\end{bmatrix} \qquad (4.2\text{-}2)$$

where

$$(S_{k\ell}) = \begin{bmatrix}-1 & 1 & -1 & 1 & 1 & -1 & 1 & -1\\ -1 & 1 & 1 & -1 & -1 & 1 & 1 & -1\\ -1 & 1 & 1 & -1 & 1 & -1 & -1 & 1\\ 1 & -1 & 1 & -1 & 1 & -1 & 1 & -1\end{bmatrix}. \qquad (4.2\text{-}2a)$$

The form (4.2-2) is deduced by simply writing the trigonometric functions in their exponential forms.

The portion of the integrands in (4.1-2) or (2.3-15) which contain the branches η can be expanded by using the series representations in Section 3.3. From (2.3-15a) and (4.2-2), the only portion of the integrands which involve η is composed of the expressions $e^{i\eta\Phi_\ell}(\cos\eta\pm\chi R\cos\chi\eta)^{-1}$ and $e^{i\eta\Psi_\ell}(\cos\eta\pm\chi R\cos\chi\eta)^{-1}$. Expansions of these expressions are required for the four sets of branches: the symmetrical and asymmetrical equivoluminal branches and the symmetrical and asymmetrical dilatational branches. The expansion which exhibits the wave fronts is a power series in $e^{-2i\eta^{(0)}}$ and $e^{-i(1-\chi)\eta^{(0)}}$ for the equivoluminal branches and in $e^{2i\eta^{(0)}}$ and $e^{i(1+\chi)\eta^{(0)}}$ for the dilatational branches. $\eta^{(0)}$ is the first term in the series representation for η given by (3.3-14), (3.3-16), (3.3-23) and (3.3-28) respectively. These expansions leave the branch numbers n and m as a linear multiple in the argument of the exponential functions making it an easy matter to sum over the branch numbers. The expansions are then simple in form and the only difficulty is in calculating the coefficients in the power series.

It is necessary to write the expressions $\cos\eta\pm\chi R\cos\chi\eta$ from the denominators of the integrals in the forms

$$\cos\eta\pm\chi R\cos\chi\eta = \frac{1}{2}e^{i\eta}\left(1\pm\chi Re^{-i(1+\chi)\eta}\right)\left(1+\frac{1\pm\chi Re^{i(1+\chi)\eta}}{1\pm\chi Re^{-i(1+\chi)\eta}}e^{-2i\eta}\right) , \tag{4.2-3a}$$

$$\cos\eta\pm\chi R\cos\chi\eta = \frac{1}{2}e^{-i\eta}\left(1\pm\chi Re^{i(1-\chi)\eta}\right)\left(1+\frac{1\pm\chi Re^{-i(1-\chi)\eta}}{1\pm\chi Re^{i(1-\chi)\eta}}e^{2i\eta}\right) \tag{4.2-3b}$$

for these expansions where (4.2-3a) is to be used when η is on an equivoluminal branch and (4.2-3b) is to be used when η is on a dilatational branch.

The expansion

$$\frac{e^{i\eta_n\Phi_\ell}}{\cos\eta_n+\chi R\cos\chi\eta_n} = \frac{2}{1+\chi}\left[\sum_{p,q=0}^{p+q=3} A_{pq}e^{i\eta_{en}^{(0)}[\Phi_\ell-1-(1-\chi)p-2q]} + O\left(\left|e^{-i(1-\chi)\eta_{en}^{(0)}}\right|,\left|e^{-2i\eta_{en}^{(0)}}\right|\right)^4\right] \tag{4.2-4}$$

is for the symmetrical equivoluminal branches η_n, n=1,2,3, ..., where $\eta_{en}^{(0)}$ is given by (3.3-3) and Φ_ℓ is given by (4.2-1). The error term in (4.2-4) means that there are possible errors $O\left(\left|e^{-i\eta_{en}^{(0)}((1-\chi)p+2q)}\right|\right)$ for any combination of p and q such that p+q=4. The coefficients A_{pq} in (4.2-4) result from the series representation (3.3-14) for the symmetrical equivoluminal branches and from the form (4.2-3a). The first ten of these coefficients are

$$A_{00} = 1$$

$$A_{10} = i(\Phi_\ell - 1 + \chi)\eta_e^{(1)}$$

$$A_{01} = -\frac{1+\chi R^2}{1+\chi}$$

$$A_{20} = -\frac{1}{2}\left[\Phi_\ell^2 - 2(1-\chi)\Phi_\ell + 1 - 3\chi + \chi^2\right]\left(\eta_e^{(1)}\right)^2 + i(\Phi_\ell - 1 + \chi)\eta_e^{(2)}$$

$$A_{11} = -i\left[\frac{1+\chi R^2}{1+\chi}\Phi_\ell - (3-2\chi)\frac{1+\chi R^2}{1+\chi} + \chi R^2\right]\eta_e^{(1)}$$

$$A_{02} = \left(\frac{1+\chi R^2}{1+\chi}\right)^2$$

$$A_{30} = -\frac{i}{6}\left[\Phi_\ell^3 - 3(1-\chi)\Phi_\ell^2 + 3(1-3\chi+\chi^2)\Phi_\ell - (1-\chi)(1-6\chi+\chi^2)\right]\left(\eta_e^{(1)}\right)^3$$
$$- \left[\Phi_\ell^2 - 2(1-\chi)\Phi_\ell + 1 - 3\chi + \chi^2\right]\eta_e^{(1)}\eta_e^{(2)} + i(\Phi_\ell - 1 + \chi)\eta_e^{(3)}$$

$$A_{21} = \frac{1}{2}\left[\frac{1+\chi R^2}{1+\chi}\Phi_\ell^2 - 2\left((3-2\chi)\frac{1+\chi R^2}{1+\chi} - \chi R^2\right)\Phi_\ell + (9-14\chi+4\chi^2)\frac{1+\chi R^2}{1+\chi}\right.$$
$$\left. - 5\chi(1-\chi)R^2\right]\left(\eta_e^{(1)}\right)^2 - i\left[\frac{1+\chi R^2}{1+\chi}\Phi_\ell - (3-2\chi)\frac{1+\chi R^2}{1+\chi} + \chi R^2\right]\eta_e^{(2)}$$

$$A_{12} = i\frac{1+\chi R^2}{1+\chi}\left[\frac{1+\chi R^2}{1+\chi}\Phi_\ell + (3\chi-5)\frac{1+\chi R^2}{1+\chi} + 2\chi R^2\right]\eta_e^{(1)}$$

$$A_{03} = -\left(\frac{1+\chi R^2}{1+\chi}\right)^3 \qquad (4.2\text{-}5)$$

where the terms $\eta_e^{(j)}$ are given by (3.3-15). The same

expansion is obviously valid with Ψ_ℓ from (4.2-1) replacing Φ_ℓ throughout (4.2-4) and (4.2-5).

From (4.2-3a), (4.2-5) and (3.3-16), it is apparent that the expansion (4.2-4) is also valid for the expression $e^{i\eta_n\Phi_\ell}(\cos\eta_n-\chi R\cos\chi\eta_n)^{-1}$ where η_n, n=1,2,3,..., are the asymmetrical equivoluminal branches if the coefficients A_{pq} are replaced by $(-1)^p A_{pq}$ and $\eta^{(0)}_{en}$ is replaced by $\eta^{(0)}_{en-\frac{1}{2}}$. $\eta^{(0)}_{en-\frac{1}{2}}$ results from (3.3-3) for $\eta^{(0)}_{en}$.

The expansions involving the dilatational branches are derived in the same manner as for those involving the equivoluminal branches, however, they can also be deduced from (4.2-4) due to the similarity between (4.2-3a) and (4.2-3b). As a result of this, the expansion

$$\frac{e^{i\eta_m\Phi_\ell}}{\cos\eta_m+\chi R\cos\chi\eta_m}=\frac{2}{1-\chi}\left[\sum_{p,q=0}^{p+q=3} A_{pq}e^{i\eta^{(0)}_{dm}[\Phi_\ell+1+(1+\chi)p+2q]}+O\left(\left|e^{i(1+\chi)\eta^{(0)}_{dm}}\right|,\left|e^{2i\eta^{(0)}_{dm}}\right|\right)^4\right] \qquad (4.2\text{-}6)$$

is for the symmetrical dilatational branches $\eta_m(\chi)$, m=0,1, 2,..., where $\eta^{(0)}_{dm}$ is given by (3.3-24) and Φ_ℓ is given by (4.2-1). The coefficients A_{pq} are given by (4.2-5) with χ and Φ_ℓ replaced by $-\chi$ and $-\Phi_\ell$ respectively and with $\eta^{(j)}_e$ replaced by $-\eta^{(j)}_d$. The terms $\eta^{(k)}_d$ are given by (3.3-25).

$R=R(\chi)$ remains unchanged. Again the expansion is obviously valid with Ψ_ℓ replacing Φ_ℓ throughout.

As for the equivoluminal branches, the expansion (4.2-6) is also valid for the expression $e^{i\eta_m\Phi_\ell}(\cos\eta_m - \chi R\cos\chi\eta_m)^{-1}$ where η_m, $m=1,2,3,\ldots$, are the asymmetrical dilatational branches if the coefficients A'_{pq} are replaced by $(-1)^p A'_{pq}$ and $\eta^{(0)}_{dm}$ is replaced by $\eta^{(0)}_{dm-\frac{1}{2}}$. $\eta^{(0)}_{dm-\frac{1}{2}}$ results from (3.3-24) for $\eta^{(0)}_{dm}$.

The expansions (4.2-4) and (4.2-6) and the similar expansions for the asymmetrical branches are expected to converge uniformly with respect to χ on the same regions in the χ-plane as did the series representations in Section 3.3 for the equivoluminal and dilatational branches. This is true in part because those series representations were used to develop these expansions, but, it is also true because a geometric series was used to expand the expressions (4.2-3a) and (4.2-3b). An additional condition for convergence is then that $\left|\frac{1\pm\chi Re^{i(1+\chi)\eta}}{1\pm\chi Re^{-i(1+\chi)\eta}}e^{-2i\eta}\right|<1$ on the equivoluminal branches, and the analogous condition with χ and η replaced by their negatives as in (4.2-3b) on the dilatational branches. These conditions are certainly not satisfied at a branch point since $\cos\eta\pm\chi R\cos\chi\eta=0$ as was found in Section 3.1, however, the presence of the factors $e^{-2i\eta}$ and $e^{2i\eta}$ in (4.2-3a) and (4.2-3b) insures that these

geometric series converge uniformly on practically the same regions as do the series representations of Section 3.3. Also, the same comments hold here as did in Section 3.3 about the regions of convergence becoming larger as the branch numbers n and m are increased. Obviously, the expansion (4.2-6) involving the symmetrical dilatational branch $\eta_0(\chi)$ cannot be valid on all of the integration path C_D since this branch has a branch point at $\chi_0=e^{i\theta_0}$ given by (2.3-8) where $0<\theta_0<\theta_{-1}$ for $0<\nu\leq\frac{1}{2}$.

Very little can be claimed about convergence of the dilatational expansions on the small indention of C_D about $\chi=1$ in the first sketch of Fig. 21. The series of Section 3.3 were not shown to converge here. Also, C_D approaches the locus of a set of branch points whose limit point is $\chi=1$. However, it is a reasonable assumption that the series do converge on this indention since this locus of branch points probably determines the boundary of the domain of convergence.

The fact that the expansions (4.2-4) and (4.2-6) and the similar expansions for the asymmetrical branches fail to converge to the desired functions on all of the integration paths C_E and C_D as $\chi=\frac{a-1}{a+1}$ is approached is the error which makes this method approximate.

The expansions (4.2-4) and (4.2-6) suggest yet another set of phase functions to simplify the notation. These are

$$\left.\begin{aligned}
\Phi_{e\ell pq} &= \frac{2}{1+\chi}[\Phi_\ell - 1 - (1-\chi)p - 2q] \\
\Psi_{e\ell pq} &= \frac{2}{1+\chi}[\Psi_\ell - 1 - (1-\chi)p - 2q] \\
\Phi_{d\ell pq} &= \frac{2}{1-\chi}[\Phi_\ell + 1 + (1+\chi)p + 2q] \\
\Psi_{d\ell pq} &= \frac{2}{1-\chi}[\Psi_\ell + 1 + (1+\chi)p + 2q]
\end{aligned}\right\} \qquad (4.2\text{-}7)$$

where Φ_ℓ and Ψ_ℓ are defined by (4.2-1). In (4.2-7) the subscripts e and d refer to the fact that these phase functions will be used in the equivoluminal and dilatational expansions respectively. The remaining subscripts refer to integers with $\ell=1,2,\ldots,8$ and $p,q=0,1,2,\ldots$.

The phase functions (4.2-7), the expansions (4.2-4) and (4.2-6), the forms (4.2-2) and the representations (4.1-2) make it possible to write (2.3-15) for the displacement component u_ξ as

$$\frac{16\pi\mu\sqrt{a^2-1}}{aI}u_\xi \cong \mathrm{Im}\sum_{n=1}^{\infty}\sum_{p,q=0}^{\infty}\sum_{\ell=1}^{8}\int_{C_E} A_{pq}S_{1\ell}\frac{1-\chi}{\chi^{\frac{3}{2}}D(\chi)}$$

$$\times\left\{[\chi^2-2(1-2\nu)\chi+1]e^{\frac{1}{2}\Phi_{e\ell pq}}\mathrm{LogR}\, e^{in\pi\Phi_{e\ell pq}}\right.$$

$$\left.-(1-\chi^2)e^{\frac{1}{2}\Psi_{e\ell pq}}\mathrm{LogR}\, e^{in\pi\Psi_{e\ell pq}}\right\}d\chi$$

$$+ \operatorname{Im} \sum_{m=0}^{\infty} \sum_{p,q=0}^{\infty} \sum_{\ell=1}^{8} \int_{C_D} A'_{pq} S_{1\ell} \frac{1+\chi}{\chi^{\frac{3}{2}} D(\chi)}$$

$$\times \left\{ [\chi^2 - 2(1-2\nu)\chi + 1] e^{-\frac{1}{2}\Phi d_{\ell pq}} \operatorname{Log} R \; e^{i\left(m+\frac{1}{2}\right)\pi\Phi d_{\ell pq}} \right.$$

$$\left. - (1-\chi^2) e^{-\frac{1}{2}\Psi d_{\ell pq}} \operatorname{Log} R \; e^{i\left(m+\frac{1}{2}\right)\pi\Psi d_{\ell pq}} \right\} d\chi$$

$$+ \operatorname{Im} \sum_{n=1}^{\infty} \sum_{p,q=0}^{\infty} \sum_{\ell=1}^{8} \int_{C_E} (-1)^p A_{pq} S_{2\ell} \frac{1-\chi}{\chi^{\frac{3}{2}} D(\chi)}$$

$$\times \left\{ [\chi^2 - 2(1-2\nu)\chi + 1] e^{\frac{1}{2}\Phi e_{\ell pq}} \operatorname{Log} R \; e^{i\left(n-\frac{1}{2}\right)\pi\Phi e_{\ell pq}} \right.$$

$$\left. - (1-\chi^2) e^{\frac{1}{2}\Psi e_{\ell pq}} \operatorname{Log} R \; e^{i\left(n-\frac{1}{2}\right)\pi\Psi e_{\ell pq}} \right\} d\chi$$

$$+ \operatorname{Im} \sum_{m=1}^{\infty} \sum_{p,q=0}^{\infty} \sum_{\ell=1}^{8} \int_{C_D} (-1)^p A'_{pq} S_{2\ell} \frac{1+\chi}{\chi^{\frac{3}{2}} D(\chi)}$$

$$\times \left\{ [\chi^2 - 2(1-2\nu)\chi + 1] e^{-\frac{1}{2}\Phi d_{\ell pq}} \operatorname{Log} R \; e^{im\pi\Phi d_{\ell pq}} \right.$$

$$\left. - (1-\chi^2) e^{-\frac{1}{2}\Psi d_{\ell pq}} \operatorname{Log} R \; e^{im\pi\Psi d_{\ell pq}} \right\} d\chi \quad . \qquad (4.2\text{-}8)$$

The Rayleigh modes, n=0, are not included in (4.2-8). Also, the expression is approximate in the sense that the

expansions (4.2-4) and (4.2-6) have been used as exact representations. The sum over p and q has been written as if all of the coefficients A_{pq} and A'_{pq} were known. The summation and integration order has been changed. This can be justified rigorously only on the portions of the integration paths C_E and C_D where (4.2-4) and (4.2-6) can be shown to converge uniformly with respect to χ to the appropriate expressions. $\eta^{(0)}_{en}$ and $\eta^{(0)}_{en-\frac{1}{2}}$ from (3.3-3) and $\eta^{(0)}_{dm}$ and $\eta^{(0)}_{dm-\frac{1}{2}}$ from (3.3-24) have been used in (4.2-8). The four integrals in (4.2-8) represent integrations over the symmetrical equivoluminal branches, the symmetrical dilatational branches, the asymmetrical equivoluminal branches and the asymmetrical dilatational branches respectively. The terms $S_{k\ell}$ are given by (4.2-2a). As can be seen from (2.3-15), a similar representation holds for the displacement component u_ζ.

The symmetrical and asymmetrical integrals for each of the equivoluminal and dilatational cases can be added in (4.2-8) to give

$$\frac{16\pi\mu\sqrt{a^2-1}}{aI}u_\xi \cong \mathrm{Im}\sum_{n=1}^{\infty}\sum_{p,q=0}^{\infty}\sum_{\ell=1}^{8}\int_{C_E} A_{pq}\frac{1-\chi}{\chi^{\frac{3}{2}}D(\chi)}$$

$$\times\left\{[\chi^2-2(1-2\nu)\chi+1]\left[S_{1\ell}+(-1)^p S_{2\ell}e^{-i\frac{\pi}{2}\Phi_{\ell pq}}\right]e^{\frac{1}{2}\Phi_{\ell pq}}\mathrm{Log}_R\, e^{in\pi\Phi_{\ell pq}}\right.$$

$$\left.-(1-\chi^2)\left[S_{1\ell}+(-1)^p S_{2\ell}e^{-i\frac{\pi}{2}\Psi_{\ell pq}}\right]e^{\frac{1}{2}\Psi_{\ell pq}}\mathrm{Log}_R\, e^{in\pi\Psi_{\ell pq}}\right\}d\chi$$

$$+\mathrm{Im}\sum_{m=1}^{\infty}\sum_{p,q=0}^{\infty}\sum_{\ell=1}^{8}\int_{C_D} A'_{pq}\frac{1+\chi}{\chi^{\frac{3}{2}}D(\chi)}$$

$$\times\left\{[\chi^2-2(1-2\nu)\chi+1]\left[S_{1\ell}e^{-i\frac{\pi}{2}\Phi_{\ell pq}}+(-1)^p S_{2\ell}\right]e^{-\frac{1}{2}\Phi_{d\ell pq}}\mathrm{Log}_R\, e^{im\pi\Phi_{d\ell pq}}\right.$$

$$\left.-(1-\chi^2)\left[S_{1\ell}e^{-i\frac{\pi}{2}\Psi_{d\ell pq}}+(-1)^p S_{2\ell}\right]e^{-\frac{1}{2}\Psi_{d\ell pq}}\mathrm{Log}_R\, e^{im\pi\Psi_{d\ell pq}}\right\}d\chi \qquad (4.2\text{-}9)$$

and similarly for u_ζ.

This operation of adding the symmetrical and asymmetrical terms is expected to cancel all of the extra wave fronts which would have resulted from a singular loading applied at the bottom face of the plate ($\xi=0$, $\zeta=-1$). It is recalled that such a loading is present in a purely symmetrical or asymmetrical loading. The cancellation must occur

as a result of the terms like $S_{1\ell}+(-1)^p S_{2\ell} e^{-i\frac{\pi}{2}\Phi} e_{\ell pq}$, etc., vanishing for certain combinations of ℓ, p and q and for certain values of the variables ξ, τ, ζ and χ.

The phase functions in (4.2-9), which are defined by (4.2-7), are complex on the integration paths C_E and C_D and the integrals are more convenient to handle if these paths are deformed so that these phase functions are either real or appear in a simpler form. This will make it possible to sum over the branch numbers n and m and then to recognize singular wave fronts.

It is very important to realize that (4.2-9) is now a term-by-term integration and the integrands possess none of the branch points which were of concern before. In fact, the only branch point of interest here is χ_{01} where R=0, so that it is a branch point of the function LogR. The locus of χ_{01} as Poisson's ratio ν varies is shown in Fig. 4 and the point is described following (A-3) in Appendix A.

With the preceding in mind, the integration paths C_E and C_D of (4.2-9) and shown in the first sketch of Fig. 21 are deformed as shown in the second and third sketches of Fig. 21. The path C_E is deformed back onto the original integration path C shown in Fig. 2 except for a vertical indention about the branch point at χ_{01}. The path C_D is just collapsed onto the real χ-axis on $\frac{a-1}{a+1} \leq \chi \leq 1$ with an

identical vertical indention for the branch point at χ_{01}.

The point χ_{01} where R=0 causes difficulties in the representation (4.2-9) with C_E and C_D deformed as described. The integrands in (4.2-9) may be singular at this point depending on the values of the phase functions as can be seen from the functions $e^{-\frac{1}{2}\Phi e\ell pq\,LogR}$, etc. Actually, it would be desirable to demonstrate mutual cancellation of the branch line integrals about this point as was done in Section 4.1 about the original branch points. It is true that the integrals along the branch cut to χ_{01} cancel by mutual cancellation when the sum over the branch number is taken with the exception of one line integral belonging to the lowest branch. However, cancellation of the integrals on the small circular path about the branch point χ_{01} is well concealed in (4.2-9) if it is present at all. The intention here is not to investigate these branch line integrals in detail, but to look at the remainder of the integrals on $\frac{a-1}{a+1}\leq\chi\leq 1$ and on $\chi=e^{i\theta}$, $0\leq\theta\leq\pi$, and to try to locate physically meaningful results.

The approach to be used is to bring the summation over the mode or branch numbers n and m inside the integrands of (4.2-9) and to sum over the terms $e^{in\pi\Phi e\ell pq}$, etc. These are the only quantities in (4.2-9) which contain the branch numbers. This interchange of the summation and integration

order is again done without justification. The summations yield generalized functions if the phase functions (4.2-7) are real and they yield ordinary functions by a simple geometric series if the phase functions are complex with positive imaginary parts.

The phase functions (4.2-7) can be examined more conveniently in terms of the variable

$$B = \frac{1}{2a}\sqrt{a^2-1}\,\frac{1+\chi}{\chi^{\frac{1}{2}}} \qquad (4.2\text{-}10)$$

with $\chi^{\frac{1}{2}}=e^{i\frac{\theta}{2}}$ on $\chi=e^{i\theta}$, $0\leq\theta\leq\pi$. B is real on all of the integration path C of Fig. 2. From (2.3-5) and (2.3-7), $B=\frac{\beta}{\omega}$ in terms of the original variables. On $\frac{a-1}{a+1}\leq\chi\leq 1$, $1\geq B\geq\frac{1}{a}\sqrt{a^2-1}$ and on $\chi=e^{i\theta}$, $0\leq\theta\leq\pi$, $\frac{1}{a}\sqrt{a^2-1}\geq B\geq 0$ where $B=\frac{1}{a}\sqrt{a^2-1}\cos\frac{\theta}{2}$. The phase functions (4.2-7) then become

$$\Phi_{e\ell pq} = \frac{1}{B}\left[\xi\sqrt{1-B^2} - (-1)^{\ell}\tau - (2p+2q+1-\zeta)\sqrt{B^2-\frac{a^2-1}{a^2}}\right] - 2q-1\pm 1 \quad ,$$

$$\Psi_{e\ell pq} = \frac{1}{B}\left[\tau - (-1)^{\ell}\xi\sqrt{1-B^2} - (2p+2q+1\mp 1)\sqrt{B^2-\frac{a^2-1}{a^2}}\right] - 2q-1+\zeta \quad ,$$

$$\Phi_{d\ell pq} = \frac{1}{\sqrt{B^2-\frac{a^2-1}{a^2}}}\left[\xi\sqrt{1-B^2} - (-1)^{\ell}\tau+(2p+2q+1\pm 1)B\right]+2q+1+\zeta \quad ,$$

$$\Psi_{d\ell pq} = \frac{1}{\sqrt{B^2-\frac{a^2-1}{a^2}}}\left[\tau-(-1)^{\ell}\xi\sqrt{1-B^2} + (2p+2q+1+\zeta)B\right]+2q+1\pm 1$$

(4.2-11)

where the upper sign still applies for $\ell=1,2,3,4$, the lower sign applies for $\ell=5,6,7,8$ and ζ is replaced by $-\zeta$ for $\ell=3,4,7,8$. In (4.2-11) all of the terms are real and the radicals are nonnegative on the integration path C except for $\sqrt{B^2-\frac{a^2-1}{a^2}} = \frac{1}{2a}\sqrt{a^2-1}\,\frac{1-\chi}{\chi^{\frac{1}{2}}}$ which is pure imaginary with the imaginary part being negative on $\chi=e^{i\theta}$, $0<\theta\leq\pi$, where $\sqrt{B^2-\frac{a^2-1}{a^2}} = -i\sqrt{\frac{a^2-1}{a^2}-B^2} = -\frac{i}{a}\sqrt{a^2-1}\sin\frac{\theta}{2}$. Thus, $\Phi_{e\ell pq}$ and $\Psi_{e\ell pq}$ have nonnegative imaginary parts on $\chi=e^{i\theta}$, $0\leq\theta\leq\pi$, and are real on $\frac{a-1}{a+1}\leq\chi\leq 1$. The phase functions $\Phi_{d\ell pq}$ and $\Psi_{d\ell pq}$ are only involved on $\frac{a-1}{a+1}\leq\chi\leq 1$ where they are also real.

It is seen from (4.2-11) that $\Psi_{e\ell pq}$ is real on all of the integration path C including $\chi=e^{i\theta}$, $0\leq\theta\leq\pi$, only for the special cases where $2p+2q+1\mp 1=0$, which means that $p=q=0$ and $\ell=1,2,3,4$ using the fact that $p,q\geq 0$. These cases will be seen to be identified with the circular equivoluminal wave

front. Likewise, $\Phi_{e\ell pq}$ is real on all of C for the special cases where $2p+2q+1-\zeta=0$, which means that $p=q=0$ for $\ell=1,2,5,6$ and $\zeta=1$ or $p=q=0$ for $\ell=3,4,7,8$ and $\zeta=-1$.

When the phase functions (4.2-11) are real, the representation

$$\sum_{n=1}^{\infty} e^{in\pi\Phi} = -\frac{1}{2} + \sum_{m=-\infty}^{\infty} \delta(\Phi-2m) + \frac{i}{2}\cot\frac{\pi}{2}\Phi \qquad (4.2\text{-}12)$$

can be used where $\delta(\Phi-2m)$ is the Dirac delta function. This is just a Fourier series representation of periodic generalized functions and it results from the representations given by Lighthill [9]. Also, (4.2-12) can be derived by differentiating the Fourier series representations $\sum_{n=1}^{\infty}\frac{1}{n}\cos n\pi\Phi=-\log\left|2\sin\frac{\pi}{2}\Phi\right|$ and $\sum_{n=1}^{\infty}\frac{1}{n}\sin n\pi\Phi$ which represents a sawtooth function. A geometric series gives

$$\sum_{n=1}^{\infty} e^{in\pi\Phi} = \frac{e^{i\pi\Phi}}{1-e^{i\pi\Phi}} \qquad (4.2\text{-}13)$$

when the phase functions have positive imaginary parts. (4.2-13) is also valid when the phase functions are real if the limiting process is carried out carefully so as to produce the generalized functions in (4.2-12).

The portion of the integrals (4.2-9) which result from integration on $\frac{a-1}{a+1}\leq\chi\leq 1$ and on $\chi=e^{i\theta}$, $0\leq\theta\leq\pi$, as shown in the

second and third sketches of Fig. 21 can now be written with the sums over the branch numbers, n and m, having been performed. These consist of Cauchy principal value integrals due to the presence of the generalized functions $\cot\frac{\pi}{2}\Phi$ and $\csc\frac{\pi}{2}\Phi$. The integrals are separated into four distinct sets of integrals, each identified with one of the four phase functions (4.2-11). Thus, by using (4.2-12) and (4.2-13), the quantity in (4.2-9) can be represented as

$$\frac{32\pi\mu\sqrt{a^2-1}}{aI}u_\xi \cong I_{de} + I_{ee} + I_{dd} + I_{ed} \tag{4.2-14}$$

where

$$I_{de} = \sum_{p,q=0}^{\infty}\sum_{\ell=1}^{8}\Bigg\{ P.V.\int_{\frac{a-1}{a+1}}^{1} A_{pq}\frac{(1-\chi)[\chi^2-2(1-2\nu)\chi+1]}{\chi^{\frac{3}{2}}D(\chi)}e^{\frac{1}{2}\Phi_{e\ell pq}}\mathrm{LogR}$$

$$\times\left[S_{1\ell}\cot\tfrac{\pi}{2}\Phi_{e\ell pq} + (-1)^p S_{2\ell}\csc\tfrac{\pi}{2}\Phi_{e\ell pq}\right]d\chi$$

$$+ 8\,\mathrm{Im}\int_0^{\pi} A_{pq}\frac{\sin\frac{\theta}{2}(\cos\theta-1+2\nu)}{|D(e^{i\theta})|}e^{i\frac{\gamma}{2}(\Phi_{e\ell pq}+1)}\left[S_{1\ell}\right.$$

$$\left.+ (-1)^p S_{2\ell}e^{-i\frac{\pi}{2}\Phi_{e\ell pq}}\right]\frac{e^{i\pi\Phi_{e\ell pq}}}{1-e^{i\pi\Phi_{e\ell pq}}}d\theta\Bigg\}\,, \tag{4.2-14a}$$

$$I_{ee} = \sum_{p,q=0}^{\infty} \sum_{\ell=1}^{8} \Bigg\{ -P.V. \int_{\frac{a-1}{a+1}}^{1} A_{pq} \frac{(1-\chi)(1-\chi^2)}{\chi^{\frac{3}{2}} D(\chi)} e^{\frac{1}{2}\Psi_{e\ell pq} \text{LogR}}$$

$$\times \left[S_{1\ell} \cot\tfrac{\pi}{2}\Psi_{e\ell pq} + (-1)^p S_{2\ell} \csc\tfrac{\pi}{2}\Psi_{e\ell pq} \right] d\chi$$

$$+ 8\text{Re} \int_0^{\pi} A_{pq} \frac{\sin\frac{\theta}{2}\sin\theta}{|D(e^{i\theta})|} e^{i\frac{\gamma}{2}(\Psi_{e\ell pq}+1)} \Bigg[S_{1\ell}$$

$$+ (-1)^p S_{2\ell} e^{-i\frac{\pi}{2}\Psi_{e\ell pq}} \Bigg] \frac{e^{i\pi\Psi_{e\ell pq}}}{1-e^{i\pi\Psi_{e\ell pq}}} d\theta \Bigg\} \quad , \qquad (4.2\text{-}14b)$$

$$I_{dd} = \sum_{p,q=0}^{\infty} \sum_{\ell=1}^{8} P.V. \int_{\frac{a-1}{a+1}}^{1} A'_{pq} \frac{(1+\chi)[\chi^2-2(1-2\nu)\chi+1]}{\chi^{\frac{3}{2}} D(\chi)} e^{-\frac{1}{2}\Phi_{d\ell pq}} \text{LogR}$$

$$\times \left[S_{1\ell} \csc\tfrac{\pi}{2}\Phi_{d\ell pq} + (-1)^p S_{2\ell} \cot\tfrac{\pi}{2}\Phi_{d\ell pq} \right] d\chi \quad , \qquad (4.2\text{-}14c)$$

$$I_{ed} = -\sum_{p,q=0}^{\infty} \sum_{\ell=1}^{8} P.V. \int_{\frac{a-1}{a+1}}^{1} A'_{pq} \frac{(1+\chi)(1-\chi^2)}{\chi^{\frac{3}{2}} D(\chi)} e^{-\frac{1}{2}\Psi_{d\ell pq}} \text{LogR}$$

$$\times \left[S_{1\ell} \csc\tfrac{\pi}{2}\Psi_{d\ell pq} + (-1)^p S_{2\ell} \cot\tfrac{\pi}{2}\Phi_{d\ell pq} \right] d\chi \quad . \qquad (4.2\text{-}14d)$$

In these integrals the form (A-6) in Appendix A defining $\gamma=\gamma(\theta)$ has been used along with $D(e^{i\theta})=|D(e^{i\theta})|e^{i\left(\theta-\frac{\gamma}{2}\right)}$

from (A-6a). The terms $S_{k\ell}$ are defined by (4.2-2a) and the coefficients A_{pq} are given by (4.2-5) for p+q=0,1,2,3. The coefficients A'_{pq} result from A_{pq} as described following (4.2-6). The phase functions $\Phi_{e\ell pq}$, $\Psi_{e\ell pq}$, $\Phi_{d\ell pq}$ and $\Psi_{d\ell pq}$ are defined by (4.2-11). The subscripts on these integrals are meant to indicate their origin such as I_{de} for the integral resulting from the dilatational potential ϕ with the integration over the equivoluminal branches and similarly for the other three integrals.

The Dirac delta functions from (4.2-12) are not present in (4.2-14a),..., (4.2-14d) simply because only the imaginary parts of the integrals in (4.2-9) are required and the delta functions always multiply the real parts of the integrands on $\frac{a-1}{a+1}\leq\chi\leq 1$. A special case is described in the following where the Dirac delta functions do remain.

The second integral in (4.2-14b) for I_{ee} must be modified for the cases p=q=0 and ℓ=1,2,3,4 since $\Psi_{e\ell 00}$ is real on $\chi=e^{i\theta}$, $0\leq\theta\leq\pi$, and the representation (4.2-12) must be used rather than (4.2-13). Thus, using A_{00}=1 from (4.2-5), the second term in (4.2-14b) for I_{ee} must be replaced with

$$8\sum_{\ell=1}^{4} P.V.\int_0^{\pi} \frac{\sin\frac{\theta}{2}\sin\theta}{|D(e^{i\theta})|}\left\{-\frac{1}{2}S_{1\ell}\cos\left[\frac{\gamma}{2}(\Psi_{e\ell 00}+1)\right]\right.$$

$$+\sum_{m=-\infty}^{\infty}\left[S_{1\ell}+(-1)^m S_{2\ell}\right]\cos\left[\left(m+\frac{1}{2}\right)\gamma\right]\delta(\Psi_{e\ell 00}-2m)$$

$$\left.-\frac{1}{2}\sin\left[\frac{\gamma}{2}(\Psi_{e\ell 00}+1)\right]\left[S_{1\ell}\cot\frac{\pi}{2}\Psi_{e\ell 00}+S_{2\ell}\csc\frac{\pi}{2}\Psi_{e\ell 00}\right]\right\}d\theta \qquad (4.2\text{-}15)$$

for $p=q=0$ and $\ell=1,2,3,4$. The second term in (4.2-14a) for I_{de} does not need to be modified even though its integrand is singular for some points on the boundaries $\zeta=\pm 1$ for $p=q=0$. It is just necessary to interpret the integral as a Cauchy principal value at these points and to realize that (4.2-12) is a limiting form of (4.2-13).

A similar representation for the displacement component u_ζ can be written by making very simple changes in (4.2-14a),..., (4.2-14d) and in (4.2-15) as suggested by (2.3-15a) and (2.3-16).

4.2.2. The Geometry of the Wave Fronts.

As usual, when dealing with generalized functions, the integrals (4.2-14a),..., (4.2-14d) and (4.2-15) are most conveniently investigated when the phase functions $\Phi_{e\ell pq}$, $\Psi_{e\ell pq}$, $\Phi_{d\ell pq}$ and $\Psi_{d\ell pq}$ replace χ or θ as the independent variable. This makes it possible to identify wave fronts

as singularities in the integrals resulting from a singular point of the generalized function coinciding with a singular point of the remainder of the integrand.

For the change of variables to the phase functions, the factor

$$d\chi = \frac{d\chi}{dB}\frac{dB}{d\Phi}d\Phi$$

replaces $d\chi$ in the integrals where Φ is any one of the phase functions (4.2-11) and B is defined by (4.2-10). A singular point in the integrands occurs if

$$\frac{dB}{d\chi}\frac{d\Phi}{dB} = 0 \quad . \tag{4.2-16}$$

From (4.2-10),

$$\frac{dB}{d\chi} = \frac{1}{2a}\sqrt{a^2-1}\,\frac{1-\chi}{\chi^{\frac{3}{2}}} = -\frac{1}{4a^2}(a^2-1)\frac{\sqrt{B^2-\frac{a^2-1}{a^2}}}{B^2-\frac{a^2-1}{a^2}-B\sqrt{B^2-\frac{a^2-1}{a^2}}}, \tag{4.2-17}$$

and from (4.2-11),

$$\frac{d\Phi}{dB}e_{\ell pq} = -\frac{1}{B^2}\left[\frac{\xi}{\sqrt{1-B^2}} - (-1)^{\ell}\tau + \frac{a^2-1}{a^2}\,\frac{2p+2q+1-\zeta}{\sqrt{B^2-\frac{a^2-1}{a^2}}}\right] ,$$

$$\frac{d_\Psi}{dB} e\ell pq = -\frac{1}{B^2}\left[\tau - (-1)^\ell \frac{\xi}{\sqrt{1-B^2}} + \frac{a^2-1}{a^2}\frac{2p+2q+1\mp 1}{\sqrt{B^2-\frac{a^2-1}{a^2}}}\right] ,$$

$$\frac{d\Phi}{dB} d\ell pq = -\frac{1}{\left(B^2-\frac{a^2-1}{a^2}\right)^{\frac{3}{2}}}\left[\frac{B\xi}{a^2\sqrt{1-B^2}} - (-1)^\ell B\tau + \frac{a^2-1}{a^2}(2p+2q+1\pm 1)\right] ,$$

$$\frac{d\Psi}{dB} d\ell pq = -\frac{1}{\left(B^2-\frac{a^2-1}{a^2}\right)^{\frac{3}{2}}}\left[B\tau - (-1)^\ell \frac{B\xi}{a^2\sqrt{1-B^2}} + \frac{a^2-1}{a^2}(2p+2q+1+\zeta)\right] .$$

(4.2-18)

$\frac{dB}{d\chi}=0$ at $\chi=1$ or at $B=\frac{1}{a}\sqrt{a^2-1}$ from (4.2-17), however, this singularity is removed by the factor $\frac{1-\chi}{\chi^{\frac{3}{2}}}$ in all of the integrals, except (4.2-14c) for I_{dd}, giving $\frac{1-\chi}{\chi^{\frac{3}{2}}}\frac{d\chi}{dB}=\frac{2a}{\sqrt{a^2-1}}$. For I_{dd}, the factor $\left(B^2-\frac{a^2-1}{a^2}\right)^{\frac{3}{2}}$ in (4.2-18) for $\frac{d\Phi}{dB} d\ell pq$ makes $\frac{d\chi}{dB}\frac{dB}{d\Phi}_{d\ell pq}$ nonsingular. The point $B=\frac{1}{a}\sqrt{a^2-1}$ is special, however, since it will be seen to be identified with the head wave. The head wave is not singular in the displacements for the loading (2.1-7) used here.

Thus, since each of the generalized functions in (4.2-14a),..., (4.2-14d) and in (4.2-15) is singular at $\Phi=2m$ for any integer m, the condition for a singular wave front is the simultaneous satisfaction of the equations

$$\left.\begin{aligned} \Phi &= 2m \quad , \\ \frac{d\Phi}{dB} &= 0 \end{aligned}\right\} \qquad (4.2\text{-}19)$$

for any integer m where Φ represents any one of the four phase functions (4.2-11). (4.2-19) represents four sets of simultaneous equations resulting from (4.2-11) and (4.2-18) each of which can be solved for ξ and ζ to give the spatial geometry of the wave fronts as a function of τ.

From (4.2-18), it is obvious that $\frac{d\Phi}{dB}=0$ is not possible for $\xi>0$ if $\ell=1,3,5,7$ since $p,q\geq 0$ and $-1\leq\zeta\leq 1$. These phase functions occur in terms which are singular only for $\xi<0$ and, therefore, are associated with wave fronts traveling in the negative ξ direction. The phase functions identified by $\ell=1,3,5,7$ and the accompanying terms in the integrals are set aside for now and only those identified by $\ell=2,4,6,8$ are considered.

It is helpful to define the normalized coordinates and parameters

$$
\left.
\begin{aligned}
L &= \frac{\xi}{\tau} \quad , \\
Z^{e}_{pq} &= \frac{2p+2q+1-\zeta}{\tau} \quad , \\
Z^{d}_{pq} &= \frac{2p+2q+1+\zeta}{\tau} \quad , \\
Q^{e}_{pq} &= \frac{2p+2q+1\mp 1}{\tau} \quad , \\
Q^{d}_{pq} &= \frac{2p+2q+1\pm 1}{\tau}
\end{aligned}
\right\} \qquad (4.2\text{-}20)
$$

where the upper sign applies for $\ell=2,4$, the lower sign applies for $\ell=6,8$ and ζ is replaced by $-\zeta$ for $\ell=4,8$.

Then from (4.2-11) and (4.2-18), simultaneous satisfaction of (4.2-19) gives the following parametric descriptions of the singular wave fronts:

for the phase functions $\Phi_{e\ell pq}$,

$$
\left.
\begin{aligned}
L &= \frac{a^2}{B}\sqrt{1-B^2}\left(B+\frac{a^2-1}{a^2}Q^{e}_{mq}\right) \quad , \\
Z^{e}_{pq} &= -\frac{a^2}{B}\sqrt{B^2-\frac{a^2-1}{a^2}}\left(B+Q^{e}_{mq}\right) \quad ;
\end{aligned}
\right\} \qquad (4.2\text{-}21a)
$$

for the phase functions $\Psi_{e\ell pq}$,

$$\left.\begin{aligned} L &= \sqrt{1-B^2}\left(1+\frac{a^2-1}{a^2}\,\frac{Q^e_{pq}}{\sqrt{B^2-\frac{a^2-1}{a^2}}}\right), \\ z^e_{mq} &= B\left(1-\frac{1}{a^2}\,\frac{Q^e_{pq}}{\sqrt{B^2-\frac{a^2-1}{a^2}}}\right); \end{aligned}\right\} \quad (4.2\text{-}21b)$$

for the phase functions $\Phi_{d\ell pq}$,

$$\left.\begin{aligned} L &= \frac{a^2}{B}\sqrt{1-B^2}\left(B-\frac{a^2-1}{a^2}Q^d_{pq}\right), \\ z^d_{-mq} &= \frac{a^2}{B}\sqrt{B^2-\frac{a^2-1}{a^2}}\left(B-Q^d_{pq}\right); \end{aligned}\right\} \quad (4.2\text{-}21c)$$

and for the phase functions $\Psi_{d\ell pq}$,

$$\left.\begin{aligned} L &= \sqrt{1-B^2}\left(1-\frac{a^2-1}{a^2}\,\frac{Q^d_{-mq}}{\sqrt{B^2-\frac{a^2-1}{a^2}}}\right), \\ z^d_{pq} &= -B\left(1+\frac{1}{a^2}\,\frac{Q^d_{-mq}}{\sqrt{B^2-\frac{a^2-1}{a^2}}}\right) \end{aligned}\right\} \quad (4.2\text{-}21d)$$

where $\ell=2,4,6,8$ throughout. These wave fronts can be sketched in the L,Z-space by taking a fixed value of Q and letting B vary in the range $1\geq B\geq\frac{1}{a}\sqrt{a^2-1}$ corresponding to $\frac{a-1}{a+1}\leq\chi\leq 1$. Also, there are singular wave fronts in (4.2-15) in the range $\frac{1}{a}\sqrt{a^2-1}\geq B\geq 0$ corresponding to $\chi=e^{i\theta}$, $0\leq\theta\leq\pi$. There is some restriction on the quantities involved in (4.2-21a),..., (4.2-21d) since all of the quantities defined by (4.2-20) are nonnegative as a result of $p,q\geq 0$, $\xi>0$, $\tau>0$ and $-1\leq\zeta\leq 1$. However, when p is replaced by the integers $\pm m$, as in Z^e_{mq}, Q^d_{-mq}, etc., the quantity may be negative since the integers m are only restricted by the fact that (4.2-19) must be satisfied.

Fig. 22 shows the equivoluminal wave fronts in dashed lines and they are present in I_{ee} given by (4.2-14b), and they result from $\Psi_{e\ell pq}$ as described by (4.2-21b). The dilatational wave fronts are shown in solid lines and they are present in I_{dd} given by (4.2-14c), resulting from $\Phi_{d\ell pq}$ as described by (4.2-21c). The sketch is at the time $\tau=6.3$ for $\nu=0.3$ which gives $a=\frac{c_d}{c_s}=\sqrt{3.5}\cong 1.871$ from (2.1-2). $\tau=6.3$ means that an equivoluminal wave has had time to cross the plate $\frac{1}{2}\tau=3.15$ times while a dilatational wave has had time to cross the plate $\frac{1}{2}a\tau\cong 5.89$ times. The top sketch of Fig. 22 is essentially the wave fronts in the L,Z-space with $L=\frac{\xi}{\tau}$ measured on the same axis as ξ and

$z=z^{e}_{mq}, z^{d}_{-mq}$ measured downward from the horizontal line on which a particular wave front terminates. Actually, this sketch just shows the right half of the plate, $\xi \geq 0$, with the thickness $-1 \leq \zeta \leq 1$ successively repeated so that all wave fronts appear as continuous lines. The geometry of the wave fronts is exactly like that for a layered half-space made up of identical layers with refraction but no reflection at the junctions. The second sketch in Fig. 22 shows the superposition of these wave fronts as they appear in the plate. The superposition just consists of folding the first sketch as an accordian at each horizontal line representing the edges of the plate to form a single thickness.

The only case in which the range $\frac{1}{a}\sqrt{a^2-1} \geq B \geq 0$ or $\chi=e^{i\theta}$, $0 \leq \theta \leq \pi$, produces a wave front is for $Q^{e}_{pq}=0$ in (4.2-21b), or $p=q=0$ and $\ell=2,4$ from (4.2-20), so that

$$L = \sqrt{1-B^2} \quad ,$$

$$z^{e}_{m0} = B \quad .$$

This is obviously the circular equivoluminal wave front since $L^2+\left(z^{e}_{m0}\right)^2=1$ or $\xi^2+\left[2m+1+(-1)^{\frac{\ell}{2}}\zeta\right]^2=\tau$ for $\ell=2,4$ and $m=0,1,2,\ldots$. This wave front is labeled 1',2',3' in Fig. 22 with the singularity on the portion 1',2' contained in

the representation (4.2-15) where $\frac{1}{a}\sqrt{a^2-1} \geq B \geq 0$ or $\chi = e^{i\theta}$, $0 \leq \theta \leq \pi$. The singularity on the remaining portion 2',3' is contained in the first term of I_{ee} in (4.2-14b) for p=q=0 and ℓ=2,4 where $1 \geq B \geq \frac{1}{a}\sqrt{a^2-1}$ or $\frac{a-1}{a+1} \leq \chi \leq 1$.

The preceding is significant because the result indicates that only the portion 1',2' of the circular equivoluminal wave front 1',2',3' in Fig. 22 comes from "the equivoluminal sector" of the ω,κ-plane as defined by (2.3-11) while all other wave fronts, equivoluminal and dilatational, come from "the dilatational sector" of the ω,κ-plane as defined by (2.3-10)

The straight equivoluminal wave front 2',4' in Fig. 22 is the head wave and it is tangent to the circular equivoluminal wave front 1',2',3'. This wave front results from the same terms, (4.2-14b) with p=q=0 and ℓ=2,4 and (4.2-15), as did 1',2',3'. However, it comes about for different reasons than the simultaneous satisfaction of the equations (4.2-19). In this case, the change in the form of the integrand, as the point χ=1 or $B=\frac{1}{a}\sqrt{a^2-1}$ is crossed on the integration path, produces the head wave. This is seen by comparing the first term in (4.2-14b) for p=q=0 and ℓ=2,4 with (4.2-15) where the Dirac delta functions $\delta(\Psi_{e\ell 00}-2m)$ are present. Thus, the head wave is associated with the line $\omega=\kappa$ which separates "the dilatational sector"

from "the equivoluminal sector." The geometry of the head wave can be deduced by setting $B=\frac{1}{a}\sqrt{a^2-1}$ and $\Psi_{e\ell 00}=2m$ for $\ell=2,4$ to obtain

$$z^e_{m0} = \frac{1}{\sqrt{a^2-1}}(a-L)$$

from (4.2-11) and (4.2-20) giving $2m+1+(-1)^{\frac{\ell}{2}}\zeta=\frac{1}{\sqrt{a^2-1}}(a\tau-\xi)$ for $m=0,1,2,\ldots$.

The remaining equivoluminal wave fronts shown in Fig. 22 are contained in the first term of I_{ee} in (4.2-14b) as described by (4.2-21b) for $Q^e_{pq}=\frac{2}{\tau},\frac{4}{\tau},\frac{6}{\tau},\frac{8}{\tau},\frac{10}{\tau}$ as labeled in the figure. Obviously, from (4.2-20), these values of Q^e_{pq} specify p+q and, since only A_{pq} with p+q=0,1,2,3 are given in (4.2-5), only the wave fronts $Q^e_{pq}=0,\frac{2}{\tau},\frac{4}{\tau},\frac{6}{\tau}$ are provided for.

The dilatational wave fronts shown in Fig. 22 result from singularities contained in I_{dd} given by (4.2-14c) and they are described by (4.2-21c) corresponding to $Q^d_{pq}=0,\frac{2}{\tau},\frac{4}{\tau},\frac{6}{\tau}$ as labeled in the figure. From (4.2-20) and (4.2-21c), $Q^d_{pq}=0$ implies that p=q=0 and $\ell=6,8$ so that

$$L = a^2\sqrt{1-B^2}$$

$$z^d_{-m0} = a^2\sqrt{B^2-\frac{a^2-1}{a^2}} \quad ,$$

which is the circular dilatational wave front $L^2+\left(z^d_{-m0}\right)^2=a^2$ or $\xi^2+\left[-2m+1-(-1)^{\frac{\ell}{2}}\zeta\right]^2=a^2\tau^2$ for $\ell=6,8$ and $m=0,-1,-2,\ldots$. This wave front is 1,2 in Fig. 22 and it, along with 3,4 from $Q^d_{pq}=\frac{2}{\tau}$ and 5,6 from $Q^d_{pq}=\frac{4}{\tau}$, is perpendicular to one of the boundaries $\zeta=\pm 1$ so that these are conditions of grazing incidence at these points. The dilatational wave front 7,8 is not at grazing incidence at point 7 ($\zeta=-1$) since it is a reflection of the portion 2',3' of the circular equivoluminal wave front which meets the boundary at an angle of incidence which is less than the critical angle $\tan^{-1}\frac{1}{\sqrt{a^2-1}}$. Again, the coefficients A'_{pq} for $p+q=0,1,2,3$ are sufficient to describe the dilatational wave fronts identified by $Q^d_{pq}=0,\frac{2}{\tau},\frac{4}{\tau},\frac{6}{\tau}$.

For all of the wave fronts shown in Fig. 22, the points at $\xi=0$ or $L=0$ come from $B=1$, $\chi=\frac{a-1}{a+1}$ or $\kappa=0$. The point 1' on the circular equivoluminal wave front 1',2',3' comes from $B=0$, $\chi=-1$ or $\frac{\omega}{\kappa}=1$ where both ω and κ are unbounded on the equivoluminal branches. The point 2' comes from $B=\frac{1}{a}\sqrt{a^2-1}$, $\chi=1$ or $\frac{\omega}{\kappa}=a$ with ω and κ bounded on the equivoluminal branches. The points 5',7',9',11' and 13' on the reflected equivoluminal wave fronts each come from a point in the range $1>B>\frac{1}{a}\sqrt{a^2-1}$, $\frac{a-1}{a+1}<\chi<1$ or from "the dilatational sector" of the ω,κ-plane. The points 1, 3 and 5 on the dilatational wave

fronts also come from $B=\frac{1}{a}\sqrt{a^2-1}$, $\chi=1$ or $\frac{\omega}{\kappa}=a$ but with ω and κ unbounded on the dilatational branches. The point 7 on the dilatational wave front 7,8 is not at grazing incidence and it comes from a point in the range $1>B>\frac{1}{a}\sqrt{a^2-1}$, $\frac{a-1}{a+1}>\chi>1$ or "the dilatational sector" of the ω,κ-plane.

It is interesting, yet certainly expected, that the number of equivoluminal wave fronts present in the plate is related directly to the number of times that the circular dilatational wave front has crossed the plate at $\xi=0$ and vice versa as seen in the top sketch of Fig. 22. The finite number of wave fronts which are present in the plate at any finite time has the desirable effect of only requiring a finite number of the coefficients A_{pq} in (4.2-5) to account for all of the wave fronts. Then only a finite number of the coefficients $\eta_e^{(j)}$ and $\eta_d^{(k)}$ for the series representations in Section 3.3 are required. In (4.2-5) it is seen that coefficients A_{pq} with p+q fixed involve $\eta_e^{(j)}$ with $j=1,2,3,\ldots,p+q$, and likewise for A'_{pq} and $\eta_d^{(k)}$. Thus, while the series representations (4.2-14a),..., (4.2-14d) involve infinite sums over $p,q=0,1,2,\ldots$, only a finite number of singular terms in (4.2-14b) for I_{ee} and (4.2-14c) for I_{dd} are identified as the representations of the wave fronts. The remaining terms do not vanish, however, they can be shown to be small until the singular wave front

with which they are identified is present in the plate.

There are wave fronts, other than those shown in Fig. 22, which are predicted by (4.2-21a),..., (4.2-21d), however, they cancel when the superposition of integrals (4.2-14) is taken. These cancellations occur in pairs. (4.2-21a) and (4.2-21c) predict wave fronts associated with $\Phi_{e\ell pq}$ and $\Phi_{d\ell pq}$ respectively, which obviously have the same geometry. However, a detailed examination of the integral sum $I_{de}+I_{dd}$ in (4.2-14) shows that the singularities corresponding to these wave fronts cancel leaving only the dilatational wave fronts shown in Fig. 22. Likewise, (4.2-21b) and (4.2-21d) predict wave fronts from $\Psi_{e\ell pq}$ and $\Psi_{d\ell pq}$ respectively, which have the same geometry. These wave fronts also cancel due to the integral sum $I_{ee}+I_{ed}$ in (4.2-14) leaving only the equivoluminal wave fronts shown in Fig. 22.

If only the wave fronts are of interest in the response, the only function of the terms I_{de} and I_{ed} in (4.2-14) is to cancel the extraneous wave fronts.

4.2.3. Discussion of Specific Terms Yielding Wave Fronts. An Example of a Solution Approximated Near a Wave Front.

In the representation (4.2-15), the terms containing the Dirac delta functions $\delta(\Psi_{e\ell 00}-2m)$ are very easy to

integrate and they yield an explicit expression, which is singular like an inverse square root in the spatial variables. These terms are singular on the portion 1',2' of the circular equivoluminal wave fron 1',2',3' in Fig. 22 and they are identically zero on the interior of 1',2',3', being nonzero only on certain regions on the exterior. Hence, this is the part of the representation (4.2-14) which proceeds the circular wave front and, along with the remaining terms in (4.2-15), this makes 1',2' the only wave front in the plate which is singular as the front is approached from both sides. This is usually called the two-sided equivoluminal (or shear) wave.

All of the remaining terms in (4.2-14), other than the delta function terms in (4.2-15), are Cauchy principal value integrals due to the presence of the generalized functions $\cot\frac{\pi}{2}\Psi_{e\ell pq}$, $\csc\frac{\pi}{2}\Psi_{e\ell pq}$, etc., and they are not so convenient to evaluate. An example is considered here to illustrate the Cauchy principal value integrals, and also to make a check with the amplitudes of the wave front expansions given by Rosenfeld [13].

The circular dilatational wave front 1,2 in Fig. 22 is considered. The singularity corresponding to this wave front has been found to be present in (4.2-14c) for I_{dd} with $p=q=0$ and $\ell=6,8$. Therefore, with $A'_{00}=1$ and the

particular values of $S_{1\ell}$ and $S_{2\ell}$ from (4.2-2a), the terms in the representation (4.2-14) for u_ξ which contain the circular dilatational wave front are

$$\frac{32\pi\mu\sqrt{a^2-1}}{aI}u_\xi' =$$

$$-P.V.\int_{\frac{a-1}{a+1}}^{1}\frac{(1+\chi)[\chi^2-2(1-2\nu)\chi+1]}{\chi^{\frac{3}{2}}D(\chi)}\left(e^{-\frac{1}{2}\Phi_{d600}}{}^{LogR}\tan\tfrac{\pi}{4}\Phi_{d600}\right.$$

$$\left. + e^{-\frac{1}{2}\Phi_{d800}}{}^{LogR}\cot\tfrac{\pi}{4}\Phi_{d800}\right)d\chi \quad . \qquad (4.2\text{-}22)$$

The prime on u_ξ' is a reminder that this term is only the part of u_ξ which contains this particular singularity. The term $\cot\frac{\pi}{4}\Phi_{d800}$ results from $S_{18}\csc\frac{\pi}{2}\Phi_{d800}+S_{28}\cot\frac{\pi}{2}\Phi_{d800}$ in (4.2-14c) and $S_{18}=S_{28}=1$ from (4.2-2a). The fact that the term is not singular at $\Phi_{d800}=4m+2$ merely shows that no wave front is present as a result of a loading at $\xi=0$ and $\zeta=-1$. Likewise, for the term $\tan\frac{\pi}{4}\Phi_{d600}$.

(4.2-22) is only a part of the total response given approximately by (4.2-14), however, no further approximations have been made and this single term is expected to be valid well behind each reflection of the circular dilatational wave front. Of course, convergence of the series

representation (4.2-14) is assumed here. Also, other terms in (4.2-14) are identified with singular wave fronts and they must be included to account for the response associated with these wave fronts.

From (4.2-11) the phase functions involved in (4.2-22) take the form

$$\Phi_{d\ell 00} = \frac{1}{\sqrt{B^2-\frac{a^2-1}{a^2}}}\left(\xi\sqrt{1-B^2}-\tau\right) + 1 - (-1)^{\frac{\ell}{2}}\zeta \qquad (4.2\text{-}23)$$

for $\ell=6,8$, and it is clear that $\Phi_{d\ell 00}\to-\infty$ as $B\to\frac{1}{a}\sqrt{a^2-1}$ $(\chi\to 1)$ if $\xi<a\tau$. Also, from (4.2-18), $\frac{d\Phi}{dB}d\ell 00=0$ at $B=\frac{1}{a^2\tau}\sqrt{a^4\tau^2-\xi^2}$ where $\Phi_{d\ell 00}=1-(-1)^{\frac{\ell}{2}}\zeta-\sqrt{a^2\tau^2-\zeta^2}$ from (4.2-23), and this is easily verified to be a maximum of the phase functions.

The portion of (4.2-22) containing Φ_{d800} can be written as

$$\text{P.V.}\int_{\frac{a-1}{a+1}}^{1} F(\chi)\cot\tfrac{\pi}{4}\Phi d\chi = \text{P.V.}\int_{1-\zeta-a\tau}^{1-\zeta-\sqrt{a^2\tau^2-\xi^2}} F(\chi_1(\Phi))\left(\frac{d\chi_1}{d\Phi}\right)\cot\tfrac{\pi}{4}\Phi d\Phi$$

$$- \text{P.V.}\int_{-\infty}^{1-\zeta-\sqrt{a^2\tau^2-\xi^2}} F(\chi_2(\Phi))\left(\frac{d\chi_2}{d\Phi}\right)\cot\tfrac{\pi}{4}\Phi d\Phi \qquad (4.2\text{-}24)$$

where $\chi_1(\Phi)$ and $\chi_2(\Phi)$ are the appropriate inverses of (4.2-23). For $4m+2 \leq 1-\zeta-\sqrt{a^2\tau^2-\xi^2} \leq 4m-2$ for a particular integer m, the second integral in (4.2-24) must be interpreted as

$$\text{P.V.}\int_{4m-2}^{1-\zeta-\sqrt{a^2\tau^2-\xi^2}} F(\chi_2(\Phi))\left(\frac{d\chi_2}{d\Phi}\right)\cot\tfrac{\pi}{4}\Phi\,d\Phi$$

$$+\sum_{m'=-m}^{\infty}\text{P.V.}\int_{-4m'-6}^{-4m'-2} F(\chi_2(\Phi))\left(\frac{d\chi_2}{d\Phi}\right)\cot\tfrac{\pi}{4}\Phi\,d\Phi =$$

$$\text{P.V.}\int_{4m-2}^{1-\zeta-\sqrt{a^2\tau^2-\xi^2}} F(\chi_2(\Phi))\left(\frac{d\chi_2}{d\Phi}\right)\cot\tfrac{\pi}{4}\Phi\,d\Phi$$

$$-\frac{4}{\pi}\int_{-\infty}^{4m-2}\frac{d}{d\Phi}\left[F(\chi_2(\Phi))\left(\frac{d\chi_2}{d\Phi}\right)\right]\log\left|\sin\tfrac{\pi}{4}\Phi\right|d\Phi \quad . \qquad (4.2\text{-}25)$$

The last term in (4.2-25) is obtained by integrating by parts so that the result is an ordinary integral.

The interpretation of the principal value integrals suggested by (4.2-25) must be used on all of the

representations (4.2-14a),..., (4.2-14d) and (4.2-15) when the phase functions become unbounded since an infinite number of singularities are then present.

(4.2-25) is a convenient form since the first term along with the first term in (4.2-24) contain the singularity identified as a portion of the circular dilatational wave front. The part of the integral (4.2-22) containing Φ_{d600} contains the remaining portion of this wave front. If only the wave front expansion is required, these terms can be combined and approximated with the nonsingular part of the integrand being evaluated at $\Phi=1-(-1)^{\ell}\zeta-\sqrt{a^2\tau^2-\xi^2}$ where $\chi_1(\Phi)=\chi_2(\Phi)$.

As a specific example, the unreflected portion of the circular dilatational wave front is considered. This is seen in Fig. 22 continuing from the point 1 through the first thickness $-1\leq\zeta\leq 1$ on 1,2, and it is associated with the phase function $\Phi=\Phi_{d800}$ and the singularity of $\cot\frac{\pi}{4}\Phi$ at $\Phi=2m=0$. The approximation of (4.2-22) suggested in the preceding is

$$\frac{32\pi\mu\sqrt{a^2-1}}{aI}u_{\xi}' \cong$$

$$-2\frac{(1+\chi)[\chi^2-2(1-2\nu)\chi+1]}{\chi^{\frac{1}{2}}D(\chi)}\frac{\xi\sqrt{a^2\tau^2-\xi^2}}{a\tau\sqrt{a^4\tau^2-\xi^2}}e^{-\frac{1}{2}\left(1-\zeta-\sqrt{a^2\tau^2-\xi^2}\right)\text{LogR}_{I(\xi,\tau,\zeta)}} \tag{4.2-26}$$

where

$$I(\xi,\tau,\zeta) = \text{P.V.}\int_{-2}^{1-\zeta-\sqrt{a^2\tau^2-\xi^2}} \frac{\cot\frac{\pi}{4}\Phi}{\sqrt{(\Phi-1+\zeta)^2+\xi^2-a^2\tau^2}}d\Phi \qquad (4.2\text{-}26a)$$

and

$$\chi = \frac{1}{a^2(a^2-1)\tau^2}\left(\sqrt{a^4\tau^2-\xi^2} - \sqrt{a^2\tau^2-\xi^2}\right)^2 \quad . \qquad (4.2\text{-}26b)$$

The singular term $\left[(\Phi-1+\zeta)^2+\xi^2-a^2\tau^2\right]^{-\frac{1}{2}}$ in (4.2-26a) results from the derivative $\frac{d\chi_1}{d\Phi}$ in the first term of (4.2-24) and the derivative $\frac{d\chi_2}{d\Phi}$ in the first term of (4.2-25). The integral (4.2-26) is an approximation of the sum of these two terms.

It is worth mentioning that, while $\frac{d\Phi}{d\chi}=0$ identifies the wave front, $\frac{d^2\Phi}{d\chi^2}\neq 0$ at the point where $\frac{d\Phi}{d\chi}=0$ or at any other point except for the wave fronts where cancellation occurs between the wave fronts of $\Phi_{e\ell pq}$ and $\Phi_{d\ell pq}$.

The Cauchy principal value integral (4.2-26a) can be evaluated approximately by expanding $\cot\frac{\pi}{4}\Phi$ about $\Phi=0$ and assuming that $\left|1-\zeta-\sqrt{a^2\tau^2-\xi^2}\right| \ll 1$, which means that the

point ξ,ζ is near the wave front, to give

$$I(\xi,\tau,\zeta) \cong \frac{-4}{\sqrt{a^2\tau^2-\xi^2-(1-\zeta)^2}} H(a^2\tau^2-\xi^2-(1-\zeta)^2)$$

$$\cong \frac{-4}{a\sqrt{2\tau_0}\sqrt{\tau-\tau_0}} H(\tau-\tau_0)$$

where $H(\tau-\tau_0)$ is the Heaviside step function. Then (4.2-26), under the same approximation, becomes

$$u_\xi' \cong \frac{I}{2\pi\mu a\sqrt{2(a^2-1)}} \frac{(1+\chi)[\chi^2-2(1-2\nu)\chi+1]}{\chi^{\frac{1}{2}}D(\chi)} \frac{\xi(1-\zeta)}{\tau_0^{\frac{3}{2}}\sqrt{a^4\tau_0^2-\xi^2}} \frac{H(\tau-\tau_0)}{\sqrt{\tau-\tau_0}} \tag{4.2-27}$$

where

$$\tau_0 = \frac{1}{a}\sqrt{\xi^2+(1-\zeta)^2} \tag{4.2-27a}$$

is the arrival time of the wave front and χ is given by (4.2-26b) with τ replaced by τ_0.

The coefficient of $\frac{H(\tau-\tau_0)}{\sqrt{\tau-\tau_0}}$ in (4.2-27) is similar to the quantities that Rosenfeld [13] calculated except that the loading $\sigma_{\zeta\zeta}=-I\delta(\xi)H(\tau)$ at $\zeta=1$ replaces (2.1-7) in that work and the coefficient of the singular term of the dilatational potential ϕ is calculated rather than a

displacement term.

With $u_\xi' \cong A\frac{H(\tau-\tau_0)}{\sqrt{\tau-\tau_0}}$ representing (4.2-27), $u_\xi' \cong$ $2A\sqrt{\tau-\tau_0}\,H(\tau-\tau_0)$ is the approximate displacement for the loading $\sigma_{\zeta\zeta}=-I\delta(\xi)H(\tau)$ by using the convolution theorem of Laplace transforms. Also, $u_\xi \cong \frac{\partial\phi}{\partial\xi}$ from (2.2-1) is valid near the wave front since ψ is not singular and this can be integrated to give $\phi \cong -\frac{4}{3}\frac{a^2\tau_0}{\xi}A(\tau-\tau_0)^{\frac{3}{2}}H(\tau-\tau_0)$. This coefficient of $(\tau-\tau_0)^{\frac{3}{2}}H(\tau-\tau_0)$ checks with the data points given by Rosenfeld [13] for $\nu=0.3$ and $a\tau_0=8$ within the accuracy indicated in that work.

Detailed work on the dilatational wave fronts is actually more convenient if the variable $\frac{a\alpha}{\omega}=\frac{1}{2}\sqrt{a^2-1}\,\frac{1-\chi}{\chi^{\frac{1}{2}}}$ from (2.3-5) and (2.3-7) is used rather than χ or B defined by (4.2-10). B is best suited for study of the equivoluminal wave fronts.

The first reflection of the dilatational wave front 1,2 in Fig. 22 results from the part of (4.2-22) which contains Φ_{d600}. This wave front results from the singularity at $\Phi_{d600}=2m=-2$ where $e^{-\frac{1}{2}\Phi_{d600}\mathrm{Log}R}=R$. The fact that one reflection has introduced the factor R in the integrand at the wave front is consistent with the interpretation of R

as the reflection coefficient as suggested in Appendix A. Subsequent reflections of this circular wave front result from the singularities at $\Phi_{d800}=-4$, $\Phi_{d600}=-6$, etc., in (4.2-22) and this introduces $R^2, R^3, \ldots$ in the integrands at the wave fronts. The same is true for all of the factors $e^{\frac{1}{2}\Psi e\ell pq}{}^{LogR}$ and $e^{-\frac{1}{2}\Phi d\ell pq}{}^{LogR}$ in the representations (4.2-14b) and (4.2-14c) since, at the wave fronts, they result in the factors R^m, $m=0,1,2,\ldots$, in the integrands. Thus, in the preceding discussion about the geometry of the wave fronts as shown in Fig. 22, the integers m from $\Phi=2m$ in (4.2-19) are associated with the reflections of wave fronts.

These interpretations point out the importance of the term $\frac{LogR(\chi)}{1+\chi}$ in (3.3-3) for $\eta_{en}^{(0)}$ and $\frac{LogR(\chi)}{1-\chi}$ in (3.3-24) for $\eta_{dm}^{(0)}$ since they are the terms which give an accurate representation of the reflection process. In contrast, the first terms in (3.3-3) and (3.3-24) contain the branch numbers n and m and the summation over the branch numbers produce the generalized functions which lead to the wave fronts.

An interesting feature of the representation (4.2-14) is that the second term in (4.2-14a) on $\chi=e^{i\theta}$, $0\leq\theta\leq\pi$,

involves the terms $e^{-\pi(2p+2q+1\pm\zeta)\sqrt{\frac{a^2-1}{a^2}-B^2}}$ which result

from $e^{i\pi\Phi_{e\ell pq}}$ and the definition (4.2-11) for $\Phi_{e\ell pq}$. This is obviously an exponential dependence on the thickness variable ζ and it is related to the usual form of the dilatational potential ϕ which is associated with harmonic equivoluminal waves reflecting from a plane boundary at an angle of incidence greater than the critical angle

$$\tan^{-1}\frac{1}{\sqrt{a^2-1}} \quad .$$

The terms $\ell=1,3,5,7$ in (4.2-9) have not entered this discussion, however, they cannot be neglected. It is recalled that these terms are identified with singular wave fronts only for $\xi<0$. The terms could be estimated on the deformed paths shown in the second and third sketches of Fig. 21, however, it seems more practical to deform the integration paths C_E and C_D as follows: C_E is deformed onto $-1\leq\chi\leq\frac{a-1}{a+1}$ and C_D onto $-1\leq\chi\leq\frac{a-1}{a+1}$ plus $\chi=e^{i\theta}$, $0\leq\theta\leq\pi$. There are no difficulties at the singularities $\chi=\pm1$ due to the form of the phase functions for $\ell=1,3,5,7$ and the fact that $\xi>0$ has been specified.

The representation (4.2-14) is quite complex, however, it only involves explicit functions of χ and it offers direct access to the high-frequency response and the accompanying singular wave fronts. This is contrasted with the modal solution (2.3-15) in which the complete details of

the high-frequency response is all but invisible. In addition, the representation (4.2-14) is apparently considerably more accurate than wave front expansions, which are only valid near the fronts.

BIBLIOGRAPHY

1. Rosenfeld, R. L. and Miklowitz, J., "Wave Fronts in Elastic Rods and Plates," Proc. Fourth U.S. Nat Congr. Appl. Mech., New York, 1962, pp. 293-303.

2. Mindlin, R. D., "Waves and Vibrations in Isotropic, Elastic Plates," Structural Mechanics, First Symp. on Naval Struct. Mech., Pergamon Press, New York, 1960, pp. 199-232.

3. Miklowitz, J., "Transient Compressional Waves in an Infinite Elastic Plate or Elastic Layer Overlying a Rigid Half-Space," Trans. ASME, Vol. 84E (J. Appl. Mech.), 1962, pp. 53-60.

4. Mencher, A. G., "Epicentral Displacement Caused by Elastic Waves in an Infinite Slab," J. Appl. Phys., Vol. 24, 1953, pp. 1240-1246, 1529.

5. Broberg, K. B., "A Problem on Stress Waves in an Infinite Elastic Plate," Trans. Roy. Inst., Stockholm, Rep. No. 139, 1959.

6. Davids, N., "Transient Analysis of Stress-Wave Penetration in Plates," J. Appl. Mech., Vol. 26, 1959, pp. 651-660.

7. Miklowitz, J., "Elastic Wave Propagation," Applied Mechanics Surveys, Spartan Books, Wash., D.C., 1966, pp. 809-839.

8. Scott, R. A. and Miklowitz, J., "Transient Compressional Waves in an Infinite Elastic Plate with a Circular Cylindrical Cavity," Trans. ASME, Vol. 31E (J. Appl. Mech.), 1964, pp. 627-634.

9. Lighthill, M. J., Fourier Analysis and Generalized Functions, Cambridge University Press, London, 1964.

10. Holden, A. N., "Longitudinal Modes of Elastic Waves in Isotropic Cylinders and Slabs," Bell System Tech. J., Vol. 30, Pt. 1, 1951, pp. 956-969.

11. Alfors, L. V., Complex Analysis, McGraw-Hill Book Co., New York, 1953.

12. Onoe, M., McNiven, H. D. and Mindlin, R. D., "Dispersion of Axially Symmetric Waves in Elastic Rods," Trans. ASME, Vol. 84E (J. Appl. Mech.), 1962, pp. 729-734.

13. Rosenfeld, R. L., Analysis of Long Compressional Waves in Rods of Arbitrary Cross Section and Elastic Wave Fronts in Plates and Circular Rods, Ph.D. Thesis, California Institute of Technology, Pasadena, California, 1962.

14. Robbins, C. I. and Smith, R. C. T., "A Table of Roots of sinz=-z," Phil. Mag. (Ser. 7), Vol. 39, 1948, pp. 1004-1005.

15. Hillman, A. P. and Salzer, H. E., "Roots of sinz=z," Phil. Mag. (Ser. 7), Vol. 34, 1943, p. 575.

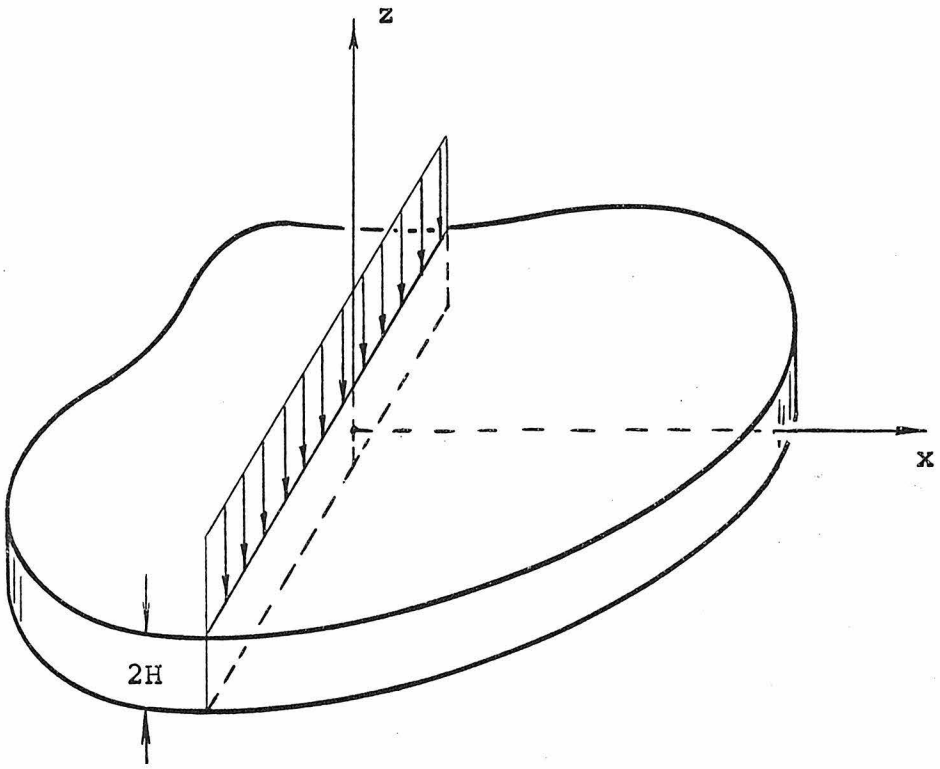

FIGURE 1

The Line Load Problem.

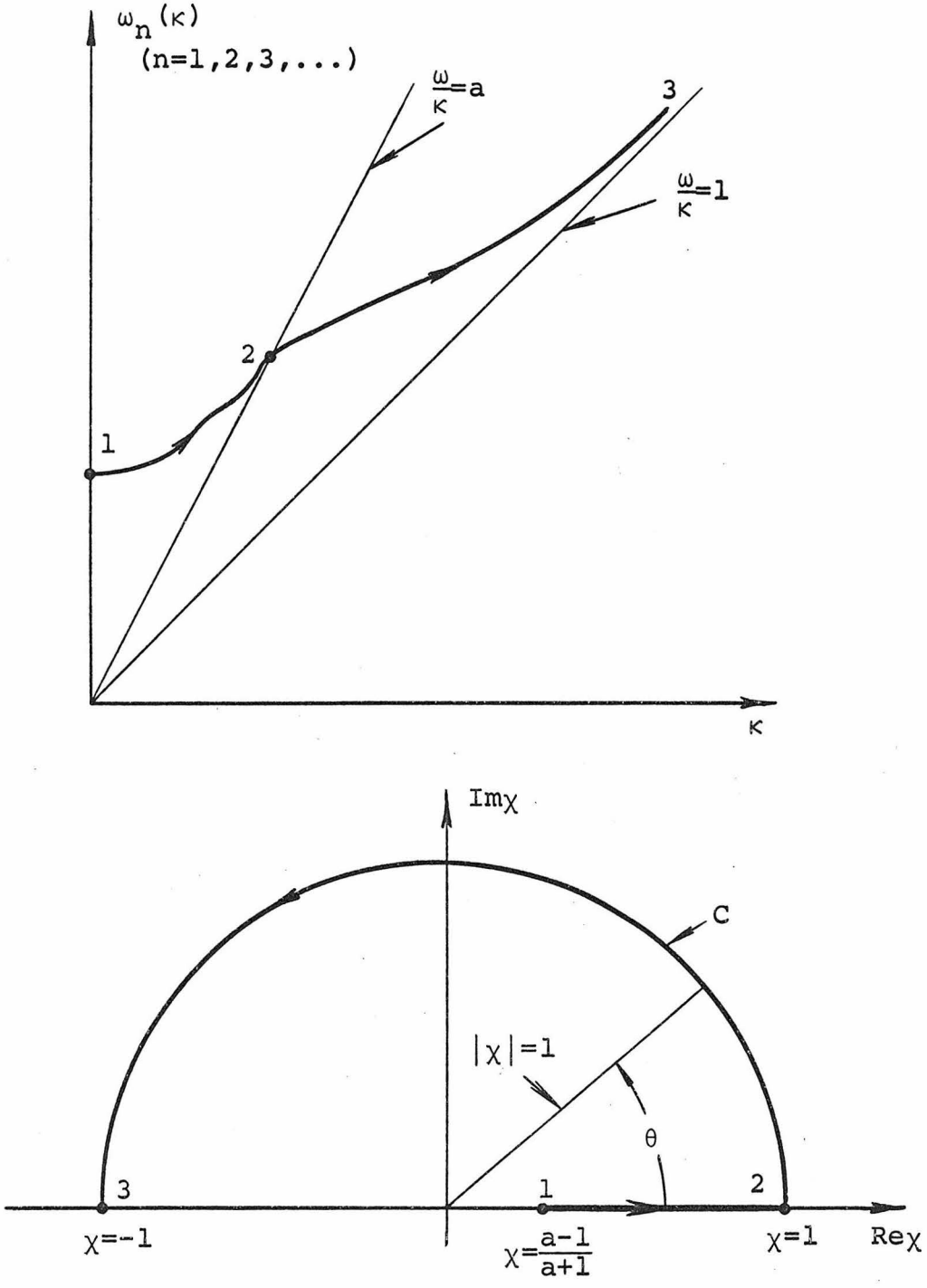

FIGURE 2

Mapping of the Real κ-Axis, $0 \to +\infty$, onto the Integration Path C in the χ-Plane.

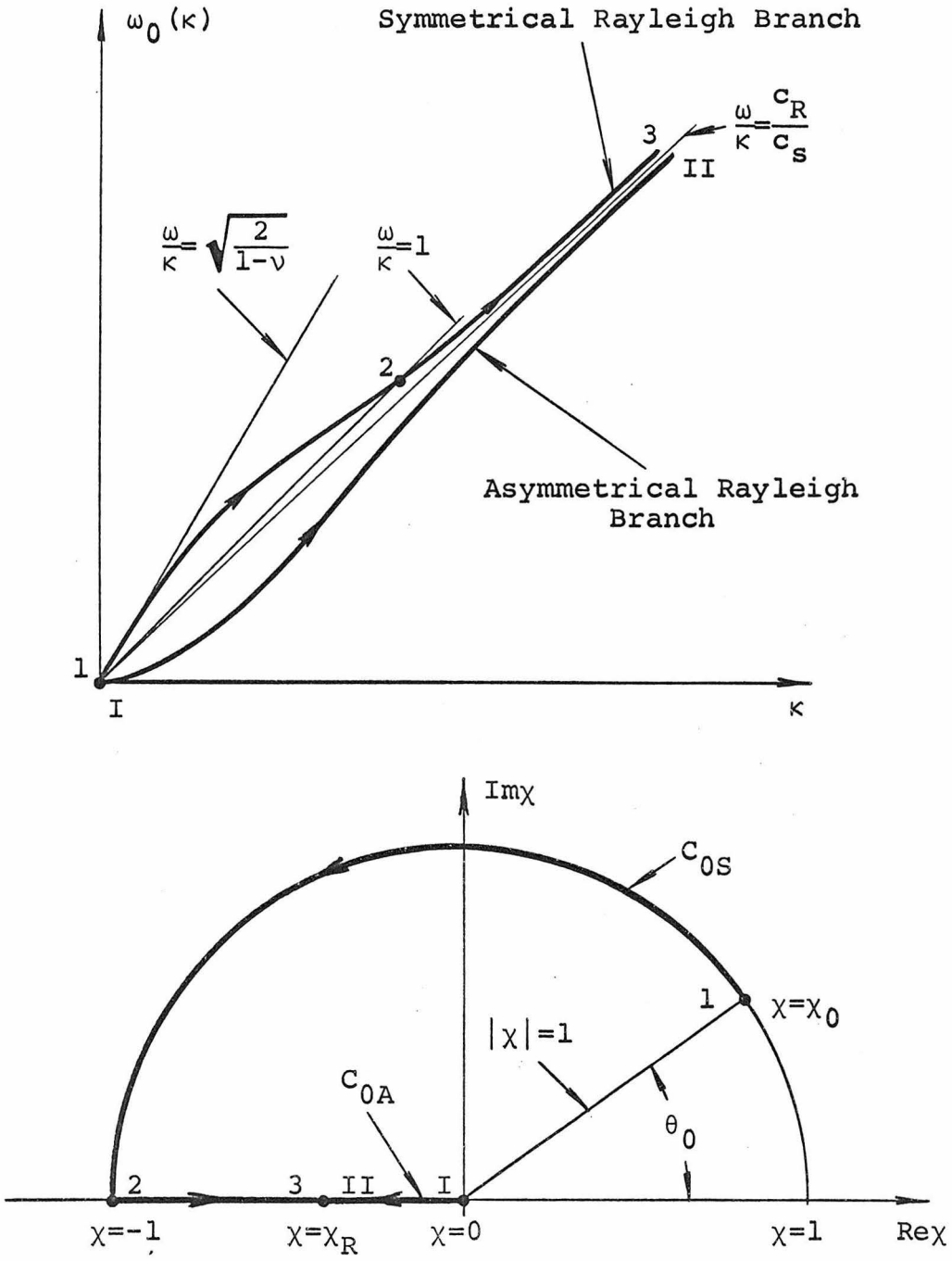

FIGURE 3

Mapping of the Real κ-Axis, $0\to+\infty$, onto the Integration Path C_{0S} for the Symmetrical Rayleigh Branch, and the Integration Path C_{0A} for the Asymmetrical Rayleigh Branch in the χ-Plane.

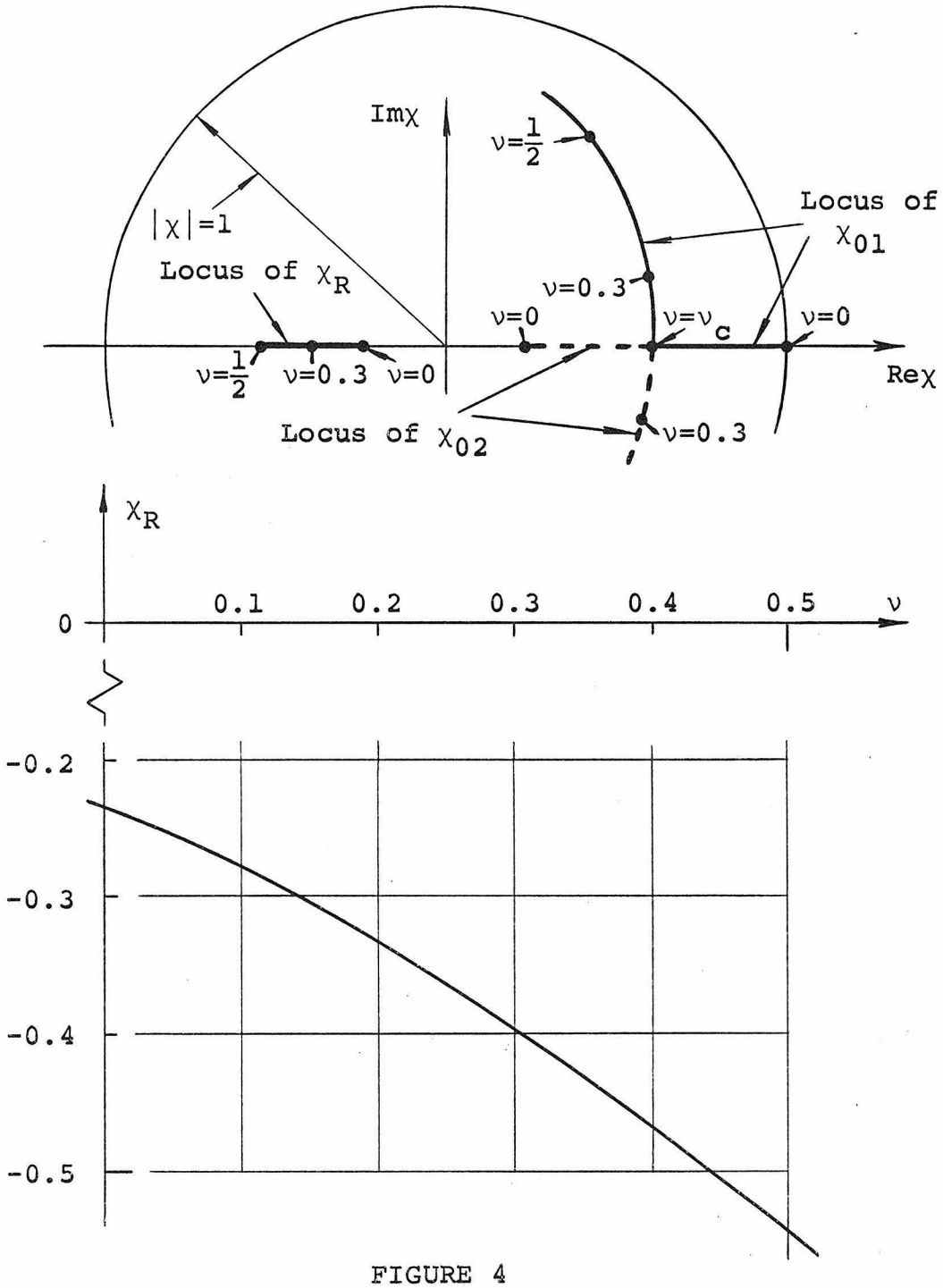

FIGURE 4

The Loci of χ_{01} and χ_{02}, where $R(\chi)=0$, and of χ_R, where $R(\chi)=\infty$, in the χ-Plane as Poisson's Ratio ν Varies. The Variation of χ_R with ν.

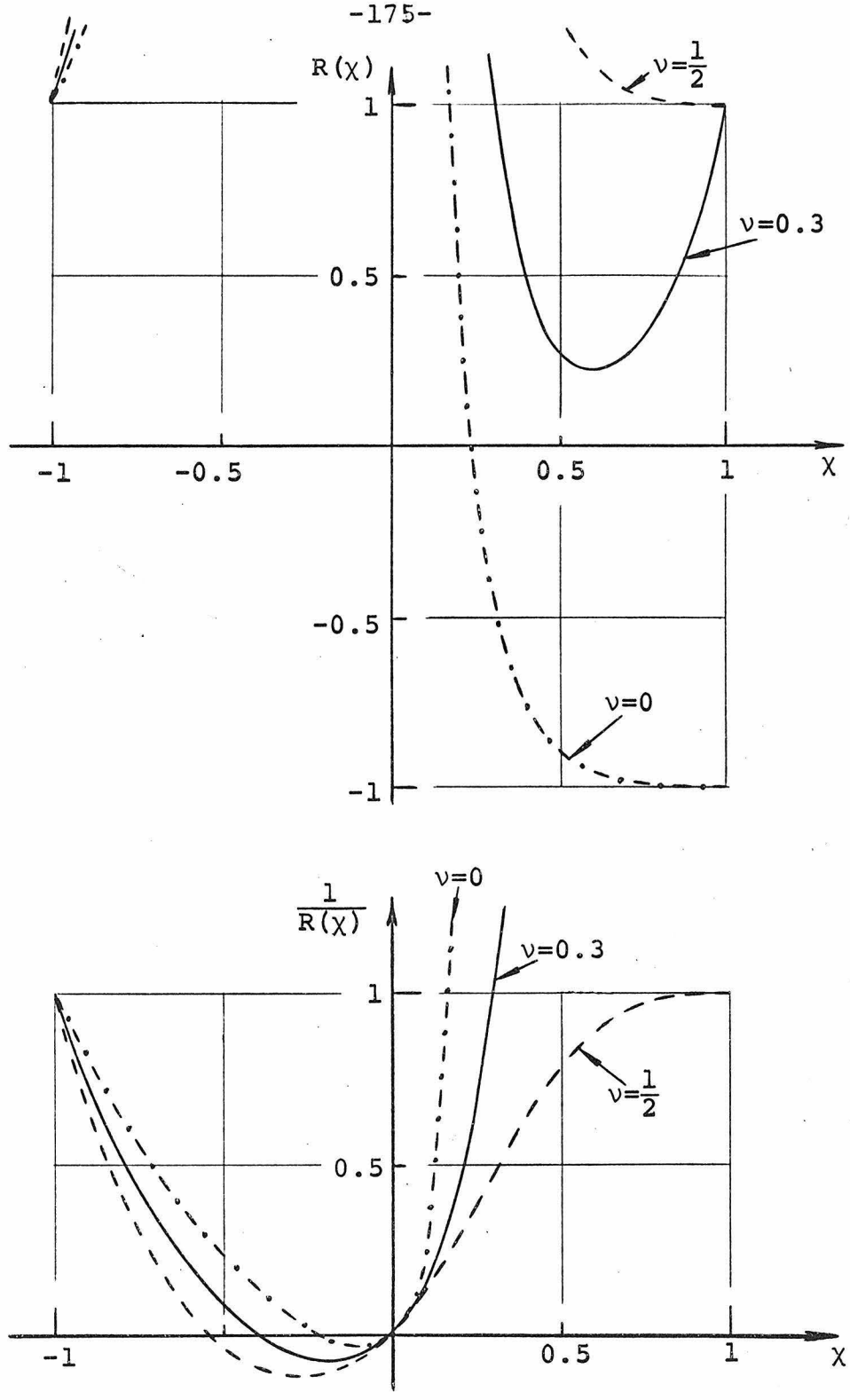

FIGURE 5

$R(\chi)$ and $[R(\chi)]^{-1}$ versus χ, $-1 \leq \chi \leq 1$, for $\nu = 0, 0.3, \frac{1}{2}$.

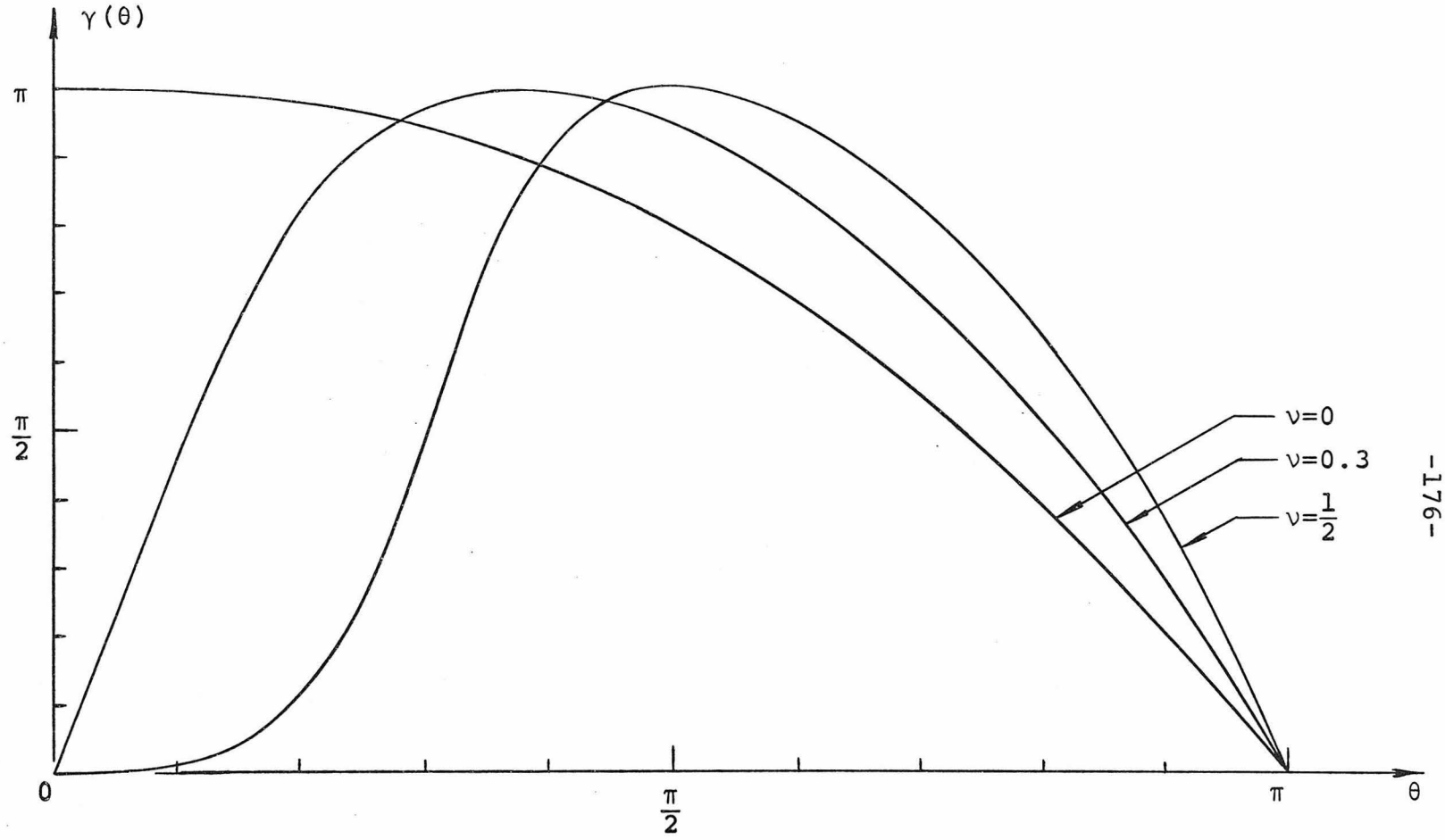

FIGURE 6

$\gamma(\theta)$, the Argument of $R(e^{i\theta})$, versus θ for $\nu=0, 0.3, \frac{1}{2}$.

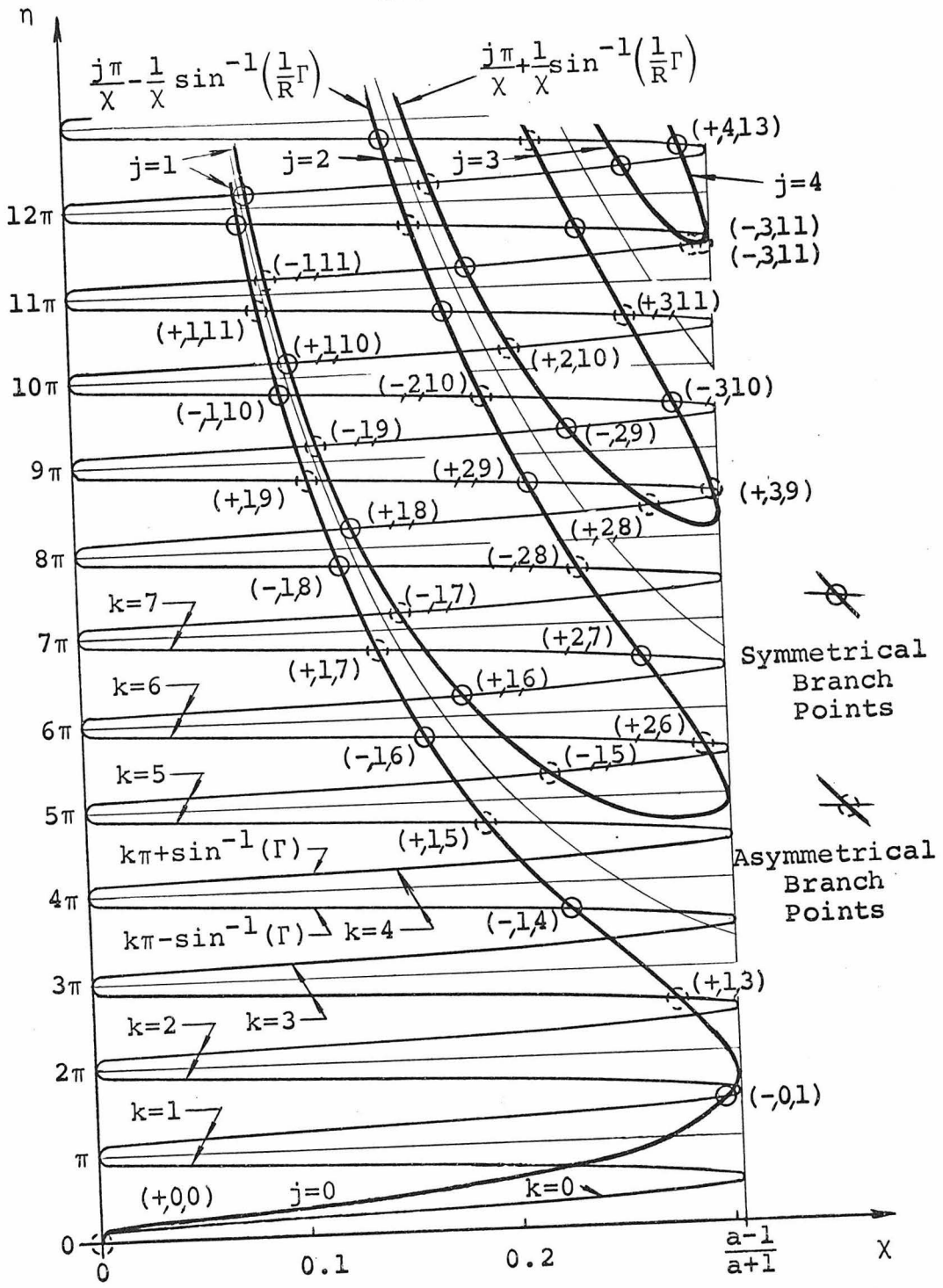

FIGURE 7

Branch Points of the Branches η on $0\leq\chi\leq\frac{a-1}{a+1}$ ($\nu=0.3$). The Triplets (±,j,k) Identify the Branch Points as Zeros of the Functions $\Delta^{\pm}_{jk}(\chi)$.

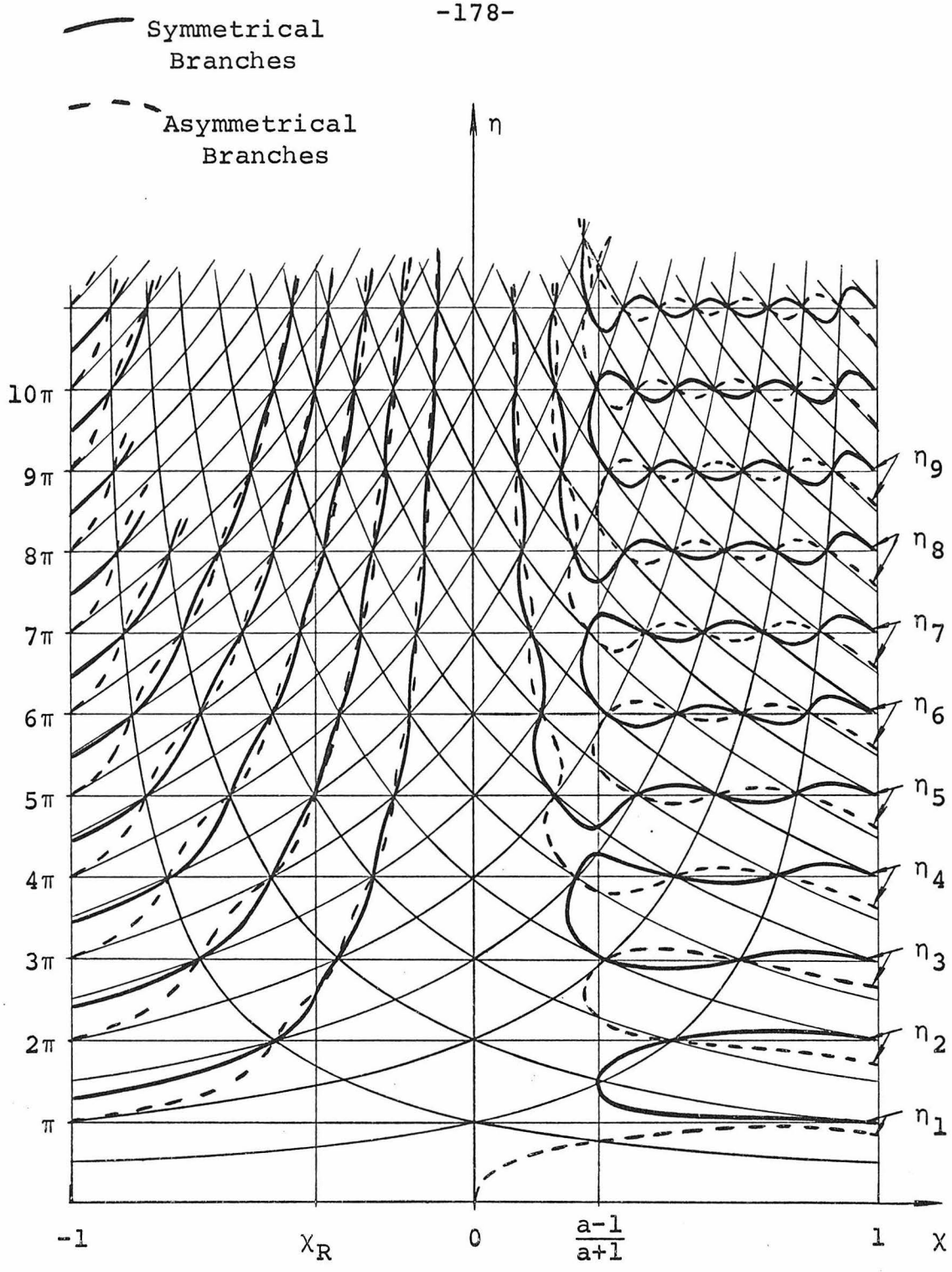

FIGURE 8

The Real Branches on the Real χ-Axis for $-1 \leq \chi \leq 1$ ($\nu=0.3$).

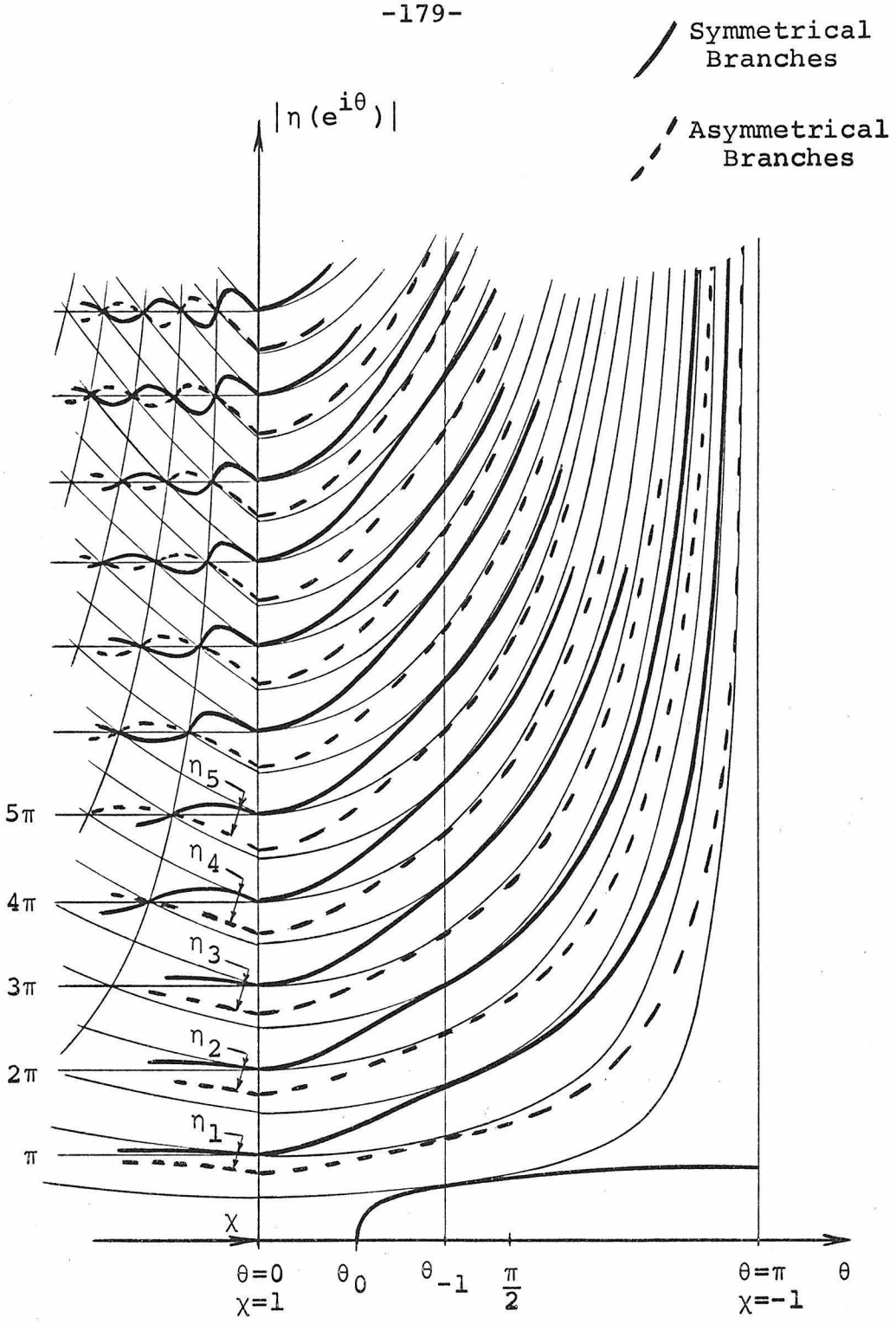

FIGURE 9

The Equivoluminal Branches on the Unit Circle $\chi=e^{i\theta}$ for $0\leq\theta\leq\pi$ ($\nu=0.3$).

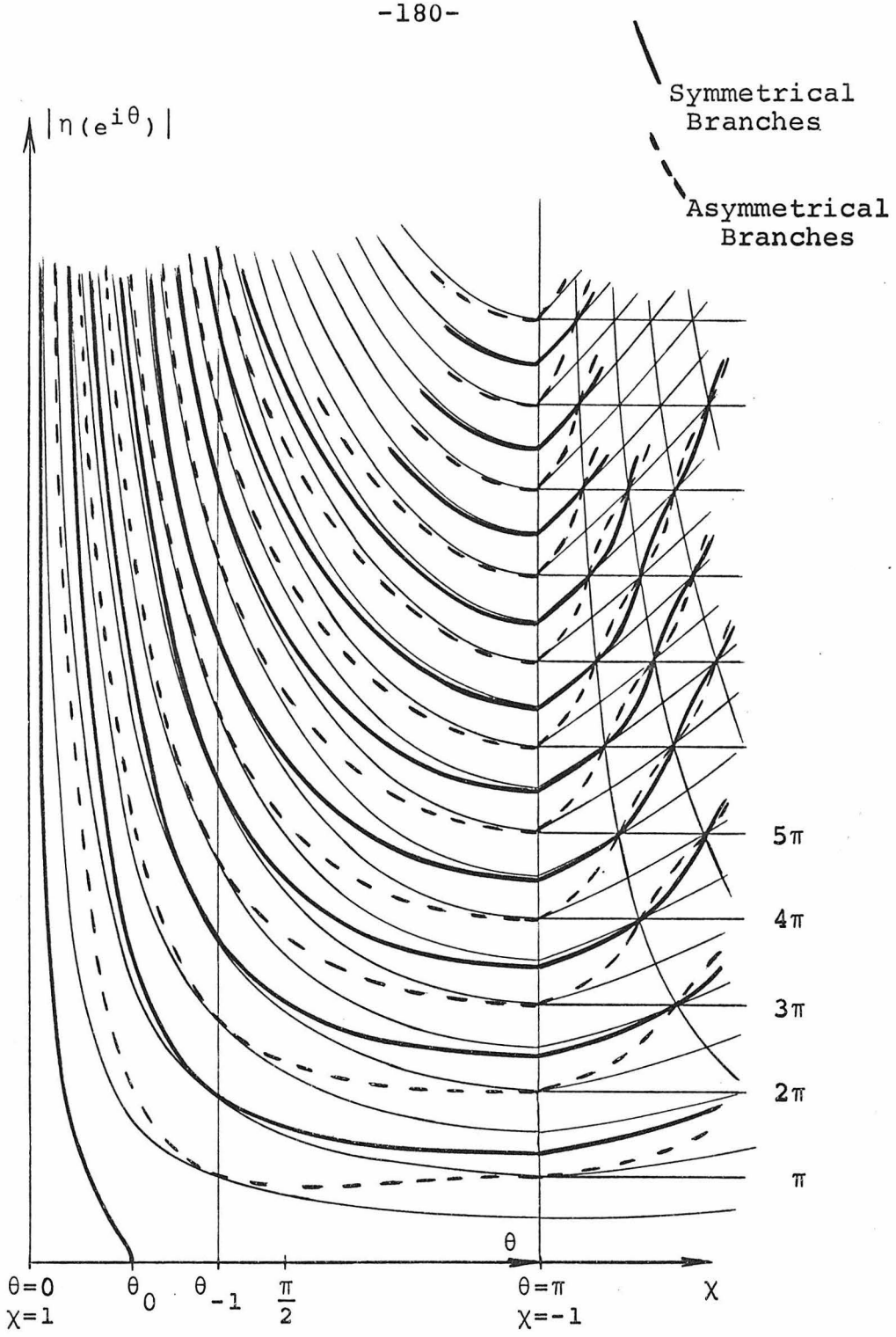

FIGURE 10

The Dilatational Branches on the Unit Circle $\chi=e^{i\theta}$ for $0\leq\theta\leq\pi$ ($\nu=0.3$).

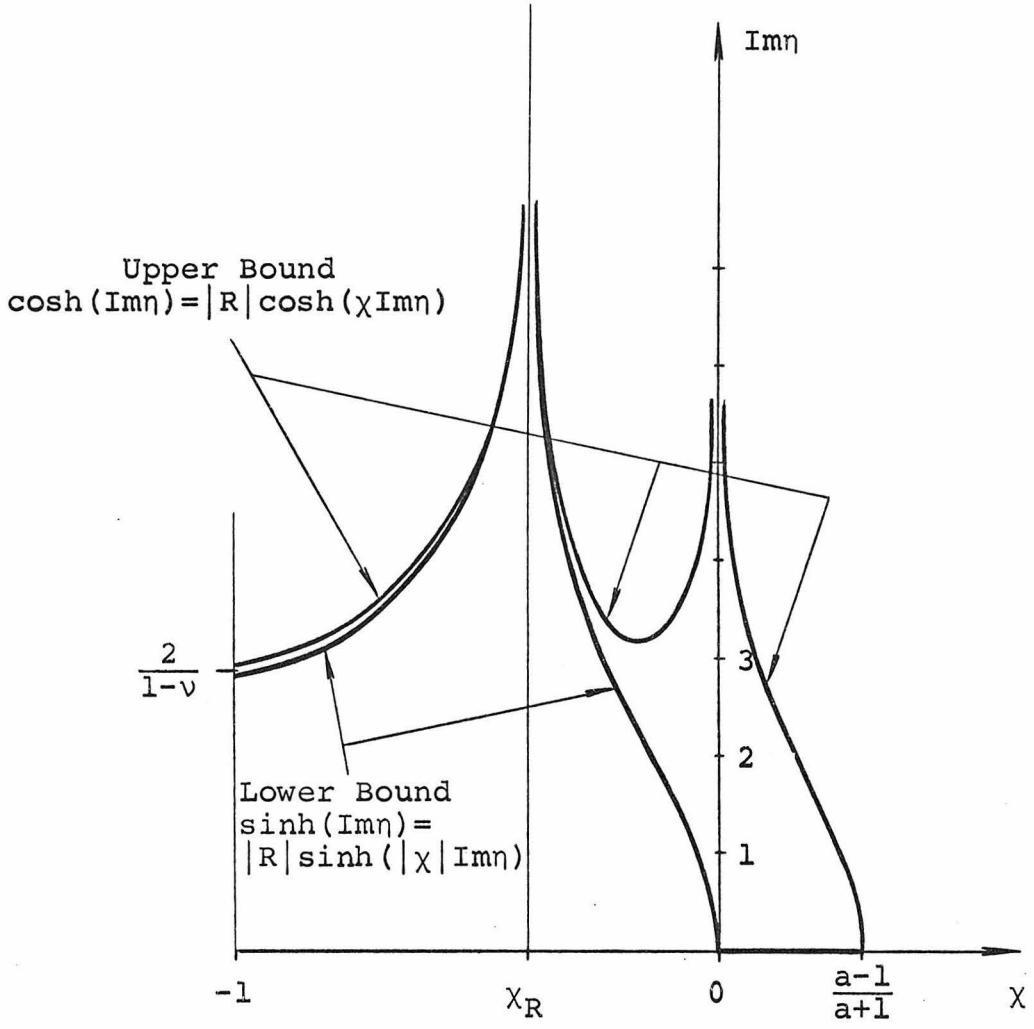

FIGURE 11

The Bounds on Imη (ν=0.3). The Lower Bound is a Portion of the Symmetrical Rayleigh Branch on $-1 \leq \chi < \chi_R$ and it is the Asymmetrical Rayleigh Branch on $\chi_R < \chi \leq 0$.

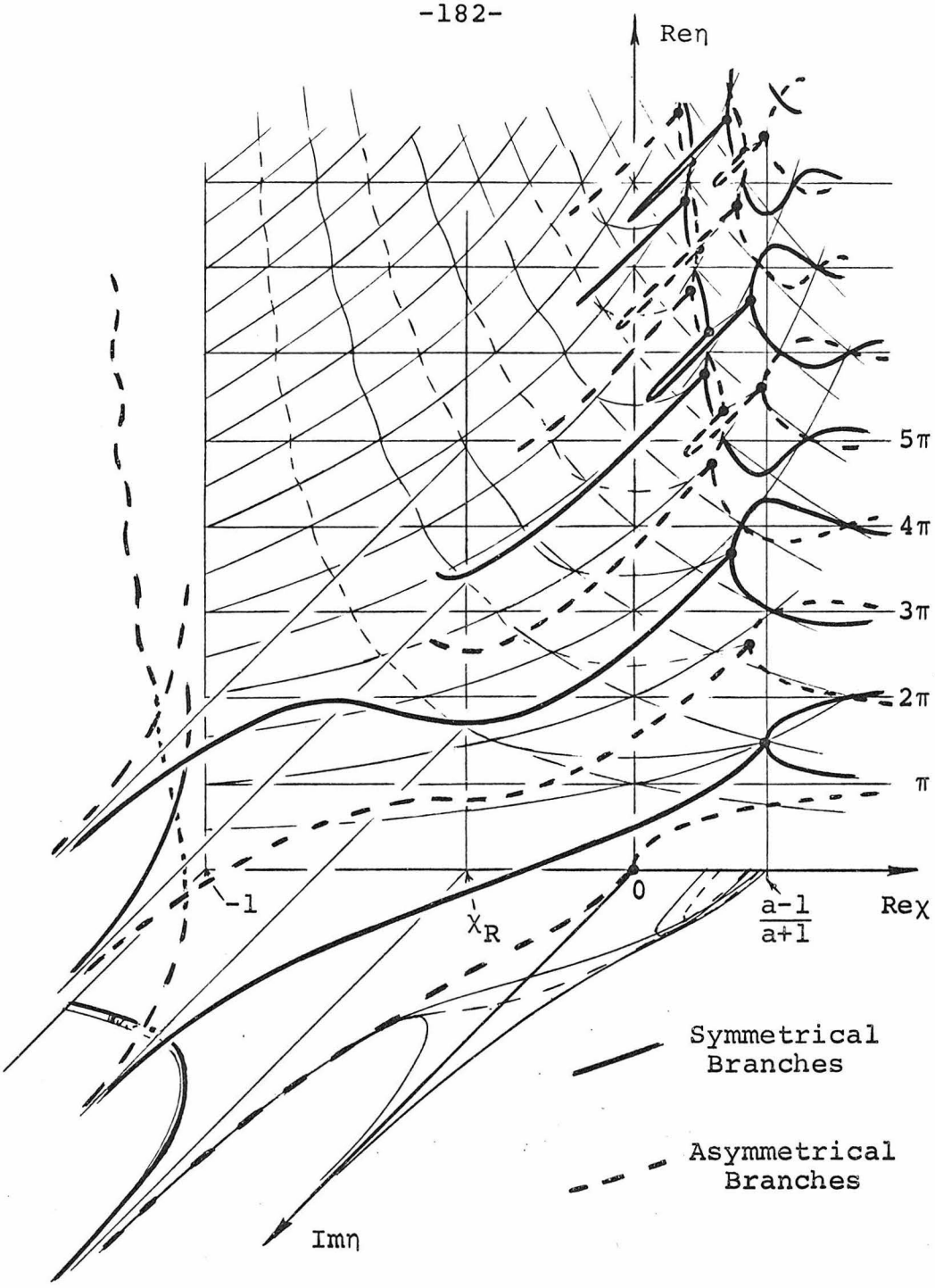

FIGURE 12

The Complex Branches on the Real χ-Axis for $-1 \leq \chi \leq \frac{a-1}{a+1}$ (ν=0.3).

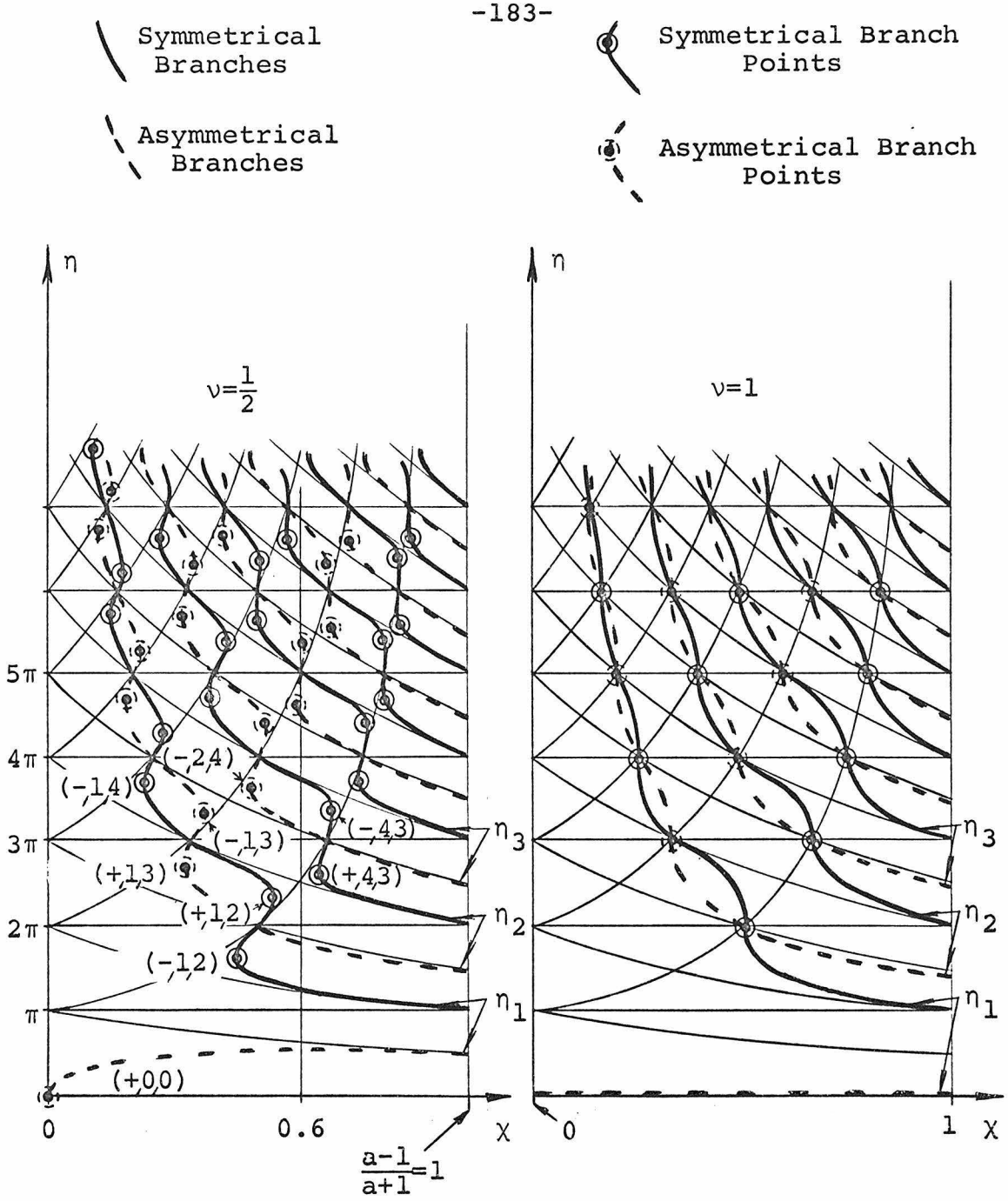

FIGURE 13

The Real Branches on $0 \leq \chi \leq 1$ for the Special Cases $\nu=\frac{1}{2}$ and $\nu=1$.

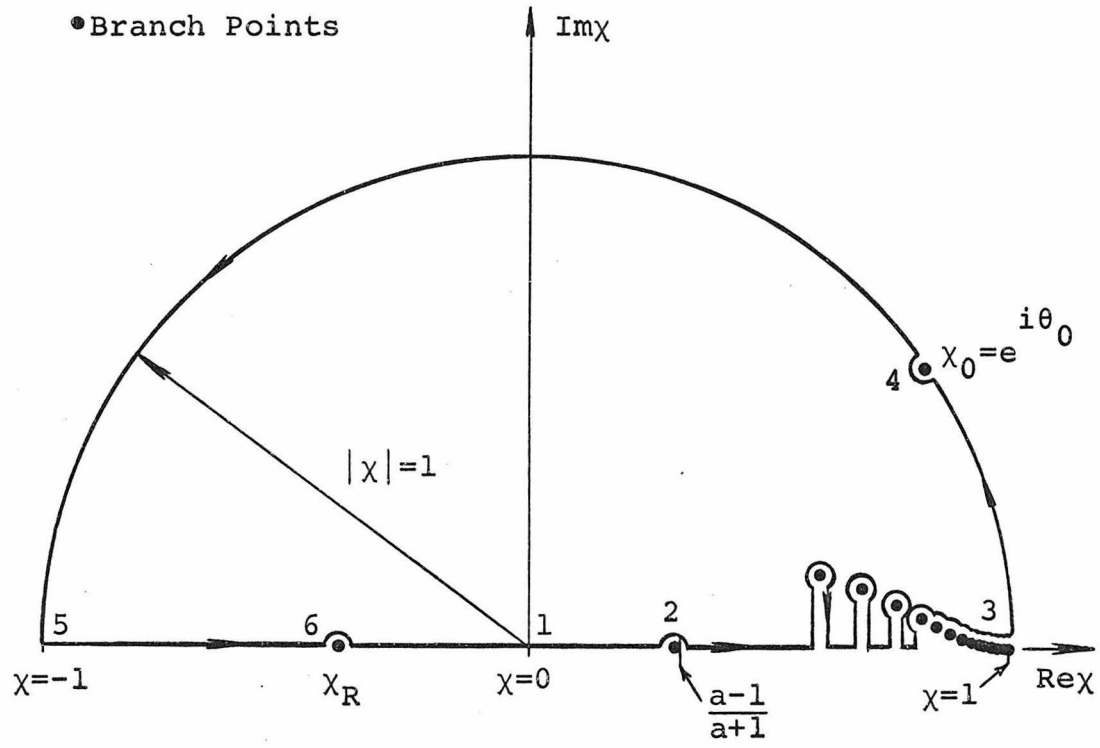

FIGURE 14

A Path in the χ-Plane for a Continuation Over Symmetrical Branches.

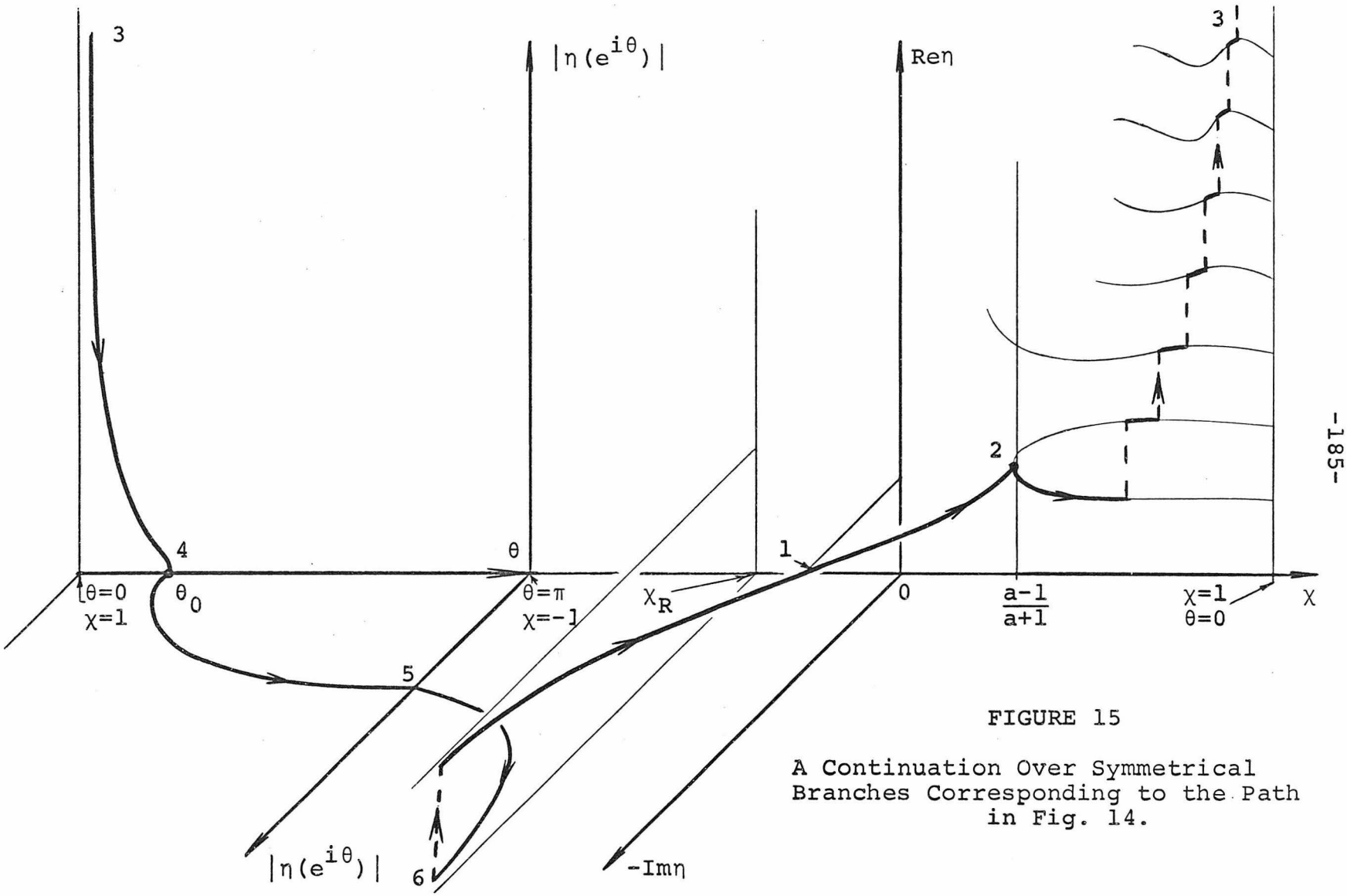

FIGURE 15

A Continuation Over Symmetrical Branches Corresponding to the Path in Fig. 14.

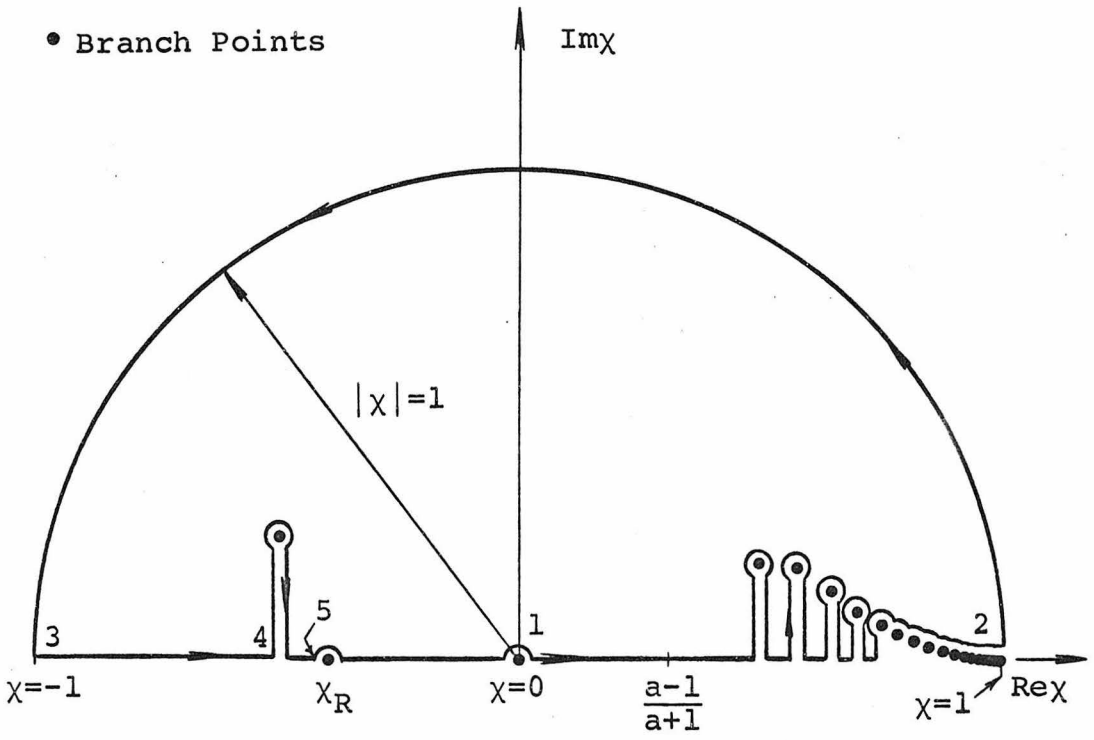

FIGURE 16

A Path in the χ-Plane for a Continuation Over Asymmetrical Branches.

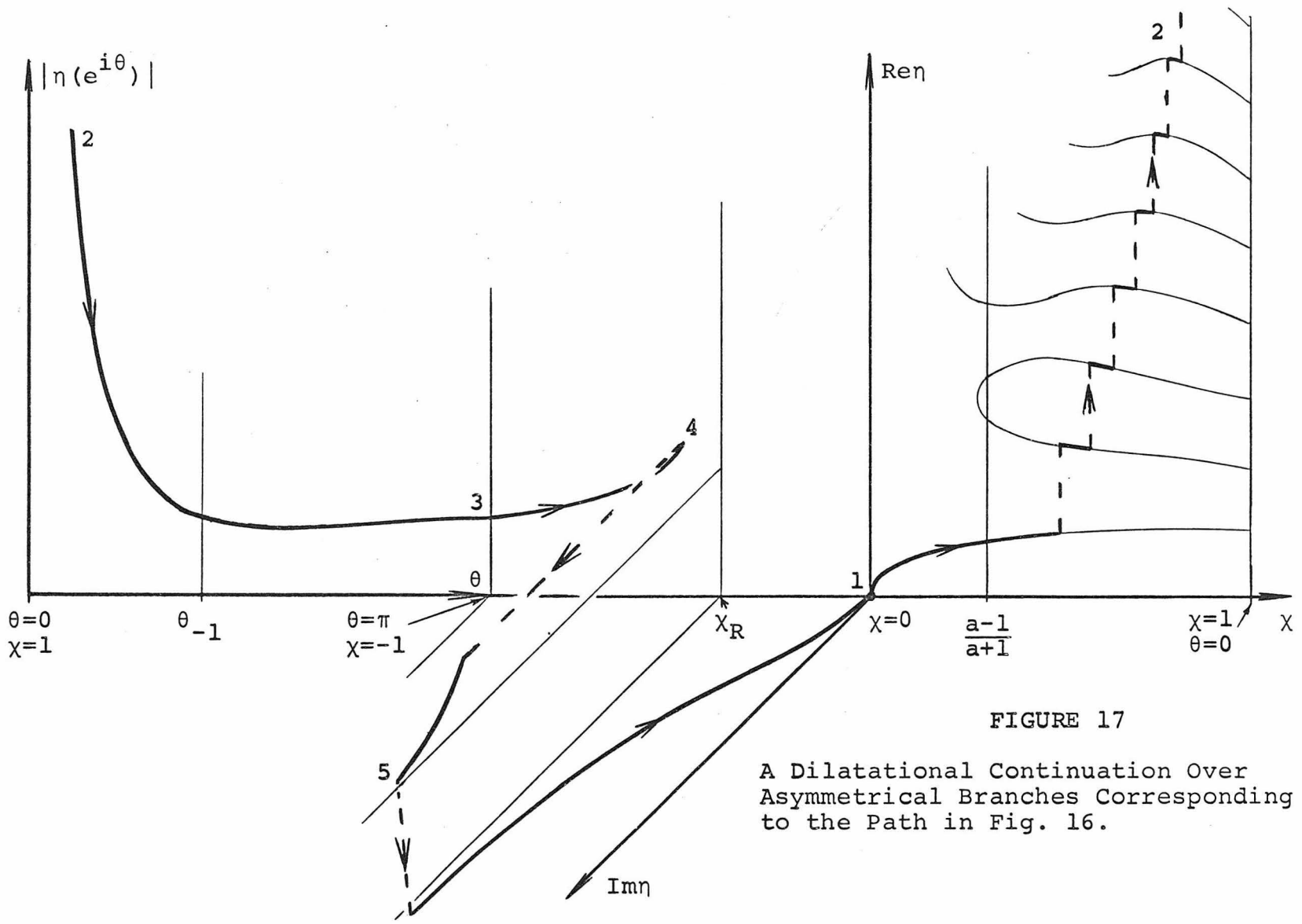

FIGURE 17

A Dilatational Continuation Over Asymmetrical Branches Corresponding to the Path in Fig. 16.

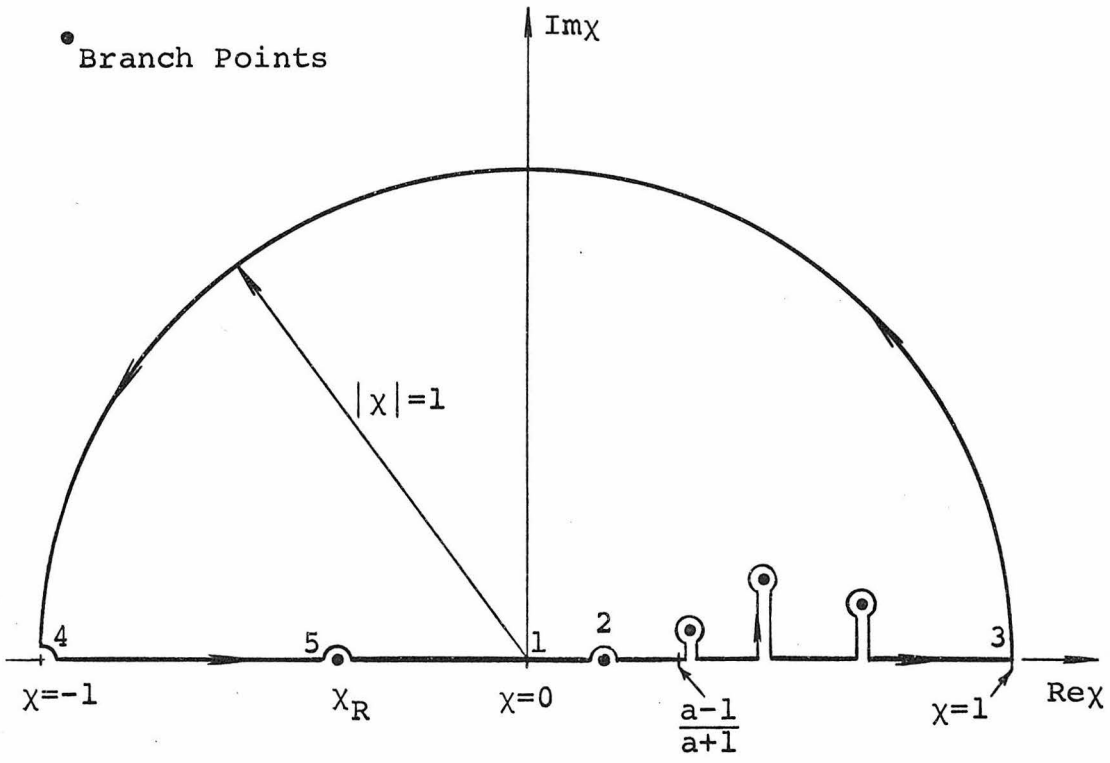

FIGURE 18

A Path in the χ-Plane for a Continuation Over Symmetrical Branches.

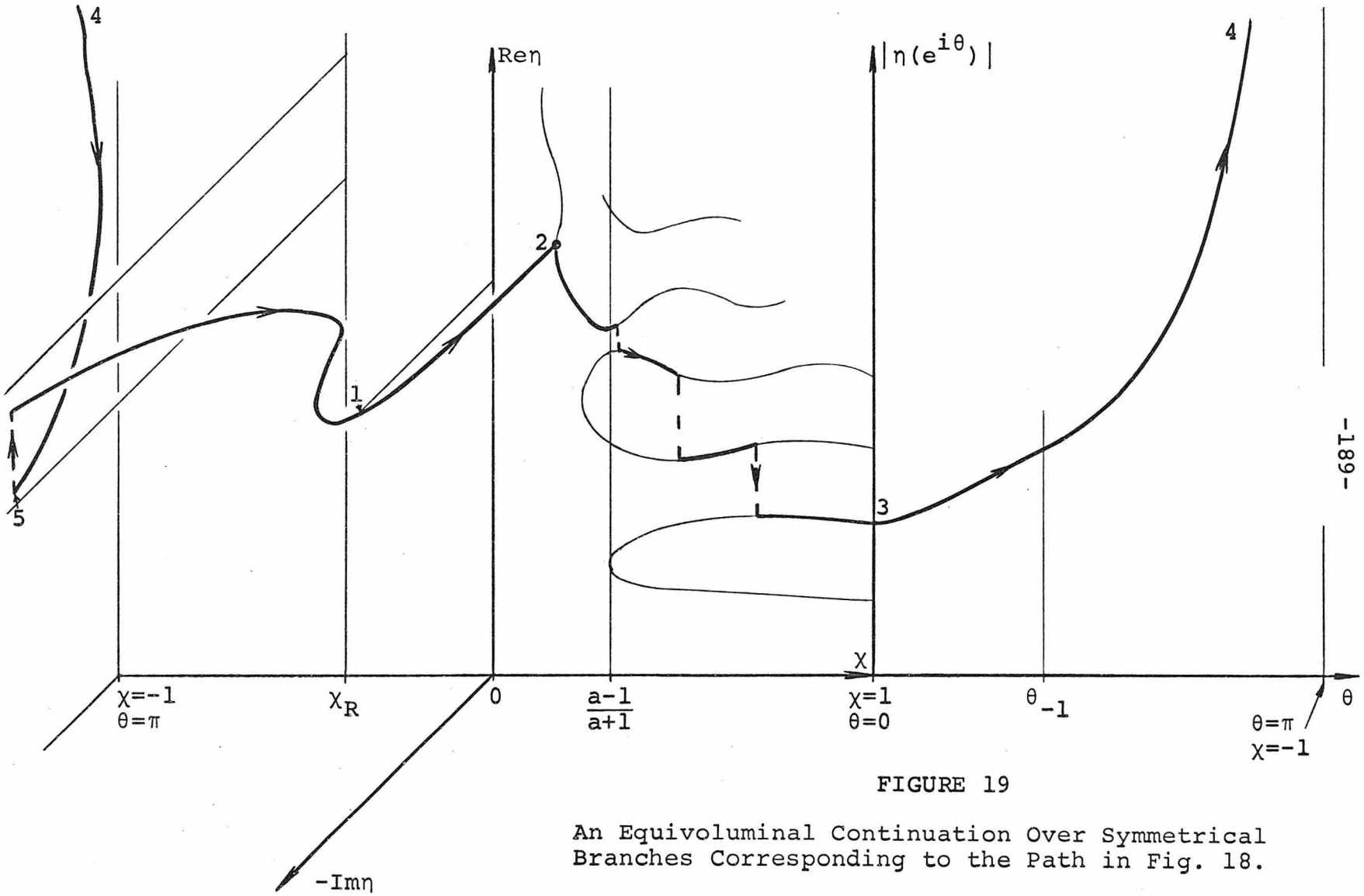

FIGURE 19

An Equivoluminal Continuation Over Symmetrical Branches Corresponding to the Path in Fig. 18.

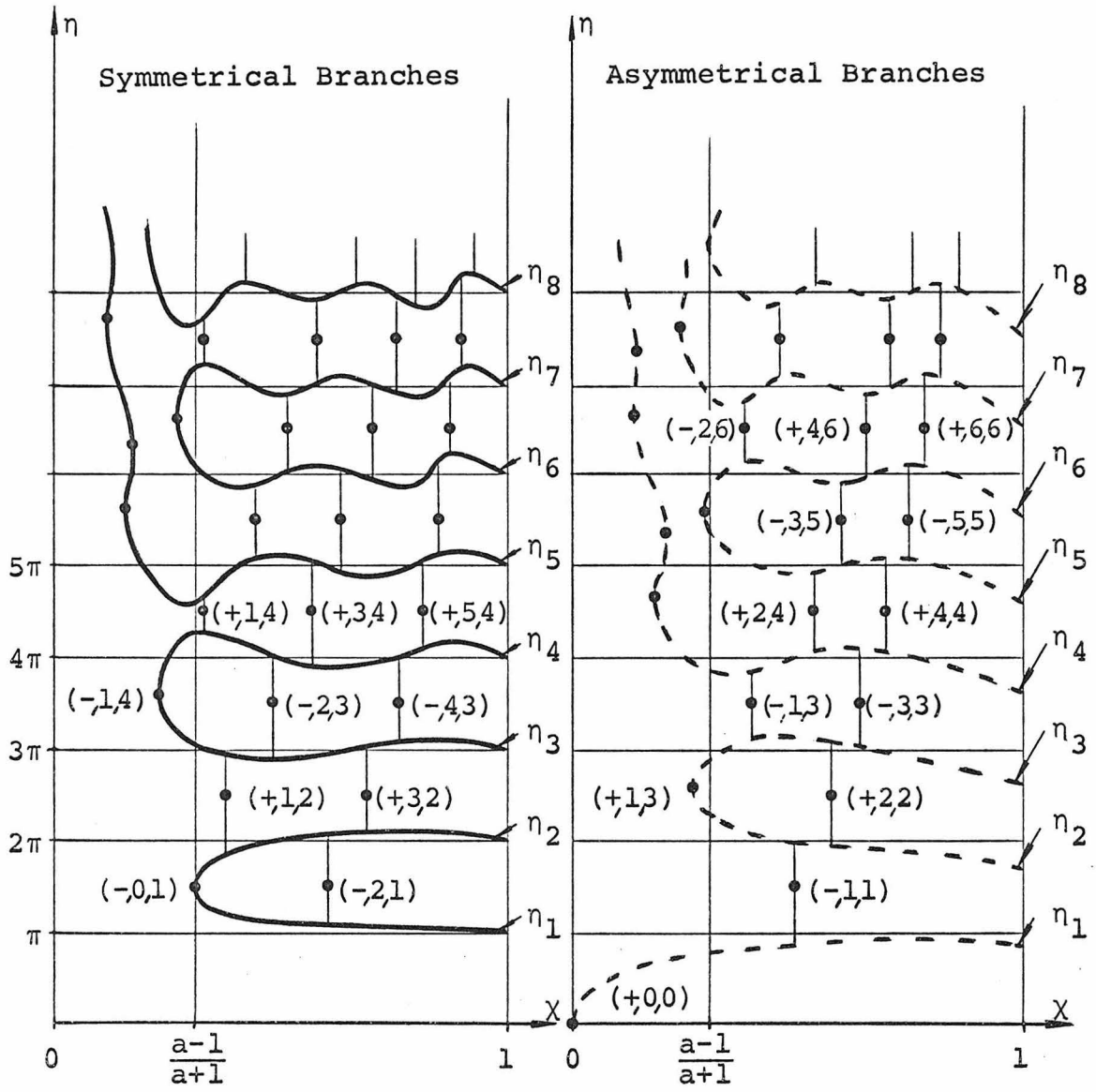

FIGURE 20

A Schematic Representation of the Branch Points Common to Pairs of Real Branches on $\frac{a-1}{a+1} \leq \chi \leq 1$ ($\nu=0.3$).

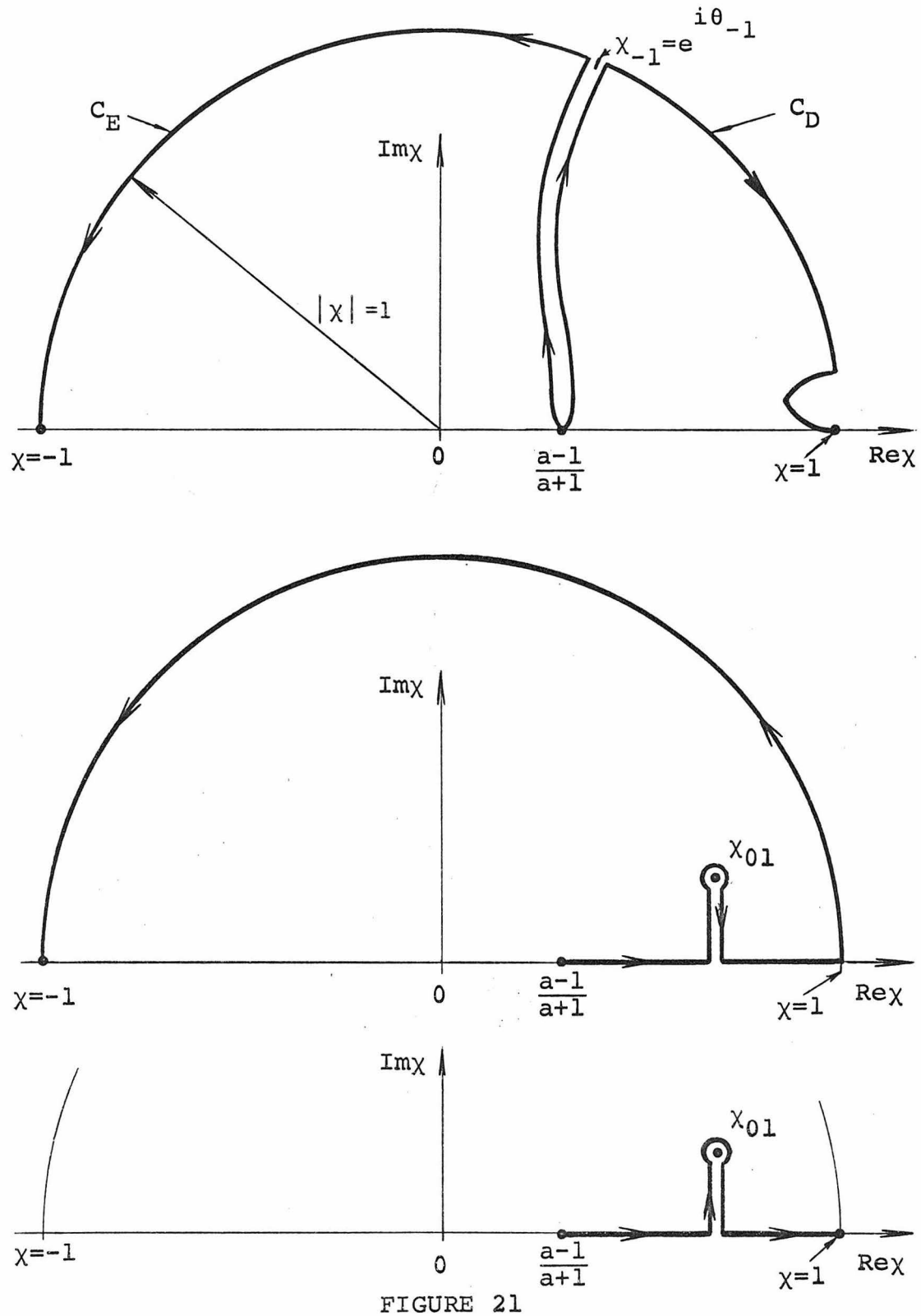

FIGURE 21

The Integration Paths C_E and C_D. A Deformation of C_E. A Deformation of C_D.

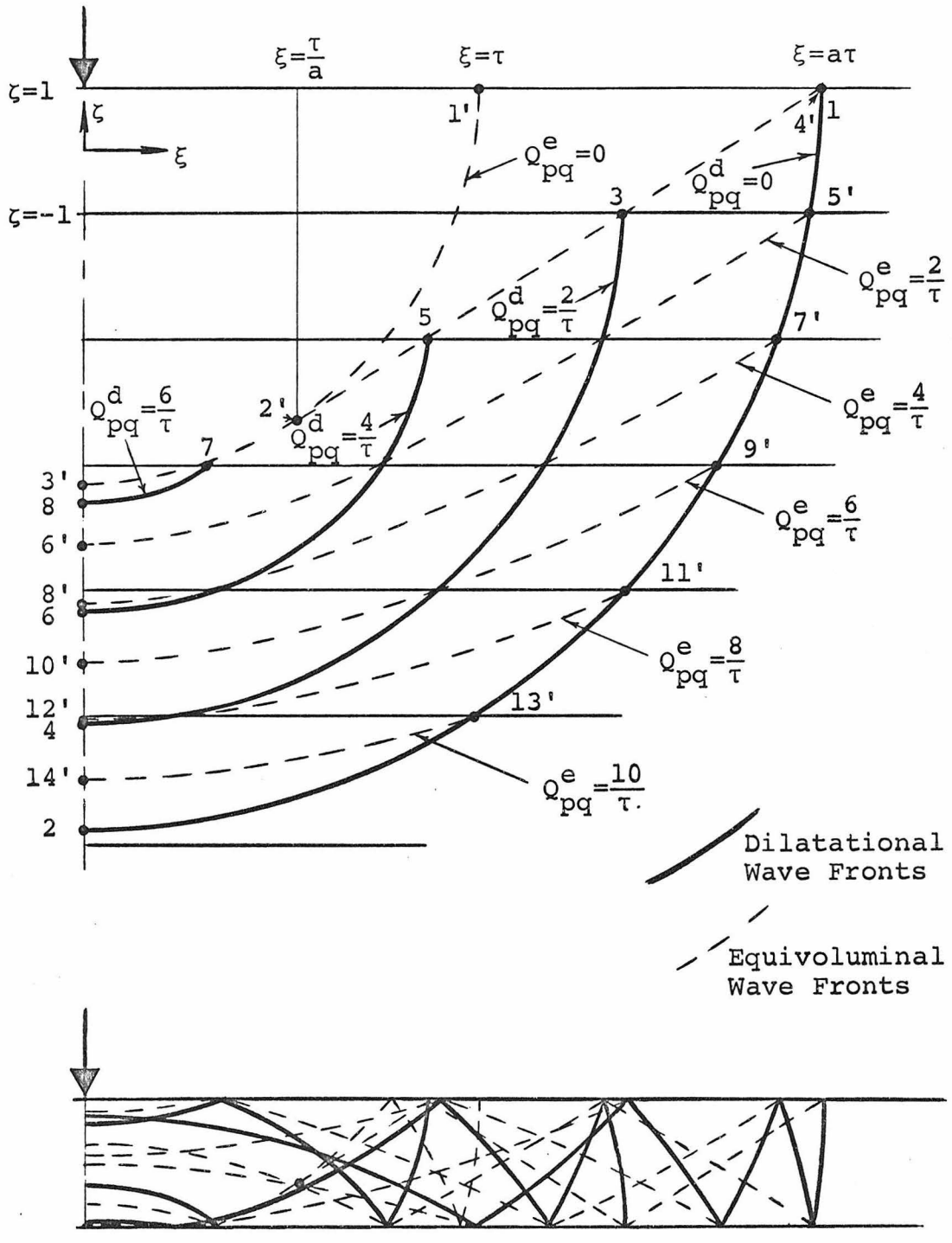

FIGURE 22

The Wave Fronts in the Plate at $\tau=6.3$ ($\nu=0.3$).

APPENDIX A

THE FUNCTION $R(\chi)$

The response of a plate to the loading (2.1-7) or to other loadings is completely characterized by the branches $\eta=\eta_n(\chi)$ through the modal solution (2.3-15). In turn, the branches η are completely characterized by the function $R(\chi)$ in (2.3-12a) through the frequency equations (2.3-13) and (2.3-14). Hence, it is necessary to know the behavior of R at all points where the behavior of η is required.

R is the same function which occurred in the wave front expansions given by Rosenfeld and Miklowitz [1]. It is interesting, in the context of that work and of the present work, that R is identical to the reflection coefficient giving the ratio of reflected to incident amplitudes of harmonic waves reflecting from a free boundary. R is a function of the angle of incidence by writing (2.3-12a) as a function of the phase velocity (2.3-1), which is given by $c_p=\frac{c}{\sin\theta_i}$ where c is the velocity of the body wave in question and θ_i is the angle of incidence measured from the normal of the boundary.

R is a rational function of both χ and ν and, therefore, it is analytic with respect to χ and ν except at the zeros of $[R]^{-1}$ (inspection shows that R is bounded and,

hence, analytic as $\chi\to\infty$ or as $\nu\to\infty$). These zeros of $[R]^{-1}$ and the points where R=0,1,-1, etc., are given in this appendix along with the behavior of R on the real χ-axis and on the unit circle $|\chi|=1$.

$R(\chi)$ can be written in several different forms each of which exhibits points in the χ-plane where it takes on special values. The notation which will be used for these points requires some explanation. Two points, χ_0 in (2.3-8) and χ_R in (2.3-9), have already been defined and the zero subscript means that this is the $\eta=0$ point of the symmetrical Rayleigh branch (the complex conjugate of χ_0 is also such a point). The R subscript refers to the fact that χ_R is the singular point of both Rayleigh branches where both ω and κ are unbounded (also, η is unbounded here). With respect to the function $R(\chi)$, it will be shown that $\chi R(\chi)=-1$ at $\chi=\chi_0$ and that $[R(\chi)]^{-1}=0$ at $\chi=\chi_R$. Other than for these two points, when a notation is required for a point, subscripts will refer to values taken by $R(\chi)$. For example, it will be seen that $R(\chi)=0$ at $\chi=\chi_{01},\chi_{02}$ and that $R(\chi)=-1$ at $\chi=\chi_{-1},\chi_{-1}^*$ (the notation χ^* is used for the complex conjugate of χ).

The forms taken by $R(\chi)$ are

$$
\left.
\begin{aligned}
R(\chi) &= \frac{1}{\chi D(\chi)}(\chi-\chi_{01})(\chi-\chi_{02})\left(\chi-\frac{1}{\chi_R}\right) \quad , \\
R-1 &= \frac{1}{\chi D(\chi)}(\chi^2-1)\left(\chi-\frac{a-1}{a+1}\right)\left(\frac{a+1}{a-1}-\chi\right) \quad , \\
R+1 &= \frac{1}{\chi D(\chi)}(\chi-\chi_{-1})^2(\chi-\chi_{-1}^*)^2 \quad , \\
\chi R-1 &= -\frac{8(1-\nu^2)}{D(\chi)}(1-\chi)\chi \quad , \\
\chi R+1 &= \frac{2}{D(\chi)}(1+\chi)(\chi-\chi_0)(\chi-\chi_0^*)
\end{aligned}
\right\} \qquad \text{(A-1)}
$$

where

$$
\chi_{-1} = e^{i\theta_{-1}} = 1 - 2\nu + 2i\sqrt{\nu(1-\nu)} \qquad \text{(A-1a)}
$$

so that $0\leq\theta_{-1}\leq\frac{\pi}{2}$ for $0\leq\nu\leq\frac{1}{2}$ ($\chi=\chi_{-1}$ maps into the Lamé point where $\omega=\sqrt{2}\kappa$), a is given by (2.1-2) with $3-2\sqrt{2}\leq\frac{a-1}{a+1}\leq 1$ for $0\leq\nu\leq\frac{1}{2}$ and $D(\chi)$ is given by (2.3-12b). Comparing the form of $R(\chi)$ in (A-1) with that in (2.3-12a), the points $\chi=\chi_{01},\chi_{02},\frac{1}{\chi_R}$ are obviously the zeros of $(1+\chi)^3-8(1-\nu)(1+\nu\chi)\chi$ and they will be discussed in more detail presently.

A useful property of R, which can be used in conjunction with the forms (A-1), is given by

$$
R\left(\frac{1}{\chi}\right) = [R(\chi)]^{-1} \qquad \text{(A-2)}
$$

and this results directly from (2.3-12a).

From (A-1) and (A-2), points in the χ-plane where R takes on special values are listed as follows:

$$
\left.
\begin{aligned}
&R = 1 \quad \text{at} \quad \chi = \frac{a+1}{a-1},\ 1,\ \frac{a-1}{a+1},\ -1 \quad ; \\
&R = -1 \quad \text{at} \quad \chi = \chi_{-1} = e^{i\theta_{-1}},\ \chi_{-1}^{*} \quad ; \\
&R = 0 \quad \text{at} \quad \chi = \chi_{01},\ \chi_{02},\ \frac{1}{\chi_R},\ \infty \quad ; \\
&[R]^{-1} = 0 \quad \text{at} \quad \chi = \chi_R,\ \frac{1}{\chi_{01}},\ \frac{1}{\chi_{02}},\ 0 \quad ; \\
&\chi R = 1 \quad \text{at} \quad \chi = 0,\ +1 \quad ; \\
&\chi R = -1 \quad \text{at} \quad \chi = -1,\ \chi_0 = e^{i\theta_0},\ \chi_0^{*} \quad .
\end{aligned}
\right\} \qquad \text{(A-3)}
$$

The three points $\chi=\chi_R,\ \frac{1}{\chi_{01}},\ \frac{1}{\chi_{02}}$ are roots of $D(\chi)=0$ with χ_R defined by (2.3-9). The loci of χ_R, χ_{01} and χ_{02} in the χ-plane and the variation of χ_R with ν for $0\leq\nu\leq\frac{1}{2}$ are shown in Fig. 4. The points χ_{01} and χ_{02} are identified by stating that $1\geq \mathrm{Re}\chi_{01}\geq \mathrm{Re}\chi_{02}>0$ and that $1>\mathrm{Im}\chi_{01}=\mathrm{Im}\chi_{02}\geq 0$ with the points being complex conjugates if $\nu_c<\nu\leq\frac{1}{2}$, real and equal if $\nu=\nu_c$, and real and unequal if $0\leq\nu<\nu_c$ where $\nu_c\cong 0.2631$. It is also true that $1\geq|\chi_{01}|\geq|\chi_{02}|>0$, the modulus being

equal to one only for χ_{01} with $\nu=0$. One exception to (A-3) occurs for $\nu=0$ in which case $\chi_{01}=\chi_{-1}=+1$ and $R(1)=-1$.

Derivatives of R with respect to χ at certain points are useful and they result directly from (A-1). Letting

$$R'(\chi_1)=\left.\frac{dR}{d\chi}\right|_{\chi=\chi_1},$$

$$\left.\begin{aligned}
&R'(1) = \frac{1-2\nu}{\nu^2} \quad \text{for} \quad 0 < \nu \leq \frac{1}{2} \ , \\
&R'(1) = 0 \quad \text{for} \quad \nu = 0 \ , \\
&R'\left(\frac{a-1}{a+1}\right) = -\frac{8(a+1)}{a^2(a-1)} \ , \\
&R'(-1) = \frac{2}{1-\nu} \ , \\
&R'(\chi_{-1}) = 0 \ , \\
&\left.\frac{d}{d\chi}\left(\frac{1}{R}\right)\right|_{\chi=0} = 1 \ , \\
&\left.\frac{d^2}{d\chi^2}\left(\frac{1}{R}\right)\right|_{\chi=0} = 16(1-\nu)^2 \ , \\
&\left.\frac{d}{d\chi}(\chi R)\right|_{\chi=0} = -8(1-\nu)^2 \ .
\end{aligned}\right\} \quad \text{(A-4)}$$

The forms in (A-1) and knowledge of the zeros of $D(\chi)$ determine the inequalities

$$\left.\begin{aligned} &-1 < R < 1 \quad \text{if} \quad \frac{a-1}{a+1} < \chi < 1 \quad , \\ &-1 < [R]^{-1} < 1 \quad \text{if} \quad -1 < \chi < \frac{a-1}{a+1} \quad , \\ &-1 < \chi R < 1 \quad \text{if} \quad 0 < \chi < 1 \quad , \\ &-1 < [\chi R]^{-1} < 1 \quad \text{if} \quad -1 < \chi < 0 \quad . \end{aligned}\right\} \tag{A-5}$$

The inequalities are evident in Fig. 5 where $R(\chi)$ and $[R(\chi)]^{-1}$ are sketched on the real χ-axis, $-1 \leq \chi \leq 1$, for the values $\nu = 0, 0.3, \frac{1}{2}$ of Poisson's ratio.

On the unit circle $\chi = e^{i\theta}$, $R(\chi)$ takes the simple form

$$R(e^{i\theta}) = e^{i\gamma(\theta)} \tag{A-6}$$

where

$$\gamma(\theta) = 2[\theta - \text{Arg}D(e^{i\theta})] \tag{A-6a}$$

with $D(\chi)$ given by (2.3-12b). For $0 \leq \theta \leq \pi$ and $0 < \nu \leq \frac{1}{2}$, $\gamma(\theta)$ satisfies $\gamma(-\theta) = -\gamma(\theta)$ and $0 \leq \gamma(\theta) \leq \pi$ with the equalities being taken only at $\theta = 0, \theta_{-1}, \pi$ where

$$\gamma(0) = \gamma(\pi) = 0, \quad \gamma(\theta_{-1}) = \pi \quad . \tag{A-7}$$

For the special case $\nu=0$ and the same range $0\leq\theta\leq\pi$, $\gamma(\theta)$ satisfies $\gamma(-\theta)=2\pi-\gamma(\theta)$ and $0\leq\gamma(\theta)\leq\pi$ with the equalities being taken only at $\theta=0,\pi$ where $\gamma(0)=\pi$, $\gamma(\pi)=0$. The function $\gamma(\theta)$ is sketched in Fig. 6 for $\nu=0,0.3,\frac{1}{2}$ and the angle $\theta_{-1}=\cos^{-1}(1-2\nu)$ is identified as the point where $\gamma(\theta_{-1})=\pi$ in each case.

There is an additional path, other than the unit circle $\chi=e^{i\theta}$, on which $|R|=1$. A portion of this path will be called C_1 and it connects the two points $\chi=\frac{a-1}{a+1}$ and $\chi=\chi_{-1}=e^{i\theta_{-1}}$ given by (A-1a). This can be shown by making local expansions of $R(\chi)$ about $\chi=\frac{a-1}{a+1}$ and $\chi=\chi_{-1}$ using $R\left(\frac{a-1}{a+1}\right)=1$ and $R(\chi_{-1})=-1$ from (A-3) and $R'(\chi_{-1})=0$ from (A-4). The path C_1 lies entirely interior to the quarter disk $\mathrm{Re}\chi>0$, $\mathrm{Im}\chi>0$, $|\chi|<1$, with the exception of its endpoints, for Poisson's ratio in $0\leq\nu\leq\frac{1}{2}$. Thus, since $|R(\chi)|=1$,

$$R(\chi) = e^{i\gamma_1(\chi)} \tag{A-8}$$

will be taken for the form of $R(\chi)$ when $\chi\in C_1$. The exact forms of C_1 and of the real function $\gamma_1(\chi)$ are very difficult to calculate, but, they are not important for this work. It can be stated with certainty that C_1 is a smooth path and that

$$\gamma_1(\chi_{-1}) = \pi, \quad \gamma_1\left(\frac{a-1}{a+1}\right) = 2\pi \quad . \tag{A-9}$$

Also, $\gamma_1(\chi)$ is a monatonic increasing function of χ for $\chi \in C_1$ (except at χ_{-1} where $\frac{dR(\chi_{-1})}{d\chi} = \frac{d\gamma_1(\chi_{-1})}{d\chi} = 0$ from (A-4)) as χ moves from χ_{-1} to $\frac{a-1}{a+1}$ on C_1. $\gamma_1(\chi)$ is monatonic on C_1 since, if it were not, there would be some point $\chi \in C_1$ $(\chi \neq \chi_{-1})$ where $\frac{dR(\chi)}{d\chi} = \frac{d\gamma_1(\chi)}{d\chi} = 0$. However, from the form (2.3-12a) of $R(\chi)$, there can be no more than six points where $\frac{dR(\chi)}{d\chi} = 0$, and it is obvious from Figs. 5 and 6 and from (A-2) and (A-6) that four such points are on the real χ-axis and that two more, χ_{-1} and χ_{-1}^*, are on the unit circle $|\chi| = 1$. Hence, there are no other points where $\frac{dR(\chi)}{d\chi} = 0$. One other aspect which clarifies (A-9) and helps to explain C_1 and $\gamma_1(\chi)$ is that, if χ traverses the closed path $\frac{a-1}{a+1} \to 1$ on the real χ-axis, $1 \to \chi_{-1}$ on the unit circle $|\chi| = 1$ and $\chi_{-1} \to \frac{a-1}{a+1}$ on C_1, then the argument of $R(\chi)$ increases by an amount 2π due to the presence of one simple zero of $R(\chi)$ at χ_{01}, which then must be interior to the closed path. This, of course, is with $\nu_c < \nu \leq \frac{1}{2}$ so that $\mathrm{Im}\chi_{01} > 0$ as shown in Fig. 4.

It is evident from the form (2.3-12a), showing that $R(\chi) = R^*(\chi^*)$, and from (A-2) that if χ is any point on C_1 then also $|R| = 1$ at the points χ^*, $\frac{1}{\chi}$ and $\frac{1}{\chi^*}$. This completes C_1 into a closed curve on which $|R(\chi)| = 1$.

APPENDIX B

ADDITIONAL INFORMATION ABOUT THE BRANCHES $\eta=\eta_n(\chi)$

B.1. THE BRANCHES AT SPECIAL POINTS

It is possible to find exact solution pairs χ,η of the frequency equations at some points in the χ-plane or for certain values of η. Such solution pairs will be helpful in understanding the branches η as continuous analytic functions of χ. The results for several points are listed here without indicating the simple calculations. Use has been made of the properties of the function $R(\chi)$ given in Appendix A and the property of analyticity of the branches as shown in Section 3.1.

(1) The case $\eta=0$.

The trivial solution $\eta\equiv 0$ for all χ is not interesting since it implies that $\omega=\kappa\equiv 0$ from (2.3-7). However, expansion of the symmetrical frequency equation shows that $|\eta|<<1$ is possible only near the points $\chi=\chi_0,\chi_0^*$ where $\chi R(\chi)=-1$ from (A-3). The expansion about $\chi=\chi_0$ is

$$\eta^2 = -\frac{3ie^{-2i\theta_0}}{\nu(1-\nu)}\sqrt{\frac{1+\nu}{1-\nu}}(\chi-\chi_0) + O\left(|\chi-\chi_0|^2\right)$$

$$= \frac{3e^{-i\theta_0}}{\nu(1-\nu)}\sqrt{\frac{1+\nu}{1-\nu}}(\theta-\theta_0) + O\left(|\theta-\theta_0|^2\right) , \qquad \text{(B.1-1)}$$

the second expression being specialized to $\chi=e^{i\theta}$ with $\theta\to\theta_0$. For $\theta>\theta_0$ this is obviously an expansion of the symmetrical Rayleigh branch $\eta_0(\chi)$ about the $\eta=0,\chi=\chi_0$ (or $\omega=\kappa=0$) point and, indeed, the branch has a square root branch point at $\chi=\chi_0$. For $\theta<\theta_0$, (B.1-1) gives a continuation of the symmetrical Rayleigh branch about the branch point.

Likewise, the asymmetrical frequency equation only admits branches with $|\eta|<<1$ near the point $\chi=0$. The expansion about $\chi=0$ takes the form

$$\eta^2 = 48(1-\nu)^2\chi + O(|\chi|^2) \quad . \tag{B.1-2}$$

For $\chi<0$ this is an expansion of the asymmetrical Rayleigh branch $\eta_0(\chi)$ about the $\eta=\chi=0$ (or $\omega=\kappa=0$) point and this branch has a square root branch point at $\chi=0$.

(2) The point $\chi=1$.

Directly from the symmetrical frequency equation (2.3-13), the branches take the values

$$\eta_n(1) = n\pi \quad , \quad n=1,2,3,\ldots, \tag{B.1-3}$$

and the branches are analytic at $\chi=1$ since the derivative (3.1-3) exists with $\left.\frac{d\eta_n(\chi)}{d\chi}\right|_{\chi=1}=-\frac{1}{2}n\pi$.

The asymmetrical frequency equation (2.3-14) can be rearranged and written as

$$\tan\eta = f(\chi,\eta)$$

where

$$f(\chi,\eta) = \frac{R\sin(\chi-1)\eta}{1-R\cos(\chi-1)\eta} \quad .$$

Assuming that bounded solutions η exist in a neighborhood of $\chi=1$ and using (A-4), results in

$$f(1,\eta) = -\frac{\eta}{R'(1)} = -\frac{\nu^2}{1-2\nu}\eta \quad .$$

Hence, asymmetrical solutions $\eta_n(1)$, n=1,2,3,..., exist and they satisfy

$$\tan\eta(1) = -\frac{\nu^2}{1-2\nu}\eta(1) \qquad \text{(B.1-4)}$$

from which $\eta_n(1)$ can be shown to be real. Only the positive set of solutions $\eta_n(1)$ satisfying $\frac{(2n-1)\pi}{2} \leq \eta_n(1) < n\pi$ for $0<\nu\leq\frac{1}{2}$ are taken, and

$$\eta_n(1) = \frac{(2n-1)\pi}{2} + \frac{2(1-2\nu)}{(2n-1)\pi\nu^2} + O(n^{-3})$$

for $n>>1$ and $0<\nu<\frac{1}{2}$.

The expression (3.1-4) for the derivative $\left.\frac{d\eta_n(\chi)}{d\chi}\right|_{\chi=1}$

of the asymmetrical branches takes the $\frac{0}{0}$ indeterminant form due to (B.1-4) and (A-4) and the derivative cannot be shown to exist from this form. However, the form $\tan\eta=f(\chi,\eta)$ of the asymmetrical frequency equation gives

$$\frac{d\eta}{d\chi} = \frac{\frac{\partial f}{\partial \chi}}{1+f^2-\frac{\partial f}{\partial \eta}} \quad ,$$

and this expression for the derivative does exist at $\chi=1$ with the assumption that bounded solutions $\eta_n(\chi)$ exist in a neighborhood of $\chi=1$ with $\eta_n(1)$ satisfying (B.1-4). Carrying out this calculation gives $\left.\frac{d\eta_n(\chi)}{d\chi}\right|_{\chi=1}=-\frac{1}{2}\eta_n(1)$; hence, the branches are analytic at $\chi=1$ and they are tangent to the hyperbolas $\eta=\frac{\eta_n(1)}{1+\chi}$ at this point as were the symmetrical branches tangent to the hyperbolas $\eta=\frac{n\pi}{1+\chi}$ at $\chi=1$.

These preceding values of the symmetrical and asymmetrical branches at $\chi=1$ map into the $\frac{\omega}{\kappa}=a$ points on the branches in the ω,κ-plane.

(3) The point $\chi=\frac{a-1}{a+1}$.

The symmetrical solutions $\eta_n\left(\frac{a-1}{a+1}\right)$, $n=1,2,3,\ldots$, with $0<\eta_1<\eta_2<\ldots$, comprise the two sets

$$\left.\begin{aligned} \eta\left(\frac{a-1}{a+1}\right) &= \left.\frac{2q\pi}{1+\chi}\right|_{\chi=\frac{a-1}{a+1}}, \quad q=1,2,3,\ldots, \\ \eta\left(\frac{a-1}{a+1}\right) &= \left.\frac{(2p-1)\pi}{1-\chi}\right|_{\chi=\frac{a-1}{a+1}}, \quad p=1,2,3,\ldots . \end{aligned}\right\} \text{(B.1-5)}$$

The asymmetrical solutions $\eta_n\left(\frac{a-1}{a+1}\right)$, n=1,2,3,..., with $0<\eta_1<\eta_2<\ldots$, comprise the two sets

$$\left.\begin{aligned} \eta\left(\frac{a-1}{a+1}\right) &= \left.\frac{(2q-1)\pi}{1+\chi}\right|_{\chi=\frac{a-1}{a+1}}, \quad q=1,2,3,\ldots, \\ \eta\left(\frac{a-1}{a+1}\right) &= \left.\frac{2p\pi}{1-\chi}\right|_{\chi=\frac{a-1}{a+1}}, \quad p=1,2,3,\ldots . \end{aligned}\right\} \text{(B.1-6)}$$

The point $\chi=\frac{a-1}{a+1}$ corresponds to cut-off $\kappa=0$ and, just as in the ω,κ variables, the branches have separated into two sets at this point; those in (B.1-5) and (B.1-6) with $1-\chi$ in the denominator correspond to motions of the plate which were called the simple thickness-stretch modes and those with $1+\chi$ in the denominator correspond to motions which were called the simple thickness-shear modes by Mindlin [2].

(4) The point $\chi=0$.

The symmetrical frequency equation admits

solutions $\eta_m(0)$, m=1,2,3,..., satisfying

$$\sin\eta(0) = -\eta(0) \quad . \tag{B.1-7}$$

$\eta_m(0)$ can be taken with $\mathrm{Re}\eta_m(0)>0$, $\mathrm{Im}\eta_m(0)>0$, and $0<|\eta_0|<|\eta_1|<\ldots$, however, the complex conjugates are equally good solutions. The first ten roots of (B.1-7) are tabulated by Robbins and Smith [14], and for m>>1

$$\eta_m(0) = \frac{(4m-1)\pi}{2} + i\mathrm{Log}(4m-1)\pi + O\left(\frac{1}{m}\mathrm{Log}m\right) \quad .$$

The asymmetrical frequency equation admits solutions $\eta_m(0)$, m=0,1,2,..., satisfying

$$\sin\eta(0) = \eta(0) \quad , \tag{B.1-8}$$

which can also be taken with $\mathrm{Re}\eta_m(0)>0$, $\mathrm{Im}\eta_m(0)>0$ for m=1,2,3,..., and $0=|\eta_0|<|\eta_1|<|\eta_2|<\ldots$. $\eta_0(0)=0$ is the $\chi=0$ point of the asymmetrical Rayleigh branch which was just discussed. The first ten roots of (B.1-8) are tabulated by Hillman and Salzer [15], and for m>>1

$$\eta_m(0) = \frac{(4m+1)\pi}{2} + i\mathrm{Log}(4m+1)\pi + O\left(\frac{1}{m}\mathrm{Log}m\right) \quad .$$

These solutions at $\chi=0$ map into $\omega=0$ and κ complex by (2.3-7) and they are related to the degenerate case of the static solution in the plate.

(5) The point $\chi=\chi_R$.

Both frequency equations admit solutions

$$\eta(\chi_R) = -\frac{m\pi}{\chi_R} \quad , \quad m=1,2,3,\ldots \; . \qquad \text{(B.1-9)}$$

(6) The point $\chi=-1$.

As in the case of the asymmetrical branches at $\chi=1$, the symmetrical frequency equation (2.3-13) can be written as

$$\tan\eta = -\frac{R\sin(1+\chi)\eta}{1-R\cos(1+\chi)\eta} \quad ,$$

which allows solution values at $\chi=-1$ for the symmetrical branches $\eta_m(-1)$, $m=0,1,2,\ldots$, satisfying

$$\tan\eta(-1) = \frac{1-\nu}{2}\eta(-1) \quad . \qquad \text{(B.1-10)}$$

The root $\eta_0(-1)=-i|\eta_0(-1)|$ is pure imaginary and it is identified as the point on the symmetrical Rayleigh branch where it crosses the equivoluminal tangent ($\chi=-1$ or $\omega=\kappa$). Other than for the conjugate of $\eta_0(-1)$, all other roots of (B.1-10) are real, and the positive set which satisfies $m\pi<\eta_m(-1)<\frac{(2m+1)\pi}{2}$ for $m=1,2,3,\ldots$, is taken where

$$\eta_m(-1) = \frac{(2m+1)\pi}{2} - \frac{4}{(2m+1)\pi(1-\nu)} + O(m^{-3})$$

for $m>>1$.

Analogous to the point $\chi=1$ on the asymmetrical branches, the derivative (3.1-3) takes the $\frac{0}{0}$ form at $\chi=-1$ for the symmetrical branches and cannot be shown to exist. However, the form given above for the symmetrical frequency equation allows calculation of the derivative giving $\left.\frac{d\eta_m(\chi)}{d\chi}\right|_{\chi=-1}=\frac{1}{2}\eta_m(-1)$ where $\eta_m(-1)$ satisfies (B.1-10). Hence, these symmetrical brances are analytic at $\chi=-1$.

The asymmetrical branches take the values

$$\eta_m(-1) = m\pi \quad , \quad m=1,2,3,\ldots, \qquad \text{(B.1-11)}$$

and they are analytic at $\chi=-1$ with the derivative (3.1-4) taking the value $\frac{d\eta_m}{d\chi}=\frac{1}{2}m\pi$.

(7) The point $\chi=\chi_{-1}$.

At this point, the symmetrical frequency equation is satisfied by each of the sets

$$\eta_n(\chi_{-1}) = \frac{(2n+1)\pi}{1+\chi_{-1}} = \frac{(2n+1)\pi}{2\sqrt{1-\nu}}e^{-i\frac{\theta_{-1}}{2}}, \quad n=0,1,2,\ldots, \qquad \text{(B.1-12)}$$

$$\eta_m(\chi_{-1}) = \frac{2m\pi}{1-\chi_{-1}} = \frac{m\pi}{\sqrt{\nu}}ie^{-i\frac{\theta_{-1}}{2}}, \quad m=1,2,3,\ldots . \qquad \text{(B.1-13)}$$

The asymmetrical frequency equation is satisfied by each of the sets

$$\eta_n(\chi_{-1}) = \frac{2n\pi}{1+\chi_{-1}} = \frac{n\pi}{\sqrt{1-\nu}} e^{-i\frac{\theta_{-1}}{2}}, \quad n=1,2,3,..., \qquad \text{(B.1-14)}$$

$$\eta_m(\chi_{-1}) = \frac{(2m-1)\pi}{1-\chi_{-1}} = \frac{(2m-1)\pi}{2\sqrt{\nu}} i e^{-i\frac{\theta_{-1}}{2}}, \quad m=1,2,3,... . \text{(B.1-15)}$$

This separation of the branches into two sets at $\chi=\chi_{-1}$ is closely related to the separation which occurs at $\chi=\frac{a-1}{a+1}$.

(8) The points $\chi=\chi_{01},\chi_{02}$.

These points are not on the real χ-axis unless $0\leq\nu\leq\nu_c$ (ν_c is described in Appendix A), however, they are interesting points since both frequency equations admit solutions

$$\eta(\chi_{01}) = \eta(\chi_{02}) = n\pi \quad , \quad n=1,2,3,... . \qquad \text{(B.1-16)}$$

These points can be made to move off the real axis, as in Fig. 4, by increasing ν, and the same values are retained by $\eta(\chi_{01})$ and $\eta(\chi_{02})$.

(9) Points χ which are real and rational.

Exact solution pairs, χ,η, satisfying the frequency equations can be found at these particular points

by finding the zeros of polynomials. Such results are important since they give exact solution pairs at points other than those already considered.

This case is illustrated by taking $\chi=\frac{m}{n}$ where n=2,3, 4,..., m=±1,±2,±3,..., and $-1<\frac{m}{n}<1$. The symmetrical frequency equation (or, likewise, the asymmetrical equation) reduces to

$$\sin\eta + R\left(\frac{m}{n}\right)\sin\left(\frac{m}{n}\eta\right) = \sin\left(\frac{1}{n}\eta\right) P_{n-1}\left(\cos\left(\frac{1}{n}\eta\right)\right) = 0$$

at $\chi=\frac{m}{n}$ where $P_{n-1}(z)$ is a polynomial of degree n-1 in z. Further, if both m and n are odd, the frequency equation takes the simpler form

$$\sin\left(\frac{1}{n}\eta\right) Q_{\frac{n-1}{2}}\left(\cos^2\left(\frac{1}{n}\eta\right)\right) = 0$$

where $Q_{\frac{n-1}{2}}$ is a polynomial of degree $\frac{n-1}{2}$. An obvious solution of these equations, which is of considerable importance for sketching the branches, results from $\sin\left(\frac{1}{n}\eta\right)=0$. Therefore, the pair

$$\chi = \frac{m}{n} \quad , \quad \eta = n\pi \qquad \text{(B.1-17)}$$

for n=2,3,4,... and m=±1,±2,±3,... satisfies both the symmetrical and asymmetrical frequency equations. The points

(B.1-17) can also be recognized as the common points of the hyperbolas $\eta=\frac{p\pi}{1-\chi}$ and $\eta=\frac{q\pi}{1+\chi}$ for p=n-m and q=m+n. These are the hyperbolas which form the grid as discussed in Subsection 3.2.1.

The remaining solution points, for χ real and rational, are given by the roots of the polynomials $P_{n-1}\left(\cos\left(\frac{1}{n}\eta\right)\right)$ or $Q_{\frac{n-1}{2}}\left(\cos^2\left(\frac{1}{n}\eta\right)\right)$. Thus, by solving nothing more difficult than for the roots of quadratic equations, the frequency equations can be solved exactly at the points $\chi=\pm\frac{1}{5},\pm\frac{1}{3},\pm\frac{1}{2}$, $\pm\frac{3}{5},\pm\frac{2}{3}$, and, by solving for the roots of cubic equations, at the points $\chi=\pm\frac{1}{7},\pm\frac{1}{4},\pm\frac{3}{7},\pm\frac{5}{7},\pm\frac{3}{4}$, etc.

For example, at the point $\chi=-\frac{3}{5}$, the symmetrical frequency equation reduces to

$$\sin\eta + R\sin\left(-\tfrac{3}{5}\eta\right) =$$

$$\sin\left(\tfrac{1}{5}\eta\right)\left[16\cos^4\left(\tfrac{1}{5}\eta\right) - 4(3+R)\cos^2\left(\tfrac{1}{5}\eta\right) + 1 + R\right] = 0$$

where $R=R\left(-\frac{3}{5}\right)>1$ for $0\leq\nu\leq\frac{1}{2}$. This equation has the solutions

$$\eta\left(-\tfrac{3}{5}\right) = 5m\pi, \quad m=1,2,3,\ldots$$

$$\eta\left(-\tfrac{3}{5}\right) = 5m\pi \pm 5\cos^{-1}\left\{\frac{1}{2\sqrt{2}}\left[3+R-(5+2R+R^2)^{\frac{1}{2}}\right]^{\frac{1}{2}}\right\},$$

$m=0,1,2,\ldots,$ (only the plus sign for $m=0$),

$$\eta\left(-\frac{3}{5}\right) = 5m\pi \pm 5i\cosh^{-1}\left\{\frac{1}{2\sqrt{2}}\left[3+R+(5+2R+R^2)^{\frac{1}{2}}\right]^{\frac{1}{2}}\right\},$$

$m=0,1,2,\ldots,$

where all of the radicals are positive and the inverse functions take their smallest real positive values. These solutions indicate a great deal about the branches η in the interval $-1<\chi<\chi_R$. For instance, in the example chosen exact solution points of the symmetrical frequency equation are found both for ω and κ pure imaginary and for ω and κ complex through (2.3-7).

B.2. THE BEHAVIOR OF THE BRANCHES UNDER THE MAPPING $\chi\rightarrow\frac{1}{\chi}$

The properties of the equivoluminal and dilatational branches, which are derived in Subsection 3.2.2, make possible some general statements about the branches η in the complex χ-plane. Use can also be made of the fact that in B.1 the branches are shown to be analytic functions of χ at $\chi=1$ and $\chi=-1$ for the cases where the branches are bounded at these points.

From (3.2-11) and (3.2-17) and from $\tan\frac{\gamma(-\theta)}{2}=-\tan\frac{\gamma(\theta)}{2}$

($\gamma(-\theta)=-\gamma(\theta)$ from Appendix A), the moduli of the equivoluminal branches are even functions of θ. That is, if $|\eta_n| = f_n(\theta)$ satisfies either (3.2-11) or (3.2-17) for n=1,2,3,..., then $f_n(-\theta)=f_n(\theta)$. Thus, the form of the branches $\eta_n(\chi)$ on the unit circle $\chi=e^{i\theta}$ is $\eta_n(e^{i\theta})=f_n(\theta)e^{-i\frac{\theta}{2}}$ from (1) of (3.2-8). Using the fact that $f_n(\theta)$ is an even function of θ results in the interesting property

$$\eta_n(e^{-i\theta}) = f_n(\theta)e^{i\frac{\theta}{2}}$$

or

$$e^{-i\theta}\eta_n(e^{-i\theta}) = f_n(\theta)e^{-i\frac{\theta}{2}} = \eta_n(e^{i\theta}) \qquad \text{(B.2-1)}$$

for $0\leq\theta<\pi$ ($f_n(\theta)$ is singular as $\theta\to\pi$).

The analytic continuations of the equivoluminal branches onto the lower half unit circle are given by (B.2-1). More significantly, the property (B.2-1) also must be valid for continuations off the unit circle $\chi=e^{i\theta}$ since the equality of these analytic functions on the unit circle implies equality everywhere in their domain of analyticity. This being the case, the equivoluminal branches have the property

$$\frac{1}{\chi}\eta_n\left(\frac{1}{\chi}\right) = \eta_n(\chi) \quad , \qquad \text{(B.2-2)}$$

which just defines the behavior of the branches $\eta_n(\chi)$ under the mapping $\chi \to \frac{1}{\chi}$.

The property (B.2-2) makes it possible to show that ω and κ defined by (2.3-7) are invariant under the mapping $\chi \to \frac{1}{\chi}$. That is, if η in (2.3-7) is an equivoluminal branch then $\omega\left(\frac{1}{\chi}\right)=\omega(\chi)$ and $\kappa\left(\frac{1}{\chi}\right)=\kappa(\chi)$. This depends on the definition of the radicals in (2.3-7). A suitable definition which leaves the point $\chi=1$ and the χ-plane near $\chi=1$ free of branch cuts is to take $\chi^{\frac{1}{2}}$ as real and positive on $\chi>0$ with the branch cut on the negative real χ-axis. Similarly, the radical in κ is taken to be real and positive on the interval $\frac{a-1}{a+1}<\chi<\frac{a+1}{a-1}$ with the branch cut on the remainder of the real χ-axis. These also are definitions which make ω and κ real and positive on the integration path C shown in Fig. 2 for $\eta=\eta_n(\chi)$, $n=1,2,3,\ldots$.

This invariance of ω and κ under the mapping $\chi \to \frac{1}{\chi}$ lends support to the statement in Section 2.3 to the effect that if ω and κ are completely known as a function of χ on the unit disk $|\chi| \leq 1$ then they are known everywhere.

Likewise, the moduli of the dilatational branches given by (3.2-12) and (3.2-18) are even functions of θ with respect to the point $\theta=\pi$. Hence, from (2) of (3.2-8), the dilatational branches have the property

$$-e^{-i\theta}\eta(e^{-i\theta}) = \eta(e^{i\theta}) \qquad \text{(B.2-3)}$$

for $0<\theta\leq\pi$ which gives the analytic continuations onto the lower half unit circle. (B.2-3) becomes

$$-\frac{1}{\chi}\eta\left(\frac{1}{\chi}\right) = \eta(\chi) \qquad \text{(B.2-4)}$$

when the dilatational branches are continued off the unit circle. ω and κ in (2.3-7) are again invariant under the mapping $\chi\rightarrow\frac{1}{\chi}$ if the positive real χ-axis is taken for the branch cut of $\chi^{\frac{1}{2}}$ and the segment $\frac{a-1}{a+1}\leq\chi\leq\frac{a+1}{a-1}$ is taken for the branch cut of the radical in κ.

The property (B.2-2) can be used to verify the value of the derivative of the equivoluminal branches at $\chi=1$ as found in B.1. $\left.\frac{d\eta_n(\chi)}{d\chi}\right|_{\chi=1}=-\frac{1}{2}\eta_m(-1)$ results directly from (B.2-2) and the fact that both the symmetrical and asymmetrical equivoluminal branches are analytic at $\chi=1$. Likewise, from (B.2-4), $\left.\frac{d\eta_m(\chi)}{d\chi}\right|_{\chi=-1}=\frac{1}{2}\eta_m(-1)$ for the symmetrical and asymmetrical dilatational branches.

B.3. THE COMPLEX BRANCHES ON THE REAL χ-AXIS

For the purpose of examining the complex branches on the real χ-axis, η is written as

$$\eta = \eta_R + i\eta_I \tag{B.3-1}$$

where $\eta_R=Re\eta$ and $\eta_I=Im\eta$. The symmetrical frequency equation (2.3-13) becomes

$$\left.\begin{aligned} \sin\eta_R\cosh\eta_I &= -R(\chi)\sin\chi\eta_R\cosh\chi\eta_I \quad , \\ \cos\eta_R\sinh\eta_I &= -R(\chi)\cos\chi\eta_R\sinh\chi\eta_I \end{aligned}\right\} \tag{B.3-2}$$

where the real parts have been equated using the fact that χ and $R(\chi)$ are real. As usual, the asymmetrical frequency equation is obtained from (B.3-2) by replacing $-R(\chi)$ with $R(\chi)$.

A simple case results from setting $\eta_R=0$ in (B.3-2) and in the corresponding asymmetrical frequency equation. These solutions, $\eta=i\eta_I$, are identified as the Rayleigh branches and they will be discussed in the context of the entire set of complex branches.

By using the fact that $-1<R(\chi)\leq 1$ on the interval $\frac{a-1}{a+1}\leq\chi<1$ (from (A-5) in Appendix A), it is possible to show that no complex solution of the form (B.3-1) exists with $\eta_I\neq 0$ which satisfies (B.3-2) on this interval. This is done by assuming that a solution with $\eta_I\neq 0$ exists and then using the inequalities $|R\sinh\chi\eta_I|<|\sinh\eta_I|$ and $|R\cosh\chi\eta_I|<\cosh\eta_I$ to obtain a contradiction. The same proof is also valid for the asymmetrical branches.

The existence and form of the complex branches are more apparent on $-1\leq\chi<\frac{a-1}{a+1}$ if the equations (B.3-2) are rearranged so that η_R and η_I can be discussed as separate functions. The first equation of (B.3-2) is multiplied by $\sinh\chi\eta_I$ and squared, the second equation is multiplied by $\cosh\chi\eta_I$ and squared, and the results are added to give

$$\sinh\eta_I = \left[\frac{R^2\cosh^2\chi\eta_I-\sin^2\eta_R}{\cosh^2\chi\eta_I-\sin^2\eta_R}\right]^{\frac{1}{2}}\sinh|\chi|\eta_I \quad . \qquad \text{(B.3-3)}$$

This equation is a result of forcing (B.3-2) into a form which is very similar to the original frequency equations (2.3-13) and (2.3-14) with $\eta_I=\text{Im}\eta$ replacing η and the radical replacing $\pm R(\chi)$. Actually, the sign of $R(\chi)$ has been lost in the squaring operations so that (B.3-3) is valid for both the symmetrical and asymmetrical complex branches, and (B.3-2) or the analogous asymmetrical frequency equations must be used to identify the particular branches. Similarly, the pair (B.3-2) can be manipulated to give

$$\sin^2(1+\chi)\eta_R = \frac{\sin^2 2\eta_R\sinh^2(1+\chi)\eta_I}{R^2\sinh^2 2\chi\eta_I} \quad ,$$

which can be combined with (B.3-3) to eliminate $\sin^2 2\eta_R = 4\sin^2\eta_R(1-\sin^2\eta_R)$, resulting in

$$\sin^2(1+\chi)\eta_R = \frac{(\sinh^2\eta_I - R^2\sinh^2\chi\eta_I)(R^2\cosh^2\chi\eta_I - \cosh^2\eta_I)}{R^2\sinh^2(1-\chi)\eta_I} \quad . \tag{B.3-4}$$

The pair (B.3-3) and (B.3-4) are especially convenient forms from which to determine both the symmetrical and asymmetrical sets of complex branches.

The following approach can be used to find exact solution points on the complex branches or to verify the existence and form of the branches: (1) $\sin^2\eta_R$ is considered as a constant parameter ($0 \leq \sin^2\eta_R \leq 1$) in (B.3-3), which can then be solved for η_I as a function of χ and the parameter; (2) this result is substituted into (B.3-4) to give η_R as a function of χ and the parameter; (3) the common points of this function η_R and the constant values of η_R from $\sin^2\eta_R$= constant give exact solution points χ, η_R, and η_I is then given by evaluating the function η_I in (1) at this point χ.

The preceding procedure depends on the fact that there exists a solution η_I of (B.3-3) for a fixed value of $\sin^2\eta_R$ and such a solution may not exist. If (B.3-3) is written as

$$\frac{\sinh\eta_I}{\sinh|\chi|\eta_I} = \left[\frac{R^2\cosh^2\chi\eta_I - \sin^2\eta_R}{\cosh^2\chi\eta_I - \sin^2\eta_R}\right]^{\frac{1}{2}} ,$$

the left side of this equation is a strictly increasing function of η_I and the right side is a nonincreasing function of η_I for $-1<\chi<\frac{a-1}{a+1}$. $\chi=0$ is an exceptional point with complex solutions already known to exist satisfying (B.1-7) and (B.1-8) in Appendix B. Also, the point $\chi=-1$ gives a limiting case which cannot be included here. Thus, a single solution $\eta_I>0$ exists if, and only if,

$$\lim_{\eta_I\to 0} \frac{\sinh\eta_I}{\sinh|\chi|\eta_I} = \frac{1}{|\chi|} < \left[\frac{R^2-\sin^2\eta_R}{\cos^2\eta_R}\right]^{\frac{1}{2}} =$$

$$\left[\frac{R^2\cosh^2\chi\eta_I-\sin^2\eta_R}{\cosh^2\chi\eta_I-\sin^2\eta_R}\right]^{\frac{1}{2}}\Bigg|_{\eta_I=0} ,$$

which is equivalent to requiring that

$$\sin^2\eta_R > \frac{1-\chi^2R^2}{1-\chi^2} \quad . \tag{B.3-5}$$

From the first of (B.3-2), this also gives a bound on $\sin^2\chi\eta_R$ which is

$$\sin^2\eta_R = R^2\,\frac{\cosh^2\chi\eta_I}{\cosh^2\eta_I}\sin^2\chi\eta_R \le R^2\sin^2\chi\eta_R$$

for $\eta_I > 0$, and this can be combined with (B.3-5) to give

$$\sin^2 \chi\eta_R > \frac{1}{R^2} \frac{1-\chi^2R^2}{1-\chi^2} \quad . \tag{B.3-6}$$

On $-1<\chi<0$, both (B.3-5) and (B.3-6) are always satisfied since $\chi^2R^2>1$ by (A-5); hence, complex branches exist on this interval by this criterion. However, on $0<\chi<\frac{a-1}{a+1}$ the inequalities (B.3-5) and (B.3-6) are not satisfied for all χ and $\eta_R \geq 0$. The limiting case $\eta_I \to 0$ on the complex branches can only occur at points χ, η_R determined by (B.3-5) and (B.3-6) with equalities replacing the inequalities. This is not meant to include all of the points on the real branches considered in Subsection 3.2.1 where $\eta_I \equiv 0$, but only the limiting points of the complex branches. But, (B.3-5) and (B.3-6) with equalities are identical to the two equations (3.1-7) with no distinction between the symmetrical and asymmetrical cases. Thus, just as is expected from a local approximation like (3.1-13), the branch points on $0<\chi\leq\frac{a-1}{a+1}$ are common points of the real and complex branches.

Bounds on the functions η_I result directly from (B.3-3) by observing that the radical on the right side of that equation is a nondecreasing function of $\sin^2\eta_R$ for $0\leq\sin^2\eta_R\leq 1$ if $R^2\geq 1$, which is the case on $-1\leq\chi\leq\frac{a-1}{a+1}$. Hence,

evaluating the right side of (B.3-3) for $\sin^2\eta_R=0$ and $\sin^2\eta_R=1$ results in the lower and upper bounds respectively for $\sinh\eta_I$, and also for η_I since $\sinh\eta_I$ is an increasing function of η_I. The bounds are then defined by the inequalities

$$|R|\sinh|\chi|\eta_I \le \sinh\eta_I \le \sqrt{R^2\cosh^2\chi\eta_I-1} \quad ,$$

which is equivalent to the pair of inequalities

$$\left.\begin{aligned} \sinh\eta_I &\ge |R|\sinh|\chi|\eta_I \quad , \\ \cosh\eta_I &\le |R|\cosh\chi\eta_I \end{aligned}\right\} \quad \text{(B.3-7)}$$

with $\eta_I \ge 0$ throughout.

The bounds (B.3-7) are taken (the equalities hold) by the imaginary part of the complex branches at various points in the $\mathrm{Re}\chi,\mathrm{Re}\eta$-plane; hence, the bounds are also envelopes with $\eta_I=\mathrm{Im}\eta$ being tangent to the curves at these points.

The lower bound is taken by η_I if $\sin^2\eta_R=0$ and $\sin^2(1+\chi)\eta_R=0$, which results from (B.3-4) under the condition that the first of (B.3-7) with the equality, or $\sinh\eta_I=|R|\sinh|\chi|\eta_I$, is satisfied. Actually, a solution $\eta_I>0$ of the first of (B.3-7) with the equality exists only on $-1\le\chi<0$ where $|\chi R|\ge 1$ by (A-5) in Appendix A. Hence, the

appropriate lower bound for η_I on $0 \leq \chi \leq \frac{a-1}{a+1}$ is just $\eta_I \equiv 0$.

The upper bound is taken by η_I if $\sin^2 \eta_R = 1$ and $\sin^2(1+\chi)\eta_R = 0$, which results from (B.3-4) and the second of (B.3-7) with the equality, or $\cosh \eta_I = |R| \cosh \chi \eta_I$. This equation has a solution $\eta_I > 0$ on all of the interval $-1 \leq \chi < \frac{a-1}{a+1}$ where $|R| \geq 1$.

The envelopes or bounds defined by (B.3-7) are shown in Fig. 11. Both the upper and lower bounds are obviously unbounded as $\chi \to \chi_R$ where $R(\chi)$ is also unbounded by (A-3). The asymptotic approximations of the bounds η_I are easily derived and they both take the form

$$\eta_I \sim \frac{1}{1+\chi} \text{Log} |R(\chi)| + O\left(|\chi - \chi_R|^{-\frac{2\chi_R}{1+\chi_R}} \right) \qquad \text{(B.3-8)}$$

as $\chi \to \chi_R$ on the real χ-axis. Hence, the imaginary part of every branch must have this approximation. The equations (B.3-7) for the bounds can be expanded near $\chi = -1$ by using $R(-1) = 1$ from (A-3) and $R'(-1) = \frac{2}{1-\nu}$ from (A-4) in Appendix A to show that η_I for the lower bound satisfies

$$\frac{1-\nu}{2} \eta_I = \tanh \eta_I$$

at $\chi = -1$, and that η_I for the upper bound satisfies

$$\frac{1-\nu}{2}\eta_I = \coth\eta_I$$

at $\chi=-1$. The lower bound equation at $\chi=-1$ is identical to (B.1-10) with $\eta=i\eta_I$. The solutions, $\eta_I(-1)$, of these equations can easily be shown to fall above and below the value $\frac{2}{1-\nu}$ with a finite separation that depends on Poisson's ratio ν.

The Rayleigh branches are a special case where $\sin^2\eta_R = \sin^2(1+\chi)\eta_R=0$ due to $\eta_R\equiv 0$ and the lower bound is an exact solution of the frequency equations. This can also be seen by setting $\eta=i\eta_I$ in the frequency equations (2.3-13) and (2.3-14). To be precise, the symmetrical Rayleigh branch $\eta=i\eta_I$ with $\eta_I\neq 0$ only exists on $-1\leq\chi<\chi_R$ where $\chi R(\chi)\leq -1$, and the asymmetrical Rayleigh branch $\eta=i\eta_I$ with $\eta_I\neq 0$ only exists on $\chi_R<\chi<0$ where $\chi R(\chi)>1$. These comments result from the forms of the frequency equations and they are a reminder that the lower bound in (B.3-7) has resulted from squaring operations which obscure the difference between the symmetrical and asymmetrical frequency equations. The lower bound in Fig. 11 is then a sketch of a portion of the symmetrical Rayleigh branch on $-1\leq\chi<\chi_R$ and of the asymmetrical Rayleigh branch on $\chi_R<\chi\leq 0$. If the negative solution η_I is taken in each case and if the radicals in (2.3-7) are taken as positive imaginary, then both ω and κ are real and positive. The positive imaginary values of the radicals

result from a natural continuation above their respective branch points, $\chi=0$ and $\chi=\frac{a-1}{a+1}$.

The asymptotic approximation of $\eta_I=Im\eta$ as $\chi\to\chi_R$ is given by (B.3-8) for all of the complex branches and the complete approximation for $\eta=\eta_R+i\eta_I$, as derived from the frequency equations (2.3-13) and (2.3-14), is

$$\eta \sim \frac{1}{1+\chi}[q\pi+iLog(R(\chi))] + O\left(|\chi-\chi_R|^{-\frac{2\chi_R}{1+\chi_R}}\right) \qquad (B.3-9)$$

as $\chi\to\chi_R$ with $q=0,2,4,\ldots$ for the symmetrical branches and $q=1,3,5,\ldots$ for the asymmetrical branches. In this approximation, $Log(R(\chi))=Log|R(\chi)|+iArg(R(\chi))$ with $-\frac{\pi}{2}$ $Arg(R(\chi))<\frac{3\pi}{2}$. (B.3-9) includes the approximation to the symmetrical Rayleigh branch $q=0$ as $\chi\to\chi_R$ on $-1\leq\chi<\chi_R$ where $Arg(R(\chi))=0$, and to the asymmetrical Rayleigh branch $q=1$ as $\chi\to\chi_R$ on $\chi_R<\chi\leq 0$ where $Arg(R(\chi))=\pi$. Every complex branch has a logarithmic branch point at $\chi=\chi_R$ and this feature is not unique to the Rayleigh branches.

(B.3-9) indicates the nature of an analytic continuation about the logarithmic branch point χ_R for every complex branch. Any symmetrical complex branch, including the Rayleigh branch, can be continued onto any other symmetrical complex branch by encircling the branch point $\chi=\chi_R$. This is equivalent to passing through the branch cut and

onto other sheets of the Riemann surface. The same holds true for the asymmetrical complex branches.

A few of the complex branches are sketched in Fig. 12 in the $\mathrm{Re}\chi, \mathrm{Re}\eta, \mathrm{Im}\eta$-space. This figure and other details about the complex branches are discussed in Subsection 3.2.3.

APPENDIX C

ADDITIONAL MATERIAL FOR ANALYTIC CONTINUATIONS

C.1. AN EXPANSION OF THE FREQUENCY EQUATIONS FOR 1-ν SMALL

The function $R(\chi)\equiv R(\chi,\nu)$ in (2.3-12a) is expanded in powers of $1-\nu$, where the assumption must be made that $1+\chi$ is not small since both R and the branches η undergo drastic changes near $\chi=-1$ as $\nu\to 1$. Then the frequency equations (2.3-13) and (2.3-14) can be approximated, under the assumptions that $1-\nu$, $\chi-\frac{j}{k}$ and $\eta-k\pi$ are small where $k=2,3,4,\ldots$, $j=\pm1,\pm2,\pm3,\ldots$ and $\chi_R<\frac{j}{k}<1$, to give

$$\chi \cong \frac{j}{k} + \frac{8(1-\nu)^2}{\pi}\,\frac{j^2(k-j)}{k(k+j)^3}(\eta-k\pi) - \frac{1}{6\pi}\,\frac{j(k^2-j^2)}{k^4}(\eta-k\pi)^3 \quad . \tag{C.1-1}$$

(C.1-1) is an approximation to the symmetrical branches for j+k odd and to the asymmetrical branches for j+k even. The requirement $\chi_R<\frac{j}{k}$, with χ_R defined by (2.3-9), only serves to avoid the vicinity of $\chi=-1$, but this is not very restrictive since $\chi_R\to-1$ as $\nu\to1$. Thus, (C.1-1) is valid near $\chi=-1$ if $1-\nu$ is sufficiently small.

In addition, (C.1-1) is valid even if $1-\nu$ is not small provided that $k\gg j$ which means this approximate

frequency equation is useful to examine the upper branches near $\chi=0$.

The simple cubic (C.1-1) vividly illustrates the nature of the branch points, which merge as $\nu\to 1$, both on $-1<\chi<0$ for $j\leq 1$ and on $0<\chi<1$ for $j\geq 1$. If (C.1-1) is taken to be exact, the branch points are identified by requiring that $\frac{d\chi}{d\eta}=0$; thus, the branch points are located at

$$\chi = \frac{j}{k} \pm \frac{64(1-\nu)^3}{3\pi} \frac{j^2(k-j)}{(k+j)^5}\sqrt{jk} \quad ,$$

$$\eta = k\pi \pm 4(1-\nu)\frac{k}{(k+j)^2}\sqrt{jk}$$

so that if j is negative both χ and η are complex at the branch points. The very important feature of this is that when $Im\chi>0$ at the branch points, identifying these as the approximate location of branch points from "the set of negative branch points," it is also true that $Im\eta>0$. Therefore, branch points belonging to "the set of negative branch points" are common only to pairs of branches consisting of a real branch on $-1<\chi<0$ and a complex branch with $Im\eta>0$. The preceding statement requires a very simple examination of the continuations about the branch points as predicted by (C.1-1). Likewise, it is seen that complex conjugates of these branch points are common to pairs of

branches consisting of a real branch on $-1<\chi<0$ (the same real branches as those just mentioned) and a complex branch with $\mathrm{Im}\eta<0$.

The simple cubic (C.1-1) has solutions which illustrate the nature of the complex branches as $\nu\to 1$. On $0\leq\chi\leq 1$ for $\frac{1}{2}\leq\nu<1$, the complex branches have complex loops between pairs of branch points just as shown in Fig. 12 on $0\leq\chi\leq\frac{a-1}{a+1}$. $\nu=1$ causes the branch points and, hence, the base points of neighboring loops to merge. On $-1\leq\chi\leq 0$ for $\nu<1$, each complex branch has an imaginary part which oscillates but is never zero as is also shown in Fig. 12. $\nu=1$ causes these minimums in $\mathrm{Im}\eta$ to reach $\mathrm{Im}\eta=0$ at the branch points and the branches become identical with those on $0\leq\chi\leq 1$.

C.2. CONTINUATIONS OF THE EQUIVOLUMINAL AND DILATATIONAL BRANCHES ABOUT THEIR SINGULAR POINTS, $\chi=-1$ AND $\chi=1$

In Subsection 3.3.3, the equivoluminal and dilatational branches were found to be singular at $\chi=-1$ and $\chi=1$ respectively. Continuations of these branches about their singular points is required and this presents a problem since none of the representations in Section 3.3 were shown to be valid except as the singular points were approached on $\chi=e^{i\theta}$, $0\leq\theta\leq\pi$.

To resolve this problem, it is easy to show that the approximation

$$\eta_n(\chi) = \frac{2n\pi}{1+\chi} - i\frac{\mathrm{Log}R}{1+\chi} + O\left(\left|e^{-2n\pi i\frac{1-\chi}{1+\chi}}\right|\right) , \qquad \text{(C.2-1)}$$

n=1,2,3,..., taken directly from the series representation (3.3-14), is valid for the symmetrical equivoluminal branches, with the error indicated, for $0<\mathrm{Arg}(1+\chi)<\pi$. The verification of this approximation is contained in the discussion following the form (3.3-6) of the symmetrical frequency equation. Thus, since the complex branches with $\mathrm{Im}\eta<0$ were found to have no branch points adjacent to the real χ-axis with $\mathrm{Im}\chi>0$, they can be continued slightly off the real χ-axis. This continuation for a complex branch with the dominant term $\frac{2n\pi}{1+\chi}$ must lead to the equivoluminal branch with the approximation (C.2-1). This argument uses the fact that $\frac{d\eta}{d\chi}$ must remain finite since no branch points are present, and the continuation must take place away from the singular point $\chi=-1$. Also, it is observed from (3.3-4) that the imaginary part of the approximation (C.2-1) is negative on the real χ-axis, which is in good agreement with the imaginary part of the complex branches since they oscillate about $-\frac{2}{1-\nu}$ on the real χ-axis near $\chi=-1$.

The complex branches with $\mathrm{Re}\eta>0$ and $\mathrm{Im}\eta>0$ continue about $\chi=-1$ onto the dilatational branches on $\chi=e^{i\theta}$, $0<\theta\leq\pi$. The reason for the difference between the continuations of complex branches with imaginary parts of different signs

is that only those branches with $\mathrm{Im}\eta>0$ have branch points with $\mathrm{Im}\chi>0$ adjacent to the real χ-axis on $-1<\chi<0$.

Similarly, the asymmetrical equivoluminal branches continue about $\chi=-1$ onto the asymmetrical complex branches with $\mathrm{Im}\eta<0$.

Also, from the approximations consisting of the leading terms of (3.3-23) and (3.3-28), the dilatational branches continue about $\chi=1$ onto the only branches available on the real χ-axis, the real branches.

C.3. THE NATURE OF "THE SET OF POSITIVE BRANCH POINTS" FOR $\nu=\frac{1}{2}$.

"The set of positive branch points" for $\nu=\frac{1}{2}$, defined in Subsection 3.4.1, has not been explained yet. The nature of these branch points is easily resolved by making analytic continuations about the closed paths described in Subsection 3.4.2, except that these branch points are ignored and remain interior to the closed paths. In doing so, it is found that none of the branches have a single-valued continuation on the closed path. Hence, one branch point from this subset must be common to each pair of neighboring real branches on $\frac{a-1}{a+1}\leq\chi\leq 1$ since this is required for a single-valued continuation. Also, the details of the continuation about each of these branch points must be the

same as for the other members of "the set of positive branch points" which are adjacent to $\frac{a-1}{a+1} \leq \chi \leq 1$. To be precise, this argument only insures that an odd number of these branch points be common to neighboring branches, however, it was found in Subsection 3.1.3 that the branch points are also zeros of $\Delta_{jk}^{\pm}$ given by (3.1-9) with $\pm(-1)^k = +1$ where $k\pi < \mathrm{Re}\eta < (k+1)\pi$ at the branch point. Consequently, it is not a reckless assumption to assign the branch point of this subset which is a zero of $\Delta_{jk}^{\pm}$ to the neighboring pair of real branches η_k and η_{k+1} on the real χ-axis. This gives the required number of branch points to make every branch continue as a single-valued, analytic function on a closed path with none of its branch points interior to or on the path.

C.4. EXAMPLES OF ANALYTIC CONTINUATIONS ON CLOSED PATHS

A closed path in the χ-plane is shown in Fig. 14 and it corresponds to the analytic continuation of the symmetrical branch shown in Fig. 15. Both the path and the corresponding values of η are indicated by a heavy, directed line. The dashed, directed lines in Fig. 15 represent transitions caused by the path going around branch points. Two axes for the modulus $|\eta(e^{i\theta})|$ versus θ, $0 \leq \theta \leq \pi$, are used on the left of

Fig. 15 to emphasize the transition from the dilatational branch $\eta_0(e^{i\theta})=i|\eta_0(e^{i\theta})|e^{-i\frac{\theta}{2}}$ to the symmetrical Rayleigh branch $\eta_0(e^{i\theta})=|\eta_0(e^{i\theta})|e^{-i\frac{\theta}{2}}$ caused by their common branch point at θ_0, where the point $\chi_0=e^{i\theta_0}$ is given by (2.3-8). The numbers 1,2,...,6 label certain corresponding points in both figures. Branch points are indicated in Fig. 14 by dots.

A description of this continuation is now given by beginning at point 1 or $\chi=0$. Point 1 is on a symmetrical complex branch with $Im\eta<0$ (Fig. 12 shows the complex conjugate of this branch). $\eta(0)=Re\eta(0)+iIm\eta(0)$ satisfies (B.1-7) and it is the root with the smallest positive real part. On 1,2, η remains on this complex branch with $Im\eta$ vanishing at 2, which is the branch point identified as (-,0,1) in Fig. 7. The continuation about the branch point at 2 takes η onto a real branch identified as the symmetrical branch $\eta_1(\chi)$ in Fig. 8. Beyond 2, branch points from "the set of positive branch points" are encountered adjacent to the real χ-axis. The continuations about these branch points are indicated by dashed lines in Fig. 15 on $\frac{a-1}{a+1}<\chi<1$. These continuations have the effect of stair-stepping up the real branches. These branch points form an infinite set with a limit point at $\chi=1$ and they are

zeros of $\Delta^{\pm}_{k+1,k}$ given by (3.1-9) for $\pm(-1)^k=+1$ and k=1,2, 3,... . These become too numerous to show near $\chi=1$ in Fig. 14 and the path just passes above all of them and onto the unit circle $\chi=e^{i\theta}$, $0<\theta\leq\pi$. In Fig. 15 this continuation connects the right and left extremes which are both labeled 3 for $\chi=1$ or $\theta=0$. On the unit circle, η goes onto the lowest dilatational branch described by (3.2-12) with m=0, which is shown in Fig. 10. This branch shares the branch point at 4 or $\chi=\chi_0=e^{i\theta_0}$ given by (2.3-8) with the symmetrical Rayleigh branch which is described by (3.2-11) with n=0 and is shown in Fig. 9. The branch is analytic at 5 ($\chi=-1$, $\theta=\pi$) and it continues onto the real χ-axis still on the symmetrical Rayleigh branch where η is pure imaginary with $Im\eta<0$ on $-1\leq\chi<\chi_R$. The branch point at 6 or $\chi=\chi_R$ given by (2.3-9) is avoided by a small indention which causes η to change as predicted by the complex conjugate of (B.3-9) with q=0. The real part of η jumps from zero to $\frac{\pi}{1+\chi_R}$ and its imaginary part is unbounded at χ_R. This puts η back on the same complex branch as the beginning point 1 and the continuation to that point is uneventful.

A similar closed path in the χ-plane is shown in Fig. 16 corresponding to the dilatational continuation (as defined in Subsection 3.4.2) of the asymmetrical branch shown in Fig. 17. In this case, there is a branch point at 1

($\chi=0$) which is common to the asymmetrical Rayleigh branch and to the asymmetrical real branch $\eta_1(\chi)$ shown in Fig. 8. The continuation from 1 to 2 ($\chi=1$) only encounters branch points adjacent to $\frac{a-1}{a+1}<\chi<1$ and these form another infinite set with a limit point at $\chi=1$. These are zeros of $\Delta^{\pm}_{kk}$ given by (3.1-9) for $\pm(-1)^k=+1$ and $k=1,2,3,\ldots$. The details of the continuation about these branch points are the same as just described for the symmetrical continuation shown in Figs. 14 and 15. At 2, η goes onto the asymmetrical dilatational branch described by (3.2-18) with $m=1$, which is shown in Fig. 10. This branch has no branch points on the unit circle $\chi=e^{i\theta}$, $0<\theta\leq\pi$, and it continues onto the lowest asymmetrical real branch at 3 ($\chi=-1$). From 3 to 4 on the real χ-axis, η remains on this real branch and then at 4 a branch point is encountered and η goes onto a complex branch with $\mathrm{Im}\eta>0$ which has the dominant term $\frac{\pi}{1+\chi}$ as $\chi\to-1$ and is shown in Fig. 12. This branch point is a zero of Δ^{-}_{-11} and it belongs to "the set of negative branch points." At 5 ($\chi=\chi_R$), η leaves the complex branch and continues onto the asymmetrical Rayleigh branch as predicted by (B.3-9) with $q=1$. The real part of η decreases from $\frac{\pi}{1+\chi_R}$ to zero on the Rayleigh branch with the imaginary part of η unbounded at χ_R. The continuation then proceeds on the asymmetrical Rayleigh branch from 5

to 1 ($\chi=0$), which was the starting point.

In Figs. 18 and 19, an equivoluminal continuation (as defined in Subsection 3.4.2) is shown and it involves the symmetrical equivoluminal branch $\eta_2(e^{i\theta})=|\eta_2(e^{i\theta})|e^{-i\frac{\theta}{2}}$, described by (3.2-11) with n=2 and shown in Fig. 9. The continuation is much like the two just described except that only three branch points from "the set of positive branch points" are involved on $\frac{a-1}{a+1}\leq\chi<1$. The branch points are zeros of Δ_{14}^{+}, Δ_{23}^{-} and Δ_{32}^{+} respectively as $\chi=1$ is approached. The continuation then goes onto the equivoluminal branch $\eta_2(e^{i\theta})$ which is analytic at $\chi=1$ and finally onto a complex branch at $\chi=-1$ which has $\mathrm{Im}\eta<0$. The complex branch has no branch points from "the set of negative branch points" as was found in C.1. The continuation about $\chi=\chi_R$ is given by the complex conjugate of (B.3-9) with q=4.